

AD-A181 836

THE SCIENCE OF AND ADVANCED TECHNOLOGY FOR
COST-EFFECTIVE MANUFACTURE OF (U) PURDUE UNIV
LAFAYETTE IN SCHOOL OF INDUSTRIAL ENGINEERING J MODREV

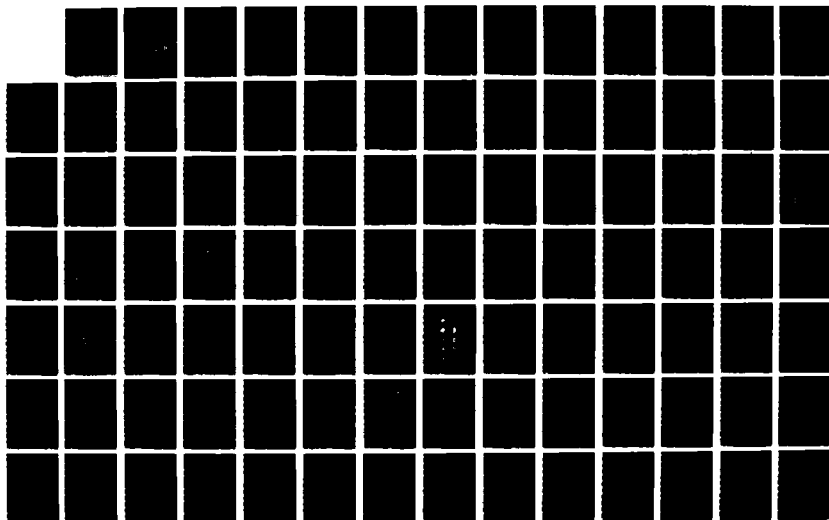
1/2

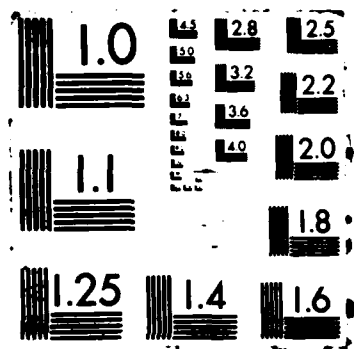
UNCLASSIFIED

DEC 86 N00014-83-K-0385

F/G 13/8

NL





AD-A181 836

THE SCIENCE OF AND ADVANCED TECHNOLOGY FOR
COST-EFFECTIVE MANUFACTURE
OF HIGH PRECISION ENGINEERING PRODUCTS

ONR Contract No. 83K0385
FINAL REPORT
Vol. 7

PRECISION ENGINEERING MONOGRAPH
ANALYTICS & DESIGN OF PRECISION LINEAR SLIDEWAYS

PREPARED BY
J. Modrey

DTIC
SELECTED
JUN 24 1987
S D

DISTRIBUTION STATEMENT A
Approved for public release
Distribution Unlimited

DECEMBER 1986

Schools of
Mechanical, Electrical and Industrial Engineering
Purdue University
West Lafayette, Indiana 47907

None

SECURITY CLASSIFICATION OF THIS PAGE

AD-A181836

REPORT DOCUMENTATION PAGE

1a REPORT SECURITY CLASSIFICATION None			1b RESTRICTIVE MARKINGS None		
2a SECURITY CLASSIFICATION AUTHORITY None			3 DISTRIBUTION / AVAILABILITY OF REPORT		
2b DECLASSIFICATION / DOWNGRADING SCHEDULE None					
4. PERFORMING ORGANIZATION REPORT NUMBER(S) Final Report Vol. 7			5 MONITORING ORGANIZATION REPORT NUMBER(S)		
6a. NAME OF PERFORMING ORGANIZATION Purdue University		6b OFFICE SYMBOL (If applicable)	7a NAME OF MONITORING ORGANIZATION Department of Defense Office of Naval Research		
6c ADDRESS (City, State, and ZIP Code) School of Industrial Engineering West Lafayette, IN 47907			7b ADDRESS (City, State, and ZIP Code) Arlington, VA 22217-5000		
8a. NAME OF FUNDING / SPONSORING ORGANIZATION		8b OFFICE SYMBOL (If applicable) 614A	9 PROCUREMENT INSTRUMENT IDENTIFICATION NUMBER N00014-83-K-0385/12/12		
8c ADDRESS (City, State, and ZIP Code)		10 SOURCE OF FUNDING NUMBERS			
		PROGRAM ELEMENT NO ONR:433	PROJECT NO	TASK NO SRO-150	WORK UNIT ACCESSION NO
11 TITLE (Include Security Classification) PRECISION ENGINEERING MONOGRAPH: ANALYTICS & DESIGN OF PRECISION LINEAR SLIDEWAYS					
12 PERSONAL AUTHOR(S) Modrey, J.					
13a TYPE OF REPORT Final		13b TIME COVERED FROM 1-1-83 TO 2-31-86		14 DATE OF REPORT (Year, Month, Day) December 1986	
15 PAGE COUNT 172					
16 SUPPLEMENTARY NOTATION					
17 COSATI CODES			18 SUBJECT TERMS (Continue on reverse if necessary and identify by block number)		
FIELD 13	GROUP	SUB-GROUP	Linear slideways; Hydrostatic guideways; Aerostatic slideways; Machine tool guideways; Precision engineering, Engineering monographs, Gas bearings; Friction, Lubrication.		
19 ABSTRACT (Continue on reverse if necessary and identify by block number) <p>Much of the hardware of high technology is characterized by miniaturization, extremely close tolerances and position control within fractions of a micron. Both national security and primacy in international economics are directly related to strength in the development of advanced precision systems and their production at low cost and high reliability. Comparing the status of precision engineering in the U.S. with that of Switzerland, Germany, and Japan, countries with enviable trade balances suggests that the time has arrived for an explicit and aggressive program focused on developing a formal discipline of precision engineering in the U.S. It is recommended here that one facet of such a program be the creation of a series of monographs dealing in depth with the basic components and metrology of high precision control and manufacturing systems. Ten to fifteen such monographs could serve to direct U.S. engineering education in this direction or retrain practicing engineers for entry into this field. This document is a suggested initial monograph and deals with the basic problem of precision mechanical linear guidance.</p> <p><i>Recommendation: This paper is a good starting point for the development of a series of monographs on precision engineering.</i></p>					
20 DISTRIBUTION / AVAILABILITY OF ABSTRACT <input type="checkbox"/> UNCLASSIFIED/UNLIMITED <input checked="" type="checkbox"/> SAME AS RPT <input type="checkbox"/> DTIC USERS			21 ABSTRACT SECURITY CLASSIFICATION None		
22a NAME OF RESPONSIBLE INDIVIDUAL Dr. A.L. Meyrowitz			22b TELEPHONE (Include Area Code) 202-696-4302		22c OFFICE SYMBOL 433

THE SCIENCE OF AND ADVANCED TECHNOLOGY FOR COST-EFFECTIVE MANUFACTURE OF HIGH PRECISION ENGINEERING PRODUCTS

ONR Contract No. 83K0385
Final Report
Vol. 7



PRECISION ENGINEERING MONOGRAPH ANALYTICS & DESIGN OF PRECISION LINEAR SLIDEWAYS

Prepared by
J. Modrey

December 1986

Accession For	
NTIS CRA&I	<input checked="" type="checkbox"/>
DTIC TAB	<input type="checkbox"/>
Unannounced	<input type="checkbox"/>
Justification	
By <i>lth on file</i>	
Distribution	
Availability Codes	
Dist	Avail and/or Special
A-1	

Schools of
Mechanical, Industrial and Electrical Engineering
Purdue University
West Lafayette, Indiana 47907

Research and data acquisition described in this report has been supported by the Office of Naval Research through Contract No. N83K0385 in the framework of the ONR Precision Engineering projects.

Work on the Precision Engineering project at Purdue University greatly benefited from the use of the technical facilities of the Purdue Computer Integrated Design, Manufacturing and Automation Center (CIDMAC) and the advice of the CIDMAC member companies*, which is gratefully acknowledged.

Moshe M. Barash
Principal Investigator

C. Richard Llu
Principal Investigator

*Member companies of CIDMAC are:

Cincinnati Milacron; TRW; Ransburg Corporation; Cummins Engine Co.; Control Data Corporation; ALCOA; Chrysler.

PREFACE

There doesn't seem to be any officially agreed upon definition of precision engineering but for purposes of this monograph the following statement could serve.

Precision Engineering: The application of higher technology and science to the design and manufacture of components or subsystems calling for geometric and position control to within fractions of a micron.

An effective graphical definition of the objectives of precision engineering in a specific discipline is by Fig. P.1 from the work of Professor Niro Taniguchi of the Tokyo Science University. While this illustration focuses on machinery accuracy it is nevertheless an excellent guideline to the comprehension of the implicit goals of precision engineering in general. Currently in the U.S., there is a belated but growing interest in precision engineering. The primary motivation for this change is the growth of high technology both for defense and commercial needs. Such products are characterized by miniaturization and very close tolerances. There is another compelling force which should activate an increased interest in precision engineering. It is the loss of markets for the kind of manufactured hard goods which might be roughly classified as the top curve of Fig. P.1. Second and even third world nations are now capable of performing at this industrial level but at less cost to our disadvantage. Product lines or methods of manufacturing which exploit more sophisticated engineering such as precision engineering could develop a more competitive edge for us. It is no coincidence that nations such as Switzerland, Germany and Japan each have a balance of trade which we envy. The common

denominator among the three nations is a history of training and education in FINE MECHANICS or its current identity PRECISION ENGINEERING. Several Japanese universities now have departments of precision engineering. They have recently coined the expression "mechatronics" giving further evidence of ferment in activities associated with precision engineering. There is even a Japan Society of Precision Engineering. Clearly the advantage to Japan is growing and might become unreconcilable for the U.S. if the current level of effort here is not stepped up.

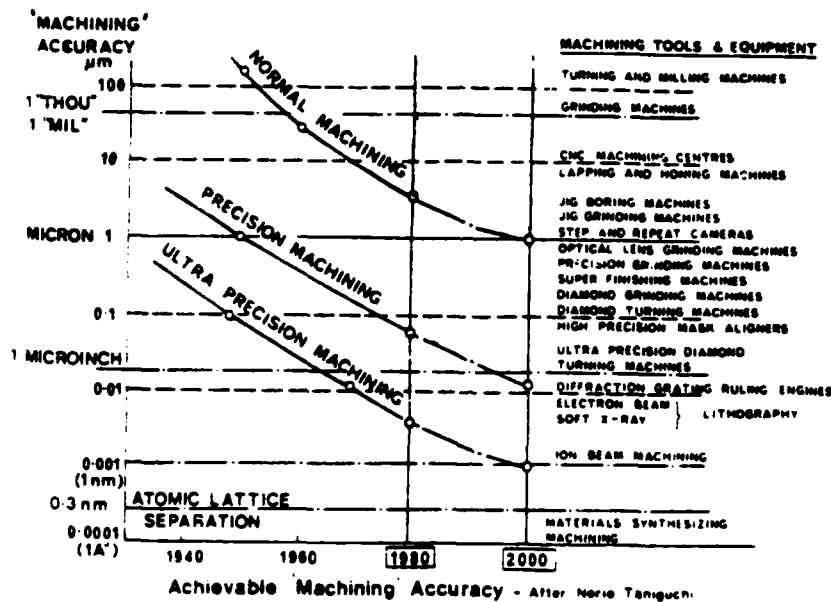


Fig. P.1

Educational programs in the ways of precision engineering aimed at not only student engineers but also practicing engineers transferring to this field is very likely the quickest avenue for the catch up program. A strategy for initializing this activity is the development of a series of short texts or monographs for beginning graduate students and engineers in practice desiring retraining. These texts would also keep

faculty, with a little formal background in precision engineering design, to transfer their skills to this movement. The conventional comprehensive design text authored by one or two generalists is probably unsuited to the program contemplated. Monographs each concentrating on a topic within the field and composed by an authority in that field will serve better.

Fig. P.2 illustrates a possible matrix of topics on which a series of monographs could be based. This report is a possible model for the very first item of the matrix. As such it is an exploratory experiment in the suggested program.

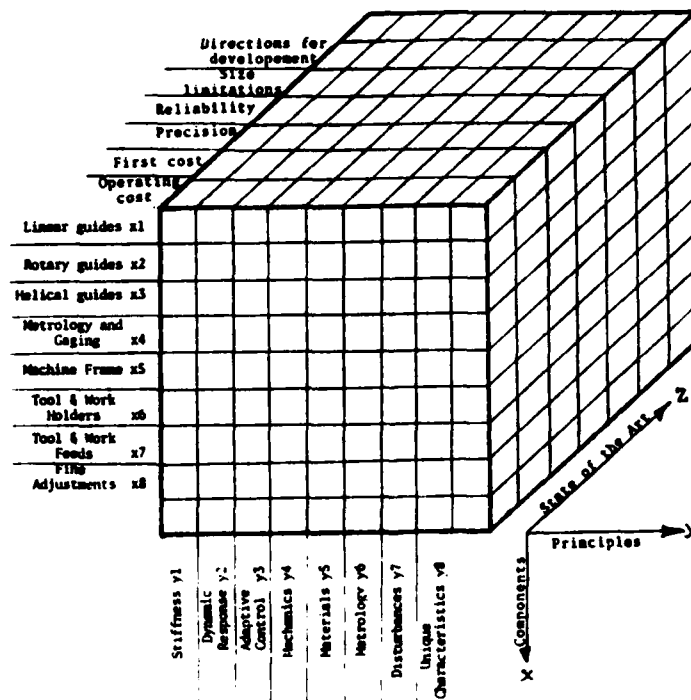


Fig. P.2 - Topics & Contents Matrix for Precision Engineering Design Monographs

TABLE OF CONTENTS

	Subpage	Page
PREFACE		iii
List of Tables		ix
List of Figures		x
CHAPTER I - INTRODUCTION	I.1	1
A Sense of Precision	I.1	1
A Modeling Language & Symbols	I.3	3
Additional Field Mechanics Symbols & Formats	I.13	13
Notational System	I.14	14
Coordinate Transformation	I.17	17
APPENDIX A1: Modeling Aids	A1.1	23
CHAPTER II - GUIDEWAYS	II.1	31
Components of Kinematic (Rigid Body) Errors	II.1	31
Shapes and Precision of Linear Guideways	II.7	37
Achieving Geometric Accuracy	II.10	40
Geometric Calibration of Precision Mechanical Systems	II.12	42
II. References	II.17	47
CHAPTER III - FRICTION OF THIN FILM SLIDEWAYS	III.1	48
Adhesion Mechanics of Friction	III.5	52
Bowden-Tabor First Analytical Approximations	III.6	53
Combined Stress Model, Junction Growth of Surface Effects	III.7	54
A Refinement to the Adhesion Theory	III.8	55
Inorganic Solid Lubricants	III.10	57
Organic Solid Lubricants	III.12	59
Boundary Lubrication, Fig. III.2b	III.14	61
Summary	III.20	67

	Subpage	Page
III. References	III.20	67
APPENDIX AIII Thermal Bowing	AIII.1	69
 CHAPTER IV THICK-FLUID FILM LUBRICATION.....	IV.1	71
Generalized Reynolds Equation	IV.2	72
Externally Pressurized Guideway (The Hydrostatic Bearing)	IV.6	76
Mechanics, Elementary Hydrostatic Bearing	IV.8	78
Lifting Capacity of Hydrostatic Bearings	IV.10	80
Flow Rate Through the Bearing	IV.12	82
Static Stiffness k_s of Linearly Sliding Hydrostatic Bearing.....	IV.13	83
Quantitative Performance of a Sample EX.P Bearing.....	IV.18	88
Lateral Guidance & Bidirectional Bearing Performance	IV.20	90
Pitching & Yawing Restraint.....	IV.22	92
Adaptive Control of Hydrostatic Slideways.....	IV.24	94
IV. References	IV.27	97
APPENDIX AIV.1	AIV.1,1	98
Reduction of Navier Stokes Equations.....	AIV.1,1	98
Simplification by Orders of Magnitude Deletions	AIV.1,3	100
Derivation of The Reynolds Equations for Thin Film Lubricants	AIV.1,5	102
APPENDIX AIV.2.....	AIV.2,1	106
Pressure Distribution in Clearance Zone 4-5	AIV.2,1	106
Flow Rate Q_{4-5} Through the Field 4-5.....	AIV.2,3	108
Coefficient of Friction $f = D/W$	AIV.2,4	109
Quantitative Evaluation of a Hydrostatic Bearing.....	AIV.2,6	111
Appropriate Resistor	AIV.2,8	113
APPENDIX AIV.3.....	AIV.3,1	116
Linear Triangular Finite Element Method.....	AIV.3,1	116
The Linear-Triangular Element.....	AIV.3,3	118
Equivalent Lumped Convectors For Element i,j,k.....	AIV.3,8	123
Equivalent Lumped Flow Sources For Element i,j,k.....	AIV.3,10	125
Conservation of Flows Into Central Node of a Cluster	AIV.3,11	126
 CHAPTER V AEROSTATIC BEARING GUIDEWAYS.....	V.1	129
Comparison of Mass Flows \mathcal{M} , Gas vs Oil.....	V.3	131
Friction Comparison & Lifting Capacity.....	V.5	133
Pneumatic Hammer Instability	V.6	134
Perturbation of Mass Flow \mathcal{M}	V.6	134
Stabilizing the EX.P. Gas Bearing with R-C Members.....	V.12	140

	Subpage	Page
Precision Levels of Aerostatic Linear Guideways	V.16	144
High Precision Positioning Straight Line Positioning	V.17	145
V. References	V.23	151
APPENDIX AV	AV.1	152
Derivation of Flow Perturbations	AV.1	152
Derivation of Capacitance Coefficient C_{3-}	AV.5	156
APPENDIX VI		157

LIST OF TABLES

Table	Page
I Specific Through & Across Variables	4
II Engineering Sciences, Constitutive Laws.....	6
III Engineering Sciences - Conservation - Compatibility.....	7
A.Ia Basic Electrical Elements.....	26
A.Ib Basic Mechanical Elements.....	27
A.Ic Basic Fluid Elements.....	28
A.Id Basic Heat Transfer Elements.....	29
II.1 Relative Potentials for the Minimization of Error Sources	39
III.1 Surfaces & Lubricants vs f.....	66
II Performance Characteristics by Restrictor, R_{2-3} Types	88
V Measured Position Errors	146

LIST OF FIGURES

Figure	Page
P.1 Achievable Machining Accuracy.....	iii
P.2 Topics & Contents Matrix for Precision Engineering Design Monographs....	v
I.1 Dimensional Spectrum of Phenomena.....	2
I.2 Representation of Potential, Dissipative & Kinetic Energy Elements.....	9
I.3 Coordinate Systems I & II Describing Position of D.....	18
AI.1 Analogue & Dualities Wheel.....	30
II.1 Machine with Composite Guidance By Components.....	32
II.2 X-Y Plane Guidance Errors Between Tables I & II of Fig. II.1.....	33
II.3 Error Vectors of Table II Relative to Table I.....	34
II.4 Types of Linear Sliding Guides.....	38
II.5 a. Box Straight Edge b. Lapping a "v" Guideway	38
II.6 Guideway With Precision Rails	42
II.7 Machine of Fig. II.1 With Calibration Stations.....	44
III.1 Classes of Lubrication by Interface Structures.....	50
III.2 Effect of Choice of Scales on Comprehension of Surface Roughness	51
III.3 Asperity Contact Geometry.....	51
III.4 Long Molecule Support of Sliding Bodies.....	63
AIII.1 Geometry of Curved Path	69
IV.1 Basic Hydrostatic Slideway	77
IV.2 Circular Hydrostatic Bearing	79
IV.3a Orifice Restrictor	85
IV.3b Inherently Compensated (Proximity) Restrictor.....	85
IV.4 Hydrostatic Guideway Two Dimensional Translatory Restraint	90
IV.5 Mechanics of Pitching Restraint	93
IV.6 Adaptive Control of Hydrostatic Guideway. Ref. 6.	96
AIV.1 Element of Thick Film Between Moving Surfaces I & II	105
AIV.2-1 Thin Bearing Film Kinematics	110
AIV.3a Finite Difference Model.....	117
AIV.3b Linear Triangular Finite Element.....	118
AIV.3c Linear Potential Field.....	120
AIV.3d Plan View Model ci With Power G_i	120
AIV.3e Network Representation of Convection Equation E.AIV.3e	124
AIV.3f Linear Element Network Representing E.AIV.3a on i,j,k	125
AIV.3g Node g Centered Cluster of Elements	128
V.1 Schematic of Aerostatic Bearing with an Added R-C Element Ref. 4	141
V.2 Zones of Stable and Unstable Operation. From Ref. 4.	144
V.3 Aerostatic Linear Slide (Hitachi Seiko) Performance. Ref. 6.	145
V.4a High Precision Straight Motion System. Ref. 7.	149
V.4b Pads, Servo Valves & Block Assembly. Ref. 7.....	149
V.5 Load, Clearance and Supply Pressure of Pads. Ref. 7.	150

I. INTRODUCTION

A SENSE OF PRECISION

The engineering design of precision machinery and devices in this monograph dwells on the practice and the analytical tools necessary for the development of mechanical systems whose performances are defined by their ability to control and measure dimensional phenomena in orders of less than two microns ($2\mu\text{m}$). It might be surmised that the intuitive comprehension of minute dimensions or displacements by the man in the street falls off rather completely at resolutions below 1mm. For most engineers the limits of intuitive comprehension of smallness falls off at about 0.1mm. In this series the focus is on minuteness less than one micron (.001mm). The "Dimensional Spectrum of Phenomena", Fig. I.1 exhibits the typical dimensions, tolerances etc. of various items of engineering and scientific phenomena. Graphical juxtapositionings such as this help the practitioner appreciate the magnitudes of accomplishment needed to achieve various levels of precision. While proficiency in engineering analysis and experimentation are paramount to the creation of successful new designs and their development, one can not overlook the power of subliminal information and patterns in the engineering of precision systems. More often than we realize problem definition, which precedes analytics, is initiated by a subconscious ordering of past observations and associations of clues. This subliminal process is variously identified with such terms as "practical experience", "insight", "creativity",

X-Rays | **Ultraviolet** | **VL** | **Infrared** | **Wave Lengths** | **Microwaves** | **Super Hi** | **Radio Waves** | **VHF**

SURFACE ROUGHNESS: **DEPTHS** **WAVE LENGTHS**

10⁻¹ **10⁻²** **10⁻³** **10⁻⁴** **10⁻⁵** **10⁻⁶** **10⁻⁷** **10⁻⁸** **10⁻⁹** **10⁻¹⁰** **10⁻¹¹** **10⁻¹²** **10⁻¹³** **10⁻¹⁴** **10⁻¹⁵** **10⁻¹⁶** **10⁻¹⁷** **10⁻¹⁸** **10⁻¹⁹** **10⁻²⁰** **10⁻²¹** **10⁻²²** **10⁻²³** **10⁻²⁴** **10⁻²⁵** **10⁻²⁶** **10⁻²⁷** **10⁻²⁸** **10⁻²⁹** **10⁻³⁰** **10⁻³¹** **10⁻³²** **10⁻³³** **10⁻³⁴** **10⁻³⁵** **10⁻³⁶** **10⁻³⁷** **10⁻³⁸** **10⁻³⁹** **10⁻⁴⁰** **10⁻⁴¹** **10⁻⁴²** **10⁻⁴³** **10⁻⁴⁴** **10⁻⁴⁵** **10⁻⁴⁶** **10⁻⁴⁷** **10⁻⁴⁸** **10⁻⁴⁹** **10⁻⁵⁰** **10⁻⁵¹** **10⁻⁵²** **10⁻⁵³** **10⁻⁵⁴** **10⁻⁵⁵** **10⁻⁵⁶** **10⁻⁵⁷** **10⁻⁵⁸** **10⁻⁵⁹** **10⁻⁶⁰** **10⁻⁶¹** **10⁻⁶²** **10⁻⁶³** **10⁻⁶⁴** **10⁻⁶⁵** **10⁻⁶⁶** **10⁻⁶⁷** **10⁻⁶⁸** **10⁻⁶⁹** **10⁻⁷⁰** **10⁻⁷¹** **10⁻⁷²** **10⁻⁷³** **10⁻⁷⁴** **10⁻⁷⁵** **10⁻⁷⁶** **10⁻⁷⁷** **10⁻⁷⁸** **10⁻⁷⁹** **10⁻⁸⁰** **10⁻⁸¹** **10⁻⁸²** **10⁻⁸³** **10⁻⁸⁴** **10⁻⁸⁵** **10⁻⁸⁶** **10⁻⁸⁷** **10⁻⁸⁸** **10⁻⁸⁹** **10⁻⁹⁰** **10⁻⁹¹** **10⁻⁹²** **10⁻⁹³** **10⁻⁹⁴** **10⁻⁹⁵** **10⁻⁹⁶** **10⁻⁹⁷** **10⁻⁹⁸** **10⁻⁹⁹** **10⁻¹⁰⁰** **10⁻¹⁰¹** **10⁻¹⁰²** **10⁻¹⁰³** **10⁻¹⁰⁴** **10⁻¹⁰⁵** **10⁻¹⁰⁶** **10⁻¹⁰⁷** **10⁻¹⁰⁸** **10⁻¹⁰⁹** **10⁻¹¹⁰** **10⁻¹¹¹** **10⁻¹¹²** **10⁻¹¹³** **10⁻¹¹⁴** **10⁻¹¹⁵** **10⁻¹¹⁶** **10⁻¹¹⁷** **10⁻¹¹⁸** **10⁻¹¹⁹** **10⁻¹²⁰** **10⁻¹²¹** **10⁻¹²²** **10⁻¹²³** **10⁻¹²⁴** **10⁻¹²⁵** **10⁻¹²⁶** **10⁻¹²⁷** **10⁻¹²⁸** **10⁻¹²⁹** **10⁻¹³⁰** **10⁻¹³¹** **10⁻¹³²** **10⁻¹³³** **10⁻¹³⁴** **10⁻¹³⁵** **10⁻¹³⁶** **10⁻¹³⁷** **10⁻¹³⁸** **10⁻¹³⁹** **10⁻¹⁴⁰** **10⁻¹⁴¹** **10⁻¹⁴²** **10⁻¹⁴³** **10⁻¹⁴⁴** **10⁻¹⁴⁵** **10⁻¹⁴⁶** **10⁻¹⁴⁷** **10⁻¹⁴⁸** **10⁻¹⁴⁹** **10⁻¹⁵⁰** **10⁻¹⁵¹** **10⁻¹⁵²** **10⁻¹⁵³** **10⁻¹⁵⁴** **10⁻¹⁵⁵** **10⁻¹⁵⁶** **10⁻¹⁵⁷** **10⁻¹⁵⁸** **10⁻¹⁵⁹** **10⁻¹⁶⁰** **10⁻¹⁶¹** **10⁻¹⁶²** **10⁻¹⁶³** **10⁻¹⁶⁴** **10⁻¹⁶⁵** **10⁻¹⁶⁶** **10⁻¹⁶⁷** **10⁻¹⁶⁸** **10⁻¹⁶⁹** **10⁻¹⁷⁰** **10⁻¹⁷¹** **10⁻¹⁷²** **10⁻¹⁷³** **10⁻¹⁷⁴** **10⁻¹⁷⁵** **10⁻¹⁷⁶** **10⁻¹⁷⁷** **10⁻¹⁷⁸** **10⁻¹⁷⁹** **10⁻¹⁸⁰** **10⁻¹⁸¹** **10⁻¹⁸²** **10⁻¹⁸³** **10⁻¹⁸⁴** **10⁻¹⁸⁵** **10⁻¹⁸⁶** **10⁻¹⁸⁷** **10⁻¹⁸⁸** **10⁻¹⁸⁹** **10⁻¹⁹⁰** **10⁻¹⁹¹** **10⁻¹⁹²** **10⁻¹⁹³** **10⁻¹⁹⁴** **10⁻¹⁹⁵** **10⁻¹⁹⁶** **10⁻¹⁹⁷** **10⁻¹⁹⁸** **10⁻¹⁹⁹** **10⁻²⁰⁰** **10⁻²⁰¹** **10⁻²⁰²** **10⁻²⁰³** **10⁻²⁰⁴** **10⁻²⁰⁵** **10⁻²⁰⁶** **10⁻²⁰⁷** **10⁻²⁰⁸** **10⁻²⁰⁹** **10⁻²¹⁰** **10⁻²¹¹** **10⁻²¹²** **10⁻²¹³** **10⁻²¹⁴** **10⁻²¹⁵** **10⁻²¹⁶** **10⁻²¹⁷** **10⁻²¹⁸** **10⁻²¹⁹**

Figure 1.1 Dimensional Spectrum of Phenomena

A MODELING LANGUAGE & SYMBOLS

Much of the analytical prediction of machine component and systems behavior is based on such engineering sciences as heat transfer, fluid mechanics, elasticity, dynamics, electrical and magnetic field theory. Each of these in its evolution developed its own languages and uniquely named laws, principles and property states. The specialist in any one of the fields by virtue of single minded activity is quite comfortable with specific names. On the other hand project, design and the administrative engineers must perform across lines of disciplines and need a more universal language to facilitate understanding and accurate communication. Fortunately, despite differing vocabularies, analogues can be established among the engineering sciences so that a unifying language and a mathematical symbology can be generated. The analytics of these monographs will be presented in one such language the principles of which are herewith described.

Generic Variables

Common to the engineering sciences, cited above, is the concept of a Through Variable. This is usually a basic extensive quantity, such as mass, energy, charge, etc. which is being transmitted along a path from one point or state to another point or state. In this monograph the generic symbol for a Through Variable is $q_{\alpha,\beta}$.

Definition: Let $q_{\alpha,\beta}$ be a vector or scalar quantity defining the transmission or flow rate of a Through Variable from point or state α towards point or state β . Because the transmission is from the prior subscript towards

the posterior subscript the sequence of subscripts is critical. It follows that:

$$q_{\beta,\alpha} = -q_{\alpha,\beta}$$

The Through Variable above is driven from α towards β by an Across Variable typified by such intensive quantities as temperature, pressure, voltage etc.. The generic Across Variable will be symbolized as $e_{\alpha/\beta}$.

Definition: Let $e_{\alpha/\beta}$ be a vector or scalar value of a generic Across Variable at α less the value at β . It follows that:

$$e_{\beta/\alpha} = -e_{\alpha/\beta}$$

Some specific examples of Through and Across Variables are illustrated by TABLE

I.

TABLE I

Engineering Science	Through Variable, q	Across Variable, e
Heat Transfer	Heat Flow; Q	Temperature θ
Fluid Mechanics	Mass Flow; M	Pressure p
Electric Fields	Current; I	Volts v
Mechanics	Force; F	Displacement s

Constitutive Law

Through and Across Variables are related by Constitutive Laws perhaps the most familiar example is Ohm's Law. The generic form of these laws is;

$$q_{\alpha,\beta} = K_{\alpha-\beta} e_{\alpha/\beta} \quad \text{EI.1}$$

Proportionality term $K_{\alpha-\beta}$ is the average property of the media or element connecting points α and β hence these subscripts apply to K as well as to q and e . In most engineering problems it may be assumed that proportionately K is approximately passive and constant such as an electrical conductance or a spring constant. In such cases the order of α and β subscripture of K is inconsequential. Recall that on the other hand the order of the subscripts when written as α,β and α/β is critical to polarity. Attention is drawn to the fact that while α and β appear in all three quantities of EI.1 there are distinctly different separating punctuations, $(.)$ $(/)$ and $(-)$, for the three distinctly different quantities shown. More on this a little later but at this point it can be stated that because of the definitions given above there is the happy consequence that if the prior subscripts and posterior subscripts appear in the same order on both sides of the equation, polarity for the equation is automatically correct. TABLE II illustrates some specific constitutive laws.

TABLE II

Engineering Science	Constitutive Law	$q_{a,j} = K_{a-j} e_{a,j}$
Heat transfer	Fourier's	$Q_{a,j} = K_{a-j} T_{a,j}$
Fluid Mechanics	D'Arcy's	$M_{a,j} = K_{a-j} P_{a,j}$
Electric Fields	Ohm's	$I_{a,j} = K_{a-j} E_{a,j}$
Elasticity	Hook's	$F_{a,j} = K_{a-j} S_{a,j}$

Conservation and Compatibility Principles

Finally two other principles, Conservation and Compatibility are needed to model the problem into differential equations. The two principles invoke the effect of geometry of related points on the derived equations.

Definition: Conservation Principle is a summation law for all Through Variables transmitted from surrounding points towards a common vertex. The generic form of this summation in terms of the subscripts defined above is:

$$\sum_{k=1}^n q_{i,j} = q_{1,j} + q_{2,j} + q_{k,j} + \cdots q_{n-1,j} + q_{n,j} = 0 \quad \text{EI.2}$$

Correct polarity is preserved if the points 1 through n surrounding j appear as the prior subscripts while the vertex j appears as the posterior subscript in all terms. Kirchoff's Current law is a familiar example of a constitutive law.

Definition: Compatibility Principle is a summation law for Across Variables relating all points connected in a chain. Kirchoff's Voltage law is a familiar example.

The generic form of this summation is:

$$e_{n/a} = e_{n/1} + e_{1/2} + e_{2/3} + \cdots + e_{n/n} = 0 \quad \text{EI.3a}$$

or

$$e_{n/b} = e_{n/1} + e_{1/2} + e_{2/3} + \cdots + e_{n/n} \quad \text{EI.3b}$$

In the form of I.3b the compatibility principle serves to generate a new value $e_{n/b}$ from the known values $e_{n/1}$, etc. in a connected chain. TABLE III illustrates some specific examples and names of these two principles.

TABLE III

Engineering Science	Conservation Principle	Compatibility Principle
Heat transfer	Conservation of energy	No name
Fluid mechanics	Conservation of momentum	No name
Electric fields	Kirchoff's Current Law	Kirchoff's Voltage Law
Dynamics	Conservation of momentum	Polygon of Velocities

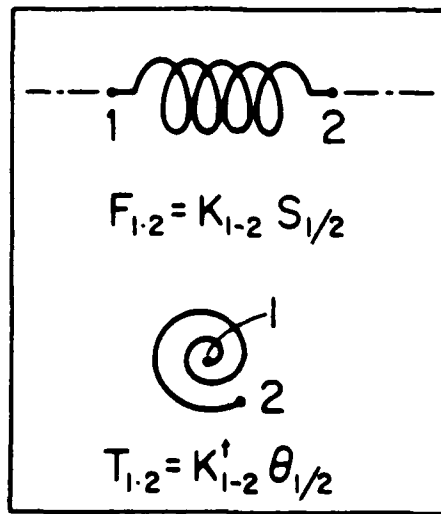
The algorithm of subscripts in EI.2 is entirely different from that of EI.3. Because of this it is imperative that, while an adjunct pair of Through and Across Variables have the same subscripts, the Through quantities have the dot subscript separators (.) while the Across quantities have the slash subscript separators (/). Equation EI.2 having the confluent algorithm of Through Variables must contain only terms with a (.) separator. Equation EI.3 on the other hand deals only with Across Variables. It has a zig-zag algorithm to its subscripts and must contain only terms with a (/) separator.

Implicit Subscript (*)

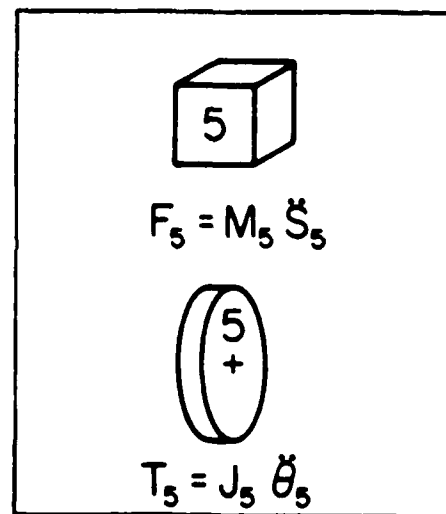
In addition to the physically apparent α, β reference to nodes, terminals or points in the field of a machine component, the language of modeling requires the recognition of a particular point or state not explicitly apparent. That is an absolute reference point henceforth identified by (*). Electrical sciences make explicit use of such an absolute datum point, it being "ground" and identified by the graphic symbol (). Curiously the other engineering sciences fail to provide a symbol for an absolute datum even though the concept prevades the language of the sciences by references to absolute temperatures, coordinates etc. By establishing an implicit terminal (*) to represent an absolute datum, ambiguity is diminished and consistency in notation is served. The lamentable omission of a graphical symbol for a ground or absolute datum in mechanical sciences makes itself felt even in the most rudimentary models such as the following observation.

The Absolute Point of Reference *

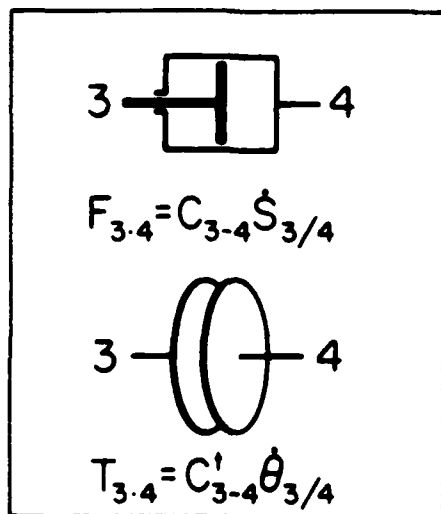
There are three fundamental structural properties to every machine component. These are flexibility (which implies an ability to store potential energy), damping (the agent of energy dissipation) and mass the basis of kinetic energy. A flexible member can be symbolized by Fig. 1.2a that is a spring with ends 1, 2. There is a corresponding constitutive equation with the ends 1, 2 playing the roles that α, β demonstrated in the introductory discussions and E1.1. The damping role of an element can be symbolized as in Fig. 1.2b by an



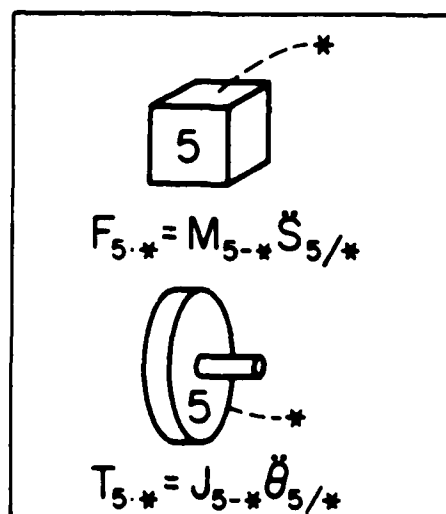
(a)



(c)



(b)



(d)

Fig. I.2 Symbolic Representation of Potential Dissipative and Kinetic Energy Elements.

elementary dash pot with terminals 3, 4 and a constitutive equation where force where force and velocity effects are in equilibrium. In both cases there is a consistency of subscripts based on reference points on both sides of the equation. Polarity is rigorously self defined by the order of these subscripts. Consider now the case of a simple mass as an inertial element. Fig. I.2c is the conventional graphical representation and the familiar constitutive equation. There is only a single reference point on this conventional representation, that is point 5, which might be a point on the surface of the mass at which an external mechanical force acts. The related constitutive equation would show only that one subscript which not only fails to show the double subscript consistency with the other two types of structural elements but even makes the nature of the acceleration ambiguous. Fig. I.2d is the suggested symbolic notation. An implicit connection of the mass to (*) is indicated. This immediately suggests that acceleration be rewritten as $\ddot{S}_{5/*}$ and so establish the acceleration as an absolute quantity. As such the symbol (*) evokes the Newtonian inertial frame of reference as a rigorous analysis should. Taking a cue from the first two examples of elements it follows that mass would be identified by two subscripts i.e. $M_{5/*}$. Subscript * now reaffirms that the property, mass, of the envelope 5 is indeed an absolute quantity invariant throughout the universe. In this way the r.h.s. of the constitutive equation is established. The l.h.s. is made to assume the two subscripts in the sequence established on the r.h.s. by the acceleration term. Even this "forcing" of subscripts to conform results in a useful interpretation. Consider the inverse force F_{*5} . By the basic definitions and the role of subscripts in a through variable, F_{*5} would be interpreted as the force transmitted from the reference point

(*) to the body (5). This interpretation squares up perfectly with the intent of the vaguely defined term "force of inertia". Finally this format of subscripts reaffirms the equivalent roles of a Newtonian equation and a corresponding D'Alembert equation. Consider four bodies 1, 2, 3, 4 exerting forces on body 5. Newton's equation becomes

$$F_{1.5} + F_{2.5} + F_{3.5} = m_{5,*} \ddot{S}_{5,*} = F_{5,*} = -F_{*,5}$$

This can be rearranged as

$$F_{1.5} + F_{2.5} + F_{3.5} + F_{4.5} + F_{*,5} = 0$$

This equation is D'Alembert's form of the dynamic problem wherein the $F_{*,5}$ plays the role of an "inertia force" applied to the system of bodies. The reader will note that the D'Alembert form assumes exactly the general format of equation E1.2. Not only does (*) serve in solid mechanics and electric theory but it also remedies an omission in thermal and fluid mechanics. In both these disciplines absolute quantities (such as temperature and pressure) are verbalized but never symbolized differently from relative quantities. An absolute reference state (*) permits one to express absolute pressure at state (1) as $P_{1,*}$ while gage pressure would be $P_{1/a}$ wherein subscript (a) identifies the atmosphere as a reference state. Similarly absolute temperature at state 1 could be identified as $T_{1,*}$ while $T_{1/f}$ might be the temperature on a Fahrenheit scale. Extended tables of Through, Across Variables and Constitutive laws are given in Appendix I.

Influence Coefficients

The above discussions dwell on the relationships between adjacent terminals in a field. Complementing this tool of analytics is the mutual influence concept for modeling linear systems. In this concept a variable at a particular point in a field is said to be influenced by a combination of variables at remote points in the field, that is:

$$e_{m/o} = G_{m,1}e_{1/o} + G_{m,2}e_{2/o} + G_{m,3}e_{3/o} + G_{m,n}e_{n/o} \quad \text{El.5a}$$

or

$$e_{m/o} = \sum_{j=1}^N G_{m,j} e_{j/o} \quad \text{El.5b}$$

Definition: $G_{m,j}$ Is an influence coefficient defining the effect on a quantity at location m by a quantity at location j .

$e_{j/o}$: The value of an Across variable at point j relative to a common reference point o .

Equation El.5a is still one more form of summation useful to modeling. It usually appears in the more ambiguous form $e_m = \sum G_{m,j} e_j$ in the literature. Coefficient $G_{m,j}$ is another doubly subscripted property but now with a $(,)$ subscript separator. Like the $(.)$ and $(/)$ subscripted variables the order of the subscripts in this case is consequential. The influence coefficients themselves must be generated from solutions of equations modeled by the constitutive laws described earlier or from some extremum

principle. Across and Through variables can also be expressed as the mutual influence on each other i.e.,

$$e_{m/o} = \sum_j G_{m,j} q_{j,o} \quad \text{or} \quad q_{s,o} = \sum_j K_{s,j} e_{j/o}$$

An array of such simultaneous equations can be expressed succinctly in matrix form

$$\{e_{m/o}\} = [G_{m,j}] \{q_{j,o}\} \quad \{q_{s,o}\} = [K_{s,j}] \{e_{j/o}\} \quad \text{EI.6}$$

The similarity of the matrix form and the constitutive equations illustrated in TABLE II is a telling and convenient modeling tool. The similarity of forms is usually not recognized because the datum subscript (o) is conventionally dropped in the matrix format as in EI.7.

$$\{e_m\} = [G_{m,j}] \{q_j\} \quad \text{EI.7}$$

ADDITIONAL FIELD MECHANICS SYMBOLS AND FORMATS

In the discussions above the subscripts took their identities from specific points in bodies. Considerations of machine kinematics, metrology, dynamics and even thermodynamic systems will call for additional indentifiers such as bodies, coordinate systems, states etc.. The following is a glossary of useful expressions and their shorthand forms used in the text that follows. Once this nomenclature is mastered it will serve to reduce ambiguity in verbalized statements and mathematical expressions. The notation suggested earlier and in the glossary below will also expedite the creation

of algorithmic formats which help in developing mathematical expressions.

NOTATIONAL SYSTEM

Numerals 0, 1, 2, 3, ... or letters a, b, c, ... will identify points on bodies or thermodynamic states.

Roman numerals, I, II, III.... and letters A, B, C, etc. will represent individual bodies and coordinate systems or thermodynamic media.

$\bar{8}\bar{7} = \bar{R}(8/7)$. A position space vector of point 8 relative to point 7. For purposes of kinematic analysis the prefix R is superfluous, since *positioning is the nature of the subject*, hence it will be dropped. On the other hand when thermodynamic analysis is involved a prefix describing the property will be retained ie $h(8/7) =$ Value of enthalpy at state 8 relative to its value at state 7.

$(\bar{8}\bar{7})_{II} = \bar{8}\bar{7}$ expressed in coordinate system II. If thermodynamic analysis is involved, II would identify the medium possessing the property whose change is being described.

$X_{II}, Y_{II}, Z_{II} = X, Y, Z$ components of a vector expressed in coordinate system II.

$\begin{bmatrix} X_{II} \\ Y_{II} \\ Z_{II} \end{bmatrix}_{8/7} =$ Matrix form of $(\bar{8}\bar{7})_{II}$

- $(\bar{3}/\bar{2}) =$ Velocity vector of point 3 relative to point 2. If a system is static the same form will be used for virtual displacements of 3 relative to 2. It will also be used to represent static errors in the position of 3 relative to 2. The context of the problem should be the guide to choice of interpretation,
- $|\bar{3}/\bar{2}| =$ The length of vector $(\bar{3}/\bar{2})$.
- $|\dot{\bar{3}}/\bar{2}| =$ Rate of change of length of vector joining point 3 to point 2. This is a scalar quantity. If system is static the same symbol will be use to represent a virtual change in the length of $(\bar{3}/\bar{2})$. The same notation will also be used to represent an error in length $|\delta \bar{3}/\bar{2}|$.
- $(\bar{3}/\bar{2}) =$ Unit vector parallel to $(\bar{3}/\bar{2})$.
- $\hat{X}_{II}, \hat{Y}_{II}, \hat{Z}_{II} =$ Unit vectors of coordinate system II.
- $n(III, II) =$ Point n in space, such as a pin connector, shared by systems III and II.
- $(\ddot{\bar{3}}/\bar{2}) =$ Acceleration vector, point 3 relative to point 2.
- $* =$ Absolute reference point. Also ground.
- $(\ddot{\bar{3}}^*) =$ Absolute acceleration of point 3.

Angles and angular motion will be represented by Greek letters and the identity of the bodies separated by the angle.

$\bar{\omega}(II/*) =$ Absolute angular velocity of body II or angular velocity of body II relative to a nonrotating body. This notation will also be used to represent the the absolute virtual angular displacement of a static system. Alternatively this symbol will be used to represent absolute angular errors in the position of body II.

$\bar{\omega}(II/III) =$ Related to above but non-absolute motion is implied. Specifically it is the angular velocity (or virtual displacement) of system II relative to system III. It follows that: $\bar{\omega}(II/III) = \bar{\omega}(II/*) - \bar{\omega}(III/*)$.

$\dot{\alpha}_{II}, \beta_{II}, \dot{\gamma}_{II} =$ X, Y, Z components of $\bar{\omega}(II/*)$.
Note $\beta_{II} = \bar{\omega}_{(II/*)}$. \hat{Y}_{II} .

$\theta(X_I/Z_{II}) =$ Angular vector position of axis X_I relative to axis Z_{II} . Illustrated on Fig. I.3.

$\dot{\theta}(X_I/Z_{II}) =$ Time rate of changes of $\theta(X_I/Z_{II})$. Alternatively virtual change or error in $\theta(X_I/Z_{II})$.

$C(q,s) =$ Influence coefficient of a property applied to point(s) on the property created at point (q).

$[C_{j,k}] =$ An array of many influence coefficients, such as $C(q,s)$, in a matrix form.

COORDINATE TRANSFORMATION

Perhaps the most frequent application of E1.6 and E1.7 in machine tool and precision engineering is for coordinate transfers from one subassembly to another. This equation appears again as a basic of the finite element method of analysis. To illustrate the application of modeling forms described in this chapter consider the derivation of the familiar coordinate transfer matrix. As an example assume that one is given a point P in the spatial coordinates of system I, Fig. I.3, and it is desired to restate the position of P in terms of system II. Furthermore the relationship of the two space systems is given in the form of the rotations of the axes of II relative to the axes of I (such as $\theta(X_{II}/Y_I)$ of Fig. I.3. Also the position of the origin (0_{II}) of system II relative to the origin (0_I) of system I is known. That is the vector $\bar{0}_{II}/\bar{0}_I$ is known. However the coordinates of this vector are given in terms of system II.

Referring to Fig. I.3, the rules for subscripture of across variables, E1.3b and the **NOTATIONAL SYSTEM** the statements above are converted to the following symbolic forms.

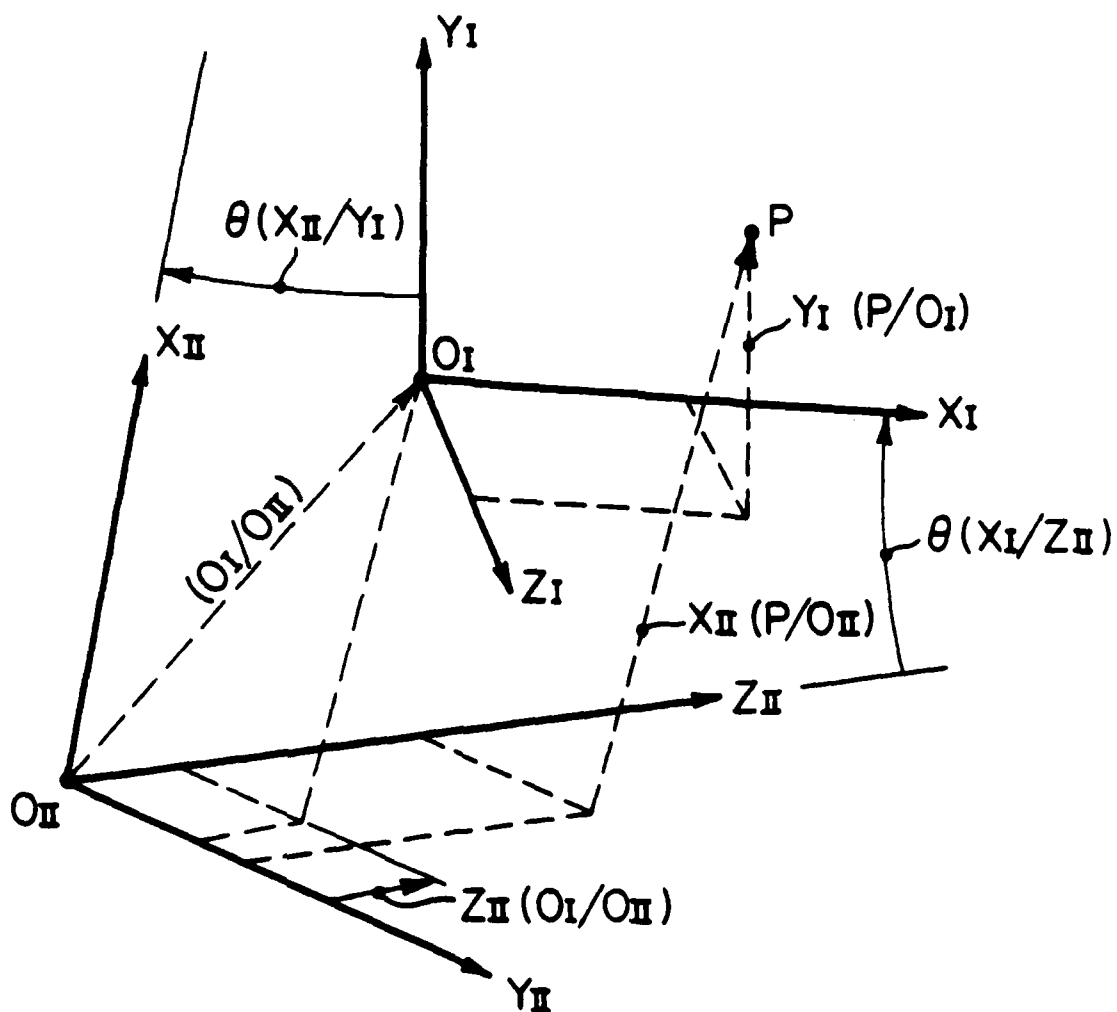


Fig. I.3 Coordinate Systems I and II Describing Position of P.
Relative Position Expressions Illustrated.

GIVEN: $\begin{bmatrix} X_I \\ Y_I \\ Z_I \end{bmatrix}_{P/O_I}$... The vector \bar{P}/\bar{O}_I in system I coordinates

$\begin{bmatrix} X_{II} \\ Y_{II} \\ Z_{II} \end{bmatrix}_{\bar{O}_{II}/O_I}$... The vector \bar{O}_{II}/O_I describing the position of origin of system II relative to the origin of system I. It is expressed in system II coordinates.

$\begin{bmatrix} \theta(X_{II}/X_I) \\ \theta(Y_{II}/Y_I) \\ \theta(Z_{II}/Z_I) \end{bmatrix}$... The angles that the coordinates of system II make relative to the coordinates of system I.

DESIRED: \bar{P}/\bar{O}_{II} that is $\begin{bmatrix} X_{II} \\ Y_{II} \\ Z_{II} \end{bmatrix}_{P/O_{II}}$

$$\text{SOLUTION: } \bar{P}/\bar{O}_{II} = \bar{P}/\bar{O}_I + \bar{O}_I/\bar{O}_{II} = \bar{P}/\bar{O}_I - \bar{O}_{II}/\bar{O}_I \quad \text{El.8}$$

that is:

$$\begin{bmatrix} X_{II} \\ Y_{II} \\ Z_{II} \end{bmatrix}_{P/O_{II}} = \begin{bmatrix} X_{II} \\ Y_{II} \\ Z_{II} \end{bmatrix}_{P/O_I} - \begin{bmatrix} X_{II} \\ Y_{II} \\ Z_{II} \end{bmatrix}_{\bar{O}_{II}/O_I} \quad \text{El.9}$$

Matrix El.9 is a more complete expression of El.8 since X_{II} , Y_{II} , Z_{II} emphasize the requirement that the equation be written in system II coordinates exclusively. Meanwhile the subscripts at the base of the column matrix inform one that the terms within the matrix deal with the relative distances between the two points cited. For

the column on l.h.s. of EI.9, the footnote indicates that elements of the matrix are actually the coordinates of P relative to the origin O_{II} .

Part of the given data of this example appears as the last vector of EI.9. On the other hand the first vector on the r.h.s. of EI.9 is not among the given data. What is actually given is $\bar{P}\bar{O}_I$ in system I coordinates. The required vector can be synthesized by a coordinate transformation in the form of EI.7 which in this case becomes

$$\begin{bmatrix} X_{II} \\ Y_{II} \\ Z_{II} \end{bmatrix}_{P/O_I} = [C_{II,I}] \begin{bmatrix} X_I \\ Y_I \\ Z_I \end{bmatrix}_{P/O_I} \quad \text{EI.10}$$

A particular element of the matrix $[C_{II,I}]$, $C_{i,j}$, is the cosine of the angle that axis i of system II makes relative to axis j of system I. That is $C_{i,j} = \cos \theta(i/j)$. Fig. I.3 illustrates the physical meaning of some terms $\theta(i/j)$. For compactness the following notation will be used:

Let $C_{i/j} = \cos \theta (\text{axis } i \text{ relative to axis } j)$

Hence $C_{(X_I/Z_{II})} = \text{Cosine of the angle that axis } X_I \text{ makes relative to axis } Z_{II}.$

Similarly $S_{(X_I/Z_{II})} = \text{Sine of the angle that axis } X_I \text{ makes relative to axis } Z_{II}$

If the direction of the relative angular positions is given graphically such as $\theta(X_{II}, Y_I)$ of Fig. I.3 the prior subscript of $\theta(i/j)$ is the axis touched by the arrow of the arc vector. The posterior subscript is the axis touched by the tail of the arc vector.

From this it follows that $\theta(j/i) = -\theta(i/j)$. It is important that correct polarities are specified when dealing with sine and tangent functions. Hence the order of the subscripts is significant again as it was in the earlier discussion of slash subscripted quantities.

Using the short hand for the cosines of the planar angles above and, setting $C_{i,j} = C_{j/i}$ the transfer matrix becomes

$$[C_{II,I}] = \begin{bmatrix} C(X_{II}/X_I) & C(X_{II}/Y_I) & C(X_{II}/Z_I) \\ C(Y_{II}/X_I) & C(Y_{II}/Y_I) & C(Y_{II}/Z_I) \\ C(Z_{II}/X_I) & C(Z_{II}/Y_I) & C(Z_{II}/Z_I) \end{bmatrix} \quad \text{EI.11}$$

Substituting EI.10 into EI.9 yields EI.12a.

$$\begin{bmatrix} X_{II} \\ Y_{II} \\ Z_{II} \end{bmatrix}_{P/O_{II}} = [C_{II,I}] \begin{bmatrix} X_I \\ Y_I \\ Z_I \end{bmatrix}_{P/O_I} + \begin{bmatrix} -X_{II} \\ -Y_{II} \\ -Z_{II} \end{bmatrix}_{O_{II}/O_I} \quad \text{EI.12a}$$

The summation on the r.h.s. of EI.12a can be compacted to form the 4 x 4 coordinate transform of EI.12b.

$$\begin{bmatrix} 1 \\ X_{II} \\ Y_{II} \\ Z_{II} \end{bmatrix}_{P/O_{II}} = \begin{bmatrix} 1 & 0 & 0 & 0 \\ a & C(X_{II}/X_I) & C(X_{II}/Y_I) & C(X_{II}/Z_I) \\ b & C(Y_{II}/X_I) & C(Y_{II}/Y_I) & C(Y_{II}/Z_I) \\ c & C(Z_{II}/X_I) & C(Z_{II}/Y_I) & C(Z_{II}/Z_I) \end{bmatrix} \cdot \begin{bmatrix} 1 \\ X_I \\ Y_I \\ Z_I \end{bmatrix}_{O_{II}/O_I} \quad \text{EI.12b}$$

where: $\begin{bmatrix} a \\ b \\ c \end{bmatrix} = \begin{bmatrix} -X_{II} \\ -Y_{II} \\ -Z_{II} \end{bmatrix}_{O_{II}/O_I}$ The vector of the offsets of the coordinate origins relative to each other.

Infinitesimal rotations of vectors are common in kinematics and error analysis of machine systems. With infinitesimal rotations the transfer matrix EI.11 is simplified to EI.13.

$$\begin{bmatrix} C_{II,I} \end{bmatrix} = \begin{bmatrix} 1 & \dot{\gamma}(II/I) & -\beta(II/I) \\ -\dot{\gamma}(II/I) & 1 & \dot{\alpha}(II/I) \\ \beta(II/I) & -\dot{\alpha}(II/I) & 1 \end{bmatrix} \quad \text{EI.13}$$

APPENDIX: AI

"Modelling Aids and Analogues With Doubly Subscripted Terms"

Across type of variables are identified by a slash separating the two subscripts identifying terminals at the end of an element. Through type variables are identified by a dot separating these two subscripts. A dash separates the two subscripts of the property of the element between the two terminals TABLES A.I.a,b,c,d organizes some of the basic Across, Through variables and element properties. These are related by the appropriate constitutive laws for electrical, mechanical, fluid flow and heat transfer mechanics. The relationships of TABLES A.I are useful for modeling a class of problems generally expressed by the partial differential equation

$$\frac{\partial}{\partial x} \left(a \frac{\partial \Lambda}{\partial x} \right) + \frac{\partial}{\partial y} \left(b \frac{\partial \Lambda}{\partial y} \right) + \frac{\partial}{\partial z} \left(c \frac{\partial \Lambda}{\partial z} \right) + d \Lambda = e \frac{\partial \Lambda}{\partial t} + f(x,y,z)$$

where $\Lambda =$ a generic symbol for across variables.

When a continuum field is approximated by a network of discrete elements such as those from TABLE I, Finite Difference equations are directly generated without first having to go through the process of determining the exact partial differential equation of the process and then decomposing it into the finite difference form. The property terms such as K_{a-b} must be determined for the specific case. For instance for heat conduction through a thin plate made of a material with a thermal conductivity k (Btu/deg sec in) and a conducting area A_{a-b} between nodes a and b, conductance would be expressed as $K_{a-b} = \frac{kB.t}{L}$ for a cartesian net.

where: $B.t = A_{a-b}$, mean cross-sectional area of the conducting branch between a and b

$L = L_{(a-b)}$ the length of the branch connecting points a and b.

The same strategy can also lead to a LINEAR FINITE ELEMENT solution of field problems. This method and the determination of K_{a-b} for an approximating mesh of irregular triangles is described in Appendix A.IV.3.




TABLES A1.1 offer iconic symbols for the elements of the different disciplines. Iconic representation in network drawings enhance communication of concepts and has long successful history in electrical engineering. There seems to be no such standard of representation in a field such as heat transfer. TABLE A.I.d offers a possible set of iconics however it is more convenient to borrow the symbols from analogous electrical elements for depicting heat transfer nets. Fig. A.I.1 is an analog wheel which helps establish the relationships between different physical systems. Both mobility and classical analogs as well as dualities are depicted.

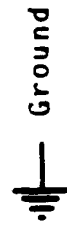
The mobility analogue (nodes go to nodes and loops go to loops) is generated by taking the symbols along a bold radial line of Fig. A.1 and transforming them into the symbols on another bold radial line. As an example a mechanical element connecting ends a and b has an electrical analog between electrical terminals a and b. The mechanical terms on the radial line at 11 o'clock are replaced with the electrical terms at 3 o'clock. Thus spring rate K is transformed to the reciprocal of inductance, $\frac{1}{L}$.

The classical analogue (nodes transform into loops and loops into nodes) is done by taking the symbols along a bold radial line of the analogue wheel and transforming

them into the symbols along a light radial line for the other physical system. As an example a mechanical element connecting points a and b has an analog in the form of an electrical element bordered by loops a and b. The mechanical elements on the bold radial line at 11 o'clock now have their analogues elements on the light radial line at 5 o'clock. Thus the mechanical spring with rate K is transformed to $\frac{1}{C}$, the reciprocal of electrical capacitance. The easy manipulation of analog and dualities is not only a very valuable tool for the numerical modeling of physical phenomena but it is also a useful aid in consultations with specialists outside one's particular expertise.

TABLE A.I.a Basic Electrical Elements

Element	Symbol	Constitutive Equation	Element Property
1 Inductor (Coil)		$\dot{i}_{a \cdot b} = \frac{1}{L_{a-b}} e_{a/b}$	$L = \text{inductance}$
2 Resistor		$\dot{i}_{a \cdot b} = \frac{1}{R_{a-b}} \dot{e}_{a/b}$	$R = \text{resistance}$
3 Capacitor		$\dot{i}_{a \cdot b} = C_{a-b} \ddot{e}_{a/b}$	$C = \text{capacitance}$




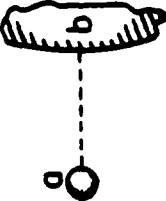
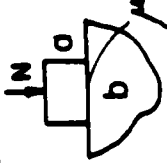


Ground

$\dot{A} = \dot{i}$ = rate of current change

$\Gamma = e$ = voltage.

TABLE A.1.b Basic Mechanical Elements

Element	Symbol	Constitutive Equation	Element Property
1 Spring		$F_{a \cdot b} = k_{a-b} x_{a/x}$	$k = \text{spring rate} \dots\dots\dots \text{lb/in}$
2 Damper		$F_{a \cdot b} = c_{a-b} \dot{x}_{a/b}$	$c = \text{damping constant} \dots\dots\dots \frac{\text{lb} \cdot \text{s}}{\text{in}}$
3 Mass		$F_{a \cdot *} = m_{a-x} \ddot{x}_{a/*}$	$m = \text{mass} \dots\dots\dots\dots\dots \frac{\text{lb} \cdot \text{s}^2}{\text{in}}$
4 Gravity Body Force		$F_{a \cdot b} = (mg)_{a-b} \hat{r}_{a/b}$	$mg = \text{weight in the field of } a-b \dots \text{lb}$
5 Coulomb Friction		$F_{a \cdot b} = (\mu N)_{a-b} \dot{x}_{a/b}$	$\mu = \text{coefficient of friction}$ $N = \text{normal load}$ $\dot{x} = \text{unit velocity vector}$



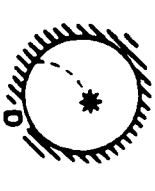
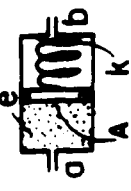
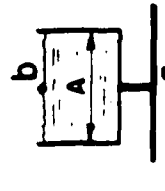
$\dot{A} = F = \text{force, lb.}$

$r = x = \text{displacement, in.}$

 Earth


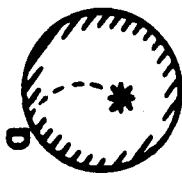
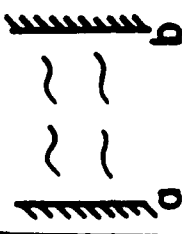
 Inertial datum

TABLE A.I.c Basic Fluidic Elements

Element	Symbol	Constitutive Equation	Element Property
1 Tube or Nozzle		$\dot{G}_{a \cdot b} = \frac{1}{I_{a \cdot b}} P_{a/b}$	$I = \text{inertance} \dots \dots \dots \text{in}^{-1}$
2 Tube or Nozzle		$\dot{G}_{a \cdot b} = \frac{1}{R_{a \cdot b}} \dot{P}_{a/b}$ laminar flow $\dot{G}_{a \cdot b} = \frac{1}{\bar{R}_{a \cdot b}} \dot{P}_{a/b}$ turbulent flow	$R = \text{laminar resistance} \dots \dots \dots \frac{1}{\text{in} \cdot \text{s}}$ $\bar{R} = \text{turbulent resistance}$ $P = p^{1/2}$
3 Pneumatic Tank		$\dot{G}_{a \cdot \cdot} = C_{a \cdot \cdot} P_{a/\cdot}$	$C = \text{capacitance due to fluid compressibility} \dots \text{in} \cdot \text{s}^2$ $C = \left(\frac{m}{nP} \right)_{\Delta \cdot \cdot}$; $n = \text{polytropic constant}$
4 Accumulator		$\dot{G}_{a \cdot b} = C_{a \cdot b} P_{a/b}$	$C = \text{capacitance due to flexible walls}$ $C = \frac{A^2 \rho}{k}$; $A = \text{area}$; $\rho = \text{mass density}$
5 Reservoir		$\dot{G}_{a \cdot b} = C_{a \cdot b} P_{a/b}$	$C = \text{capacitance due to volume change}$ $G = \frac{A}{g}$; $g = \text{gravitational constant}$

$\dot{A} = \dot{G} = \text{rate of change of mass flow rate, lb/in.}$ $P = \text{pressure drop, lb/in}^2$.

TABLE A.I.d Basic Heat Transfer Elements

Element	Symbol	Constitutive Equation	Element Property
1 Conductor		$\dot{Q}_{a \cdot b} = k_{a-b} T_{a/b}$	$k = \text{conductivity} \dots \frac{\text{BTU}}{\text{s} \cdot \text{O}}$
2 Thermal Accumulator		$\dot{Q}_{a \cdot \star} = C_{a-\star} \dot{T}_{a/\star}$	$C = \text{capacitance} \dots \frac{\text{BTU}}{\text{O}}$ $C = m \times sh$ $sh: \text{specific heat}$
3 Radiant Heat Transfer		$\dot{Q}_{a \cdot b} = B_{a-b} \theta_{a/b}$	$B = \text{radiation constant}$ $\theta_{a/\star} = T_{a/\star}^4$

$\dot{A} = \dot{Q} = \text{heat flow rate, BTU/s.}$ $T = \text{temperature}$

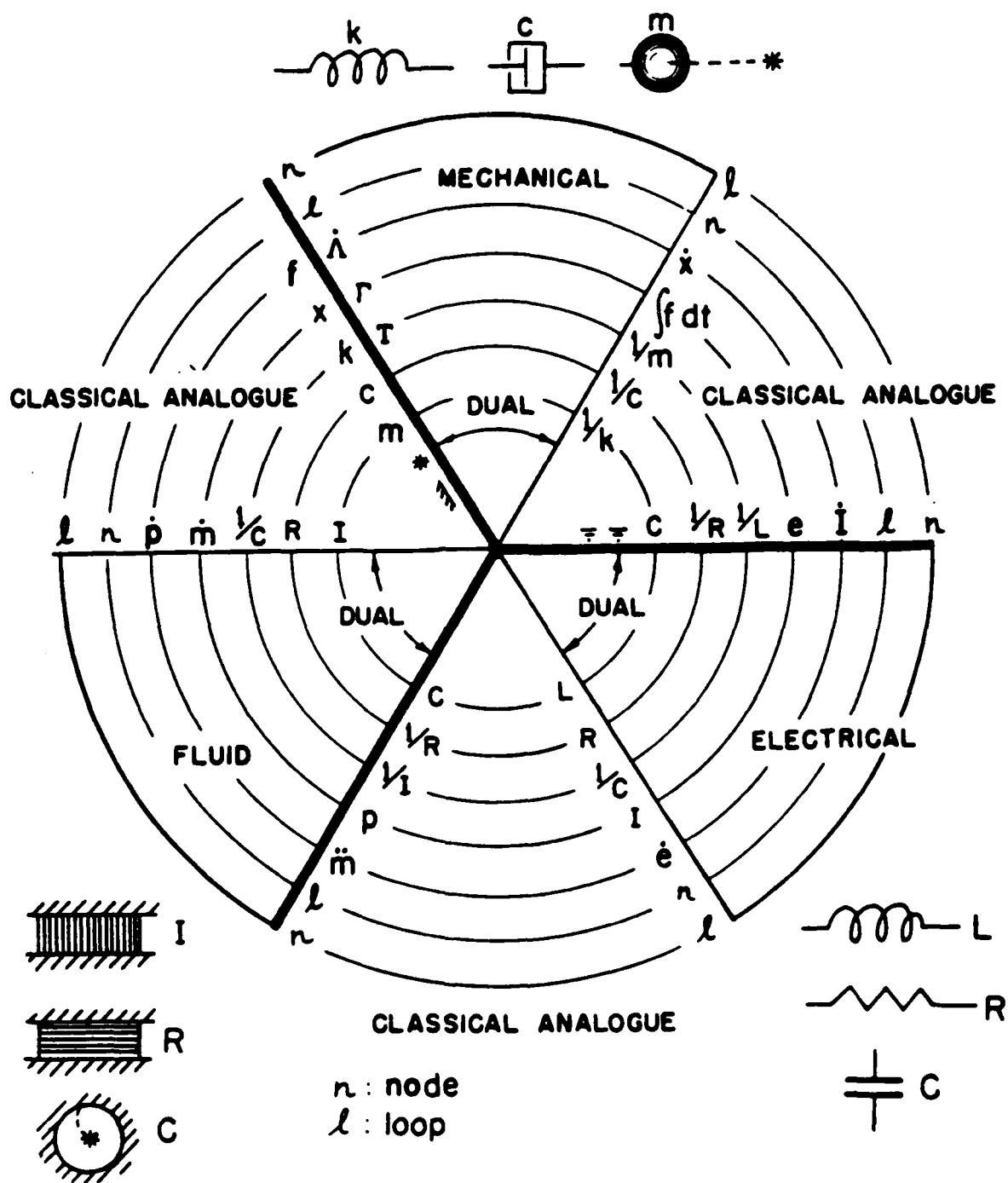


Fig. AI.1 Analogue and Dualities Wheel

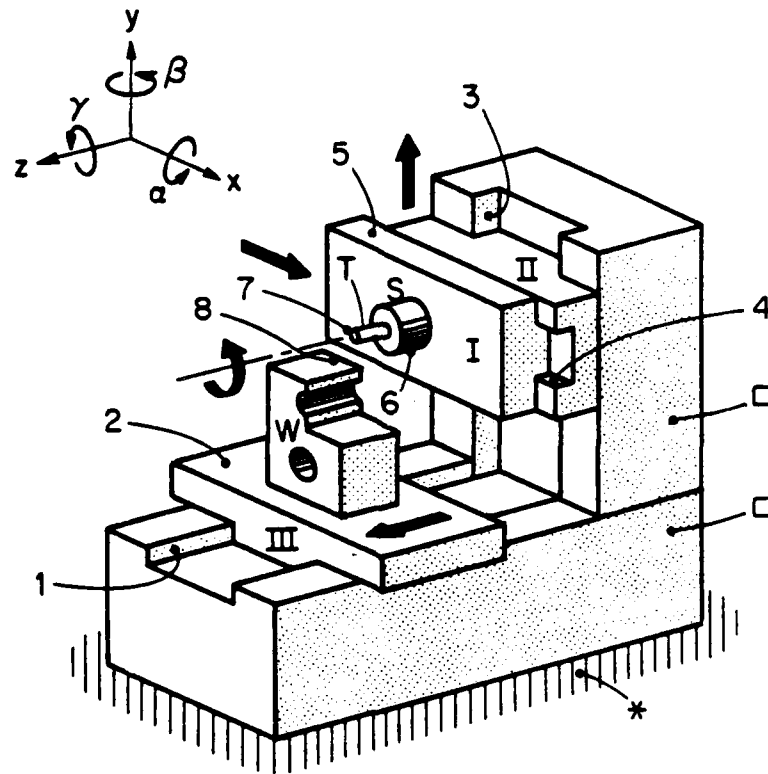
II. GUIDE-WAYS

The essence of the quality of a machine tool or a mechanical actuator is the precision of its guide ways. The machine tool of Fig. II.1 illustrates the implicit role of several interconnected guide ways and sliding tables. The slides are driven in a fashion as to move the workpiece and cutting edge in three dimensional space. The expectation is that point 7 of the tool comes in in contact with a predetermined point 8 of the work piece. If that is actually the case the relative position vector is $\bar{8/7} = 0$. This defines ideal conditions. In reality each of the interconnected bodies suffers errors which combined produce a mismatch and therefore an error in the work equal to the error vector ${}^1(\bar{8/7})$. The error $(\bar{8/7})$ is itself a chain rule summation of error contributions by all the connecting members of Fig. II.1. It is therefore necessary to examine each of the component errors in turn.

Components of Kinematic (Rigid Body) Errors

To illustrate the nature of localized kinematic errors consider the limited case of bodies I and II sliding on each other without elastic or thermal distortions. Figure II.2 is a rudimentary representation of the pair with Fig. II.2a representing an ideal geometry and Figs. II 2b, c, d depicting various malformed guide ways. Consider measurements taken with table II fixed and table I positioned along the X axis of II by

¹ Refer to NOTATIONAL SYSTEM of Section I for interpretation of symbols and abbreviations.



COORDINATE SYSTEMS		REFERENCE POINTS	
Name of body	Symbol	Point	Host
Main frame	□	0	□
X Slide	I	1	□
Y Slide	II	2	III
Z Slide	III	3	□
Work Piece	W	4	II
Tool or Probe	T	5	I
Spindle	S	6	S
		7	T
		8	W

Fig. II.1 Machine With Composite Guidance By Components.

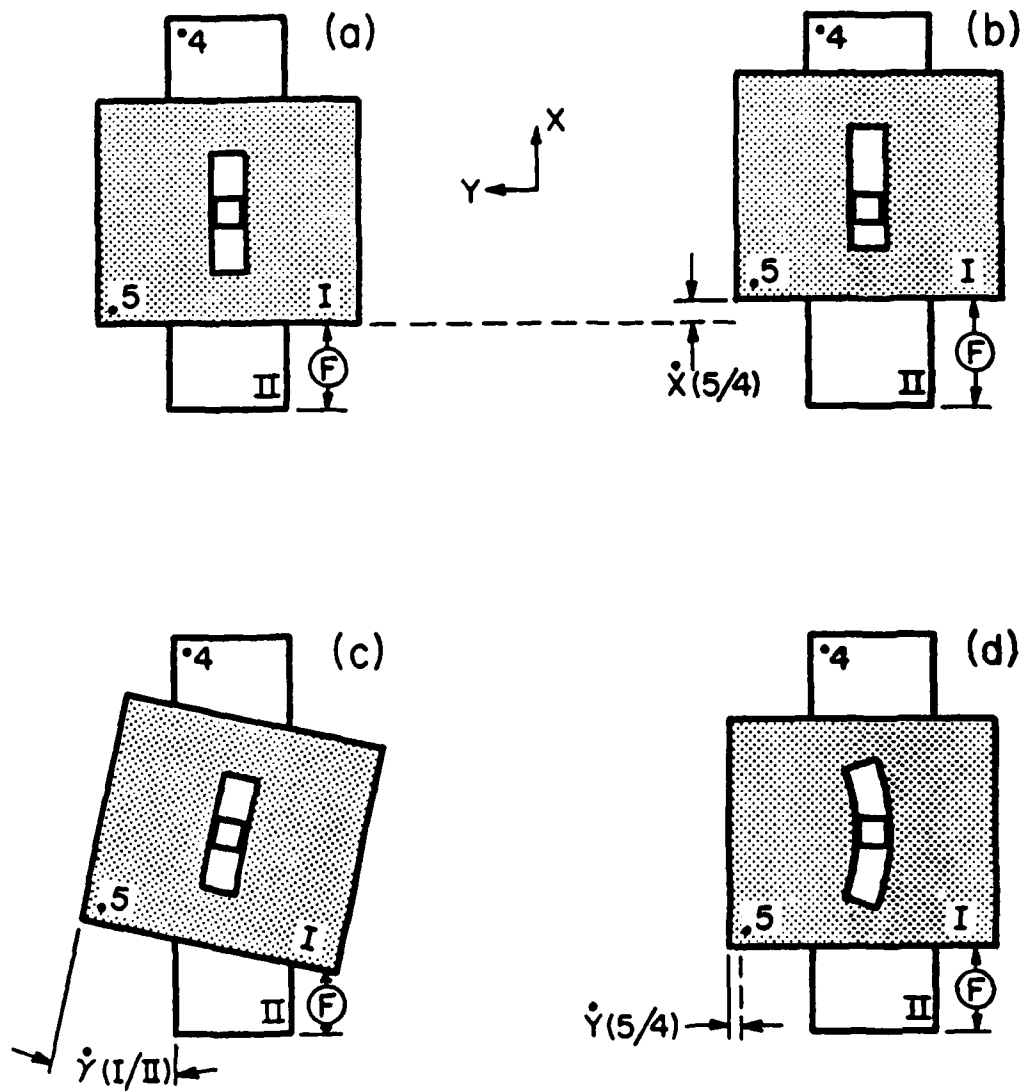


Fig. II.2 X-Y Plane Guidance Errors Between Tables I & II of Fig. II.1.

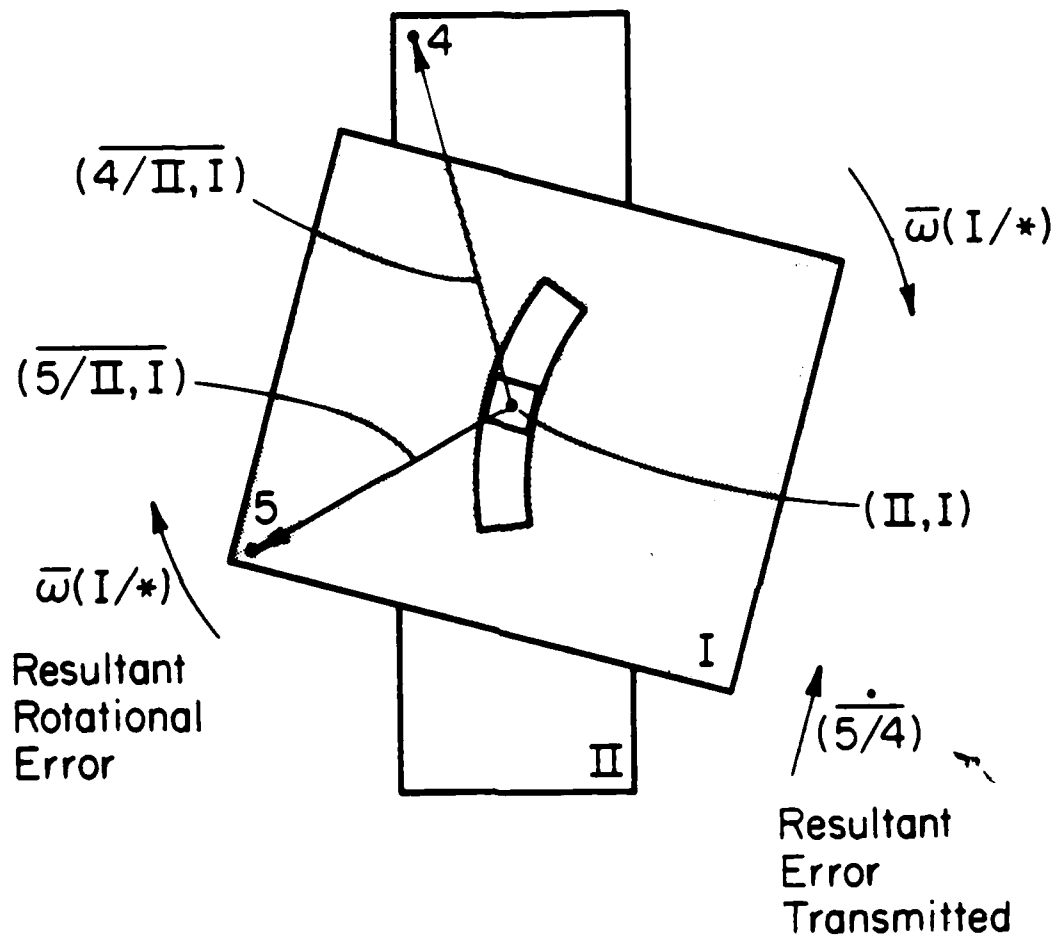


Fig. II.3 Errors Vectors of Table II Relative to Table I due to a Malformed Guide.

the actuator F. Control imperfections of this feed create the first observable error, that being along X as in Fig. II.2b. Points 4 and 5 are reference points which would serve as gaging points for measuring this error. The observed error is therefore identified as $\dot{X}_{II}(5/4)$. It is the error component along the X axis of II due to a pure translatory error between I and II. The actual points 5 and 4 would normally be chosen as convenient stations at which to mount the two parts of an experimental measuring gage. While analytical convenience might suggest other reference points the physical limitation of locating instruments must prevail.

Figure II.2c shows the error imposed by a skewed guide. The error is a rotation, around the ZII axis, of II about I, that is $\dot{\gamma}_{II}(I/II)$.

The curved guide of Fig. II.2d causes a sideways translation of table II hence an error $\dot{Y}_{II}(I/II)$. In real world examples the guides of Figs II.2b and .2c become one in the form of a skewed curved guide as in Fig. II.3.

For convenience only a view along the Z axis was illustrated in Fig. II.2. Similar studies would need to be made by sights along the X axis of body II as well as along its Y axis. Combining the three studies would enable one to extract the six components which would describe the total translatory and rotary errors between the members I and II due to the geometric errors in the mutual guide way. These errors are $\dot{X}_{II}(5/4)$, $\dot{Y}_{II}(5/4)$, $\dot{Z}_{II}(5/4)$ and $\dot{\alpha}_{II}(I/II)$, $\dot{\beta}_{II}(I/II)$, $\dot{\gamma}_{II}(I/II)$. If similar studies are made of all the pairs of bodies of Fig. II.1 the results could be combined in a chain form as suggested by eqtn EI.3b to arrive at the total error $(\overline{8/7})$ described by eqtn EII.1.

$$\overline{(8/7)} = \overline{(8/2)} + \overline{(2/1)} + \overline{(1/3)} + \overline{(3/4)} + \overline{(4/5)} + \overline{(5/6)} + \overline{(6/7)} \quad \text{EII.1}$$

Actually several other types of error sources, besides the as-manufactured-errors just described, must be considered for eqtn EII.1. A listing of this type of error and some of the more important agents of error is:

1. Geometric or rigid member kinematics errors. These arise from imperfect fabrication and positioning of assembled members. These imperfections manifest themselves as out of straightness, skewed and twisted guides, displaced constraints, non orthogonality of axes etc.. These errors are essentially invariant with time.
2. Wear and backlash are temporal factors whereby errors resulting from a mode of operations are superimposed on the geometric errors.
3. Thermal drift represents the most conspicuous form of temporal errors. The kinematic constants now vary with operating time. Errors arise from the changing thermal expansion and contractions of the components involved.
4. Elastic and or plastic deformations of components due to static and dynamic loads caused by the weights of the system members and forming loads applied to work pieces. These again change the kinematic constants with time and operating sequence.
5. In addition to distortion of "solid" members implied in 4 above, there are fluid films and elastomers between members which have an influence on the kinematic parameters of the system.

Shapes and Precision of Linear Guideways

Commercial linear guideways take on various profiles as in Fig. II.4. The fundamental objective of such slideways is to provide only one degree of freedom that being unrestricted and pure translation along the X axis (refer to Fig. II.2a,b and Fig. II.4). Existence of any movements in the other five coordinates are recognized as errors. For illustrative clarity the guideways shown in Fig. II.1 are indicated as squared-off surfaces (surfaces 1,3,4). Other possible commercial forms are depicted in Fig. II.4. The squared-off profile (a) is a very popular choice for horizontal installations being a good compromise between accuracy and fabrication costs. The double "V", Fig. II.4e, offers the highest accuracy possibilities but with the highest fabrication costs of the series shown.

As depicted in Fig. II.4 only shapes (b) and (c) seem to have the necessary five constraints needed for the ideal linear guide. Tables (a),(d),(e) have the theoretical freedom to lift off in the Z direction as well as to rotate in the β mode hence only three restraints would remain. However the practical application of these profiles is such that the external force W preloads the surfaces sufficiently to force contact at all times so that five constraints are actually preserved.

Earlier the agents of error in guideways were listed. Let us use some of the listings to compare the designs of Fig. II.4 by way of the score sheet TABLE II.1.

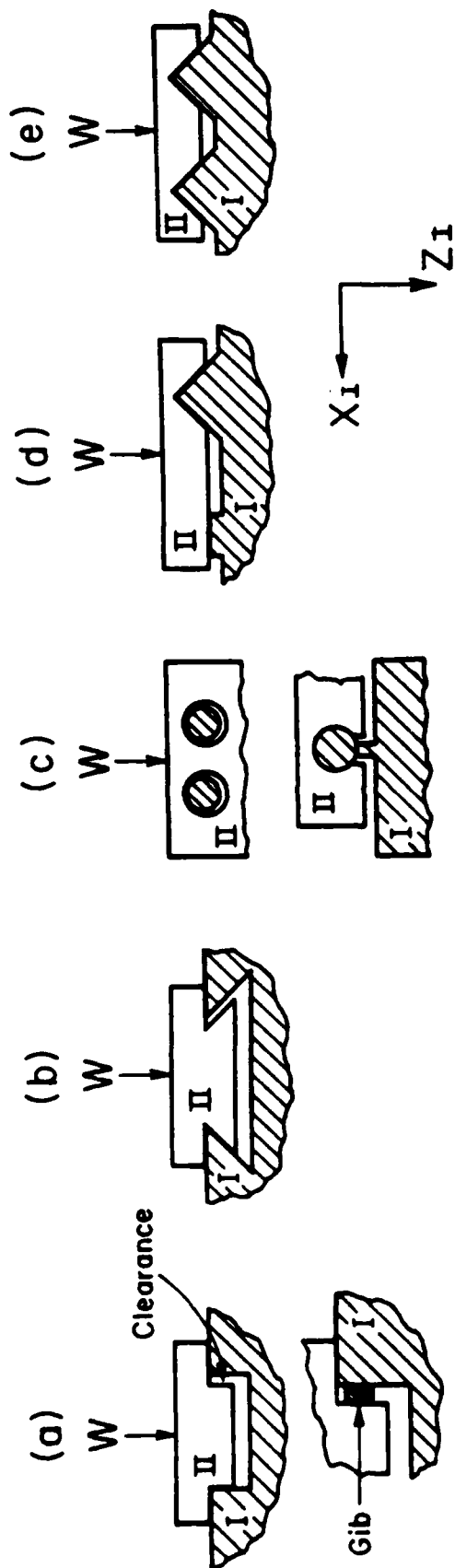
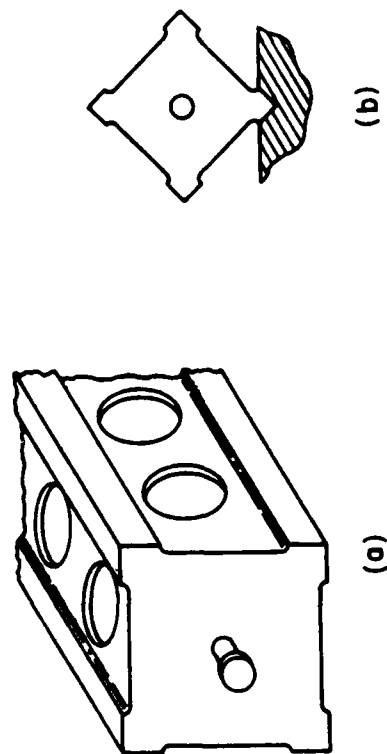


Fig. II.4 Types of Linear Sliding Guides.



b. Lapping a "V" Guideway

a. Box Straight Edge

TABLE II.1

Relative Potentials for the Minimization of Error Sources					
(5 = Best 1 = Poorest)					
Guideway Design					
Error Source	a	b	c	d	e
Geometric	3	2	1	4	5
Wear	5	2	1	4	4
Play	3	2	1	5	5
Flexibility	5	5	1	5	5

Play (Back Lash) Guidance Error

The sliding interface surfaces of Fig. II.4 are identified by the bolder lines. In design (d) the load W forces intimate contact at these surfaces. By contrast W will not close up the inherent clearance on the sides profile of (c). There is therefore an opportunity for undesirable movement in the \dot{Y} and $\dot{\gamma}$ modes. The apparent one degree of freedom of design (c) is actually three degrees of freedom even with load W applied. Hence the poor score, of 1, for play control in design c. Consider the squared-off, design (a), which must also have an assembly clearance between its side walls. That and the tolerance on parallelism of the side walls will result in some \dot{Y} and $\dot{\gamma}$ play. To raise the performance of (a) to a score of 3 a gib (tailored to a particular pair of members I, II as to minimize the clearance and out of parallelism) is inserted on one of the side walls. Dove tail guide (b) has the same problem just described. Forming a quality dove tail and a possible gib is obviously a more expensive design than (a) but a dove tail guide is a necessary alternative to (a) if the load W is insufficient to force full contact on the horizontal surfaces.

Flexibility

Rail designs a,b,d,e impose no particular limitations on the stiffness of the supporting bed II. Guide design (c) is however very much more flexible in bending because the cylindrical rails are supported only at their ends. The free span, approximately the length of carriage travel, is given to excessive bending. Supporting these rails along their entire lengths, as in the supplementary detail to Fig. II.4c, helps to reduce flexure in the vertical and horizontal planes but the latter mode is still severely compromised by the thinness of the fin.

Achieving Geometric Accuracy

W. R. Moore⁽¹⁾ gives an excellent discourse on the mechanics of fabrication of accurate guide ways. Very persuasive arguments are offered for the superiority of guide profiles (d) and (c). Quality of linear guides stems from the accuracy of master surfaces and straight edges which are used as gauges and laps. Accuracy starts with the generation of master flat surfaces by the three plate method. In this three nominally flat plates are abrasively rubbed against each other in a systematic cross matching and successive 90° turning on each other. The plates in a natural fashion work each other into highly accurate plane surfaces. Flatness accuracy is enhanced still further by reducing residual hills and valleys by hand scraping and local lapping. The objective is to create a surface flat to approximately 0.6 μm over a span of 1000 mm. From

(1) Cited references are listed at the end of each section.

these master surfaces four sided master straight edges are derived Fig. II.5. The four sided (box) geometry possesses several critical advantages for attaining and maintaining straightness and parallelism. The axi-symmetric form insures maximum flexural stiffness in all positions as well as minimum thermal distortion. The process of generation also results in very accurate 90° corners. By setting the box straight edge on the master surface plate the eight gage surfaces can be effectively checked for straightness, squareness and parallelism with respect to the master surface and therefore with respect to each other. Finally the 90° corner and straightness are self-proving in the generation of the masters and the machine ways. This cannot be said of straight edges with non square rectangular cross-sections or of V shaped straight edges. Because the accurate 90° corners derive naturally from matching the box straight edge to the master surface plate, these corners are then the ideal tool for marking and lapping female V guides Fig. II.5. By tipping the box master straight edge end for end as well as rotating sequentially through 90° while checking for high spots or lapping, a female V guide can be formed which is truer than any of the individual eight working surfaces of the box straight edge. So it is, because it is naturally derived from gaging and forming surfaces inherently superior in accuracy, the 90° V track is a superior guideway. The double V of (e) has a slight advantage over (d). The V and flat tracks wear at somewhat different rates, hence twist error is somewhat less likely in symmetrical arrangements such as e.

Cast iron is an excellent material for masters and machine guideways because it responds well to scraping. Furthermore cast iron machine beds possess good internal vibration damping. On the other hand cast iron sliding on cast iron wears many times faster than cast iron on steel (W, Moore⁽¹⁾ observes a 10:1 wear ratio). Hardened and

ground inserts, Fig. II.6, add wear resistance to the latent accuracy of the V guide concept. In this arrangement the female V's of the C. I. base are scraped to a male double V master to about $2.5 \mu\text{m}$ straightness and parallelism. Although these V's will not be used as final slide ways the accuracy will minimize possible distortions created by bolting the steel inserts to the bed. The upper C.I. sliding table is prepared in the same fashion as described for the bed V'ways. After the steel rails are ground true in assembly, the upper table is lapped into the steel guides achieving accuracy by matching.

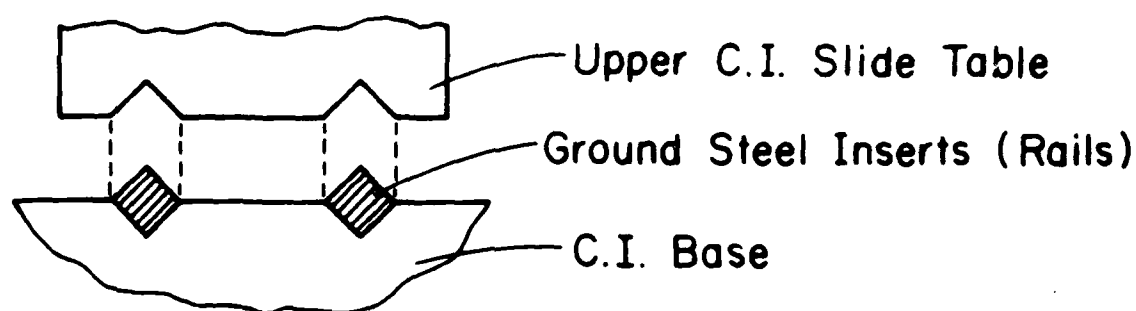


Fig. II.6 Guideway With Precision Rails

Geometric Calibration of Precision Mechanical Systems

Superior accuracy of each component is fundamental to accurate positioning by mechanical systems. Yet the accumulation of errors, as suggested by EII.1 flaws the over-all accuracy. On the other hand over-all repeatability from an assembly of accurate components could be very high. The principle objective of precise and accurate performance can be served by calibrating a full machine system. Several calibration

techniques are described in publications (2,3,4,5,6).

Using the minimal number of reference points, the N.B.S. method⁽²⁾ involves two interferometer metrology stations A and B, Fig. II.7. A third metrology station G (representing work piece W of Fig. II.1) contains gage points such as g one of which could be the surrogate for point 8 of the work piece W. Metrology posts A and B vector onto each other, the gage point g and onto the probe p. The latter is the surrogate for the tool tip 7 of Fig. II.1. There are three coordinate systems A, B, G and their origins are at a, b, g respectively. For analytic simplification the three coordinate systems are set parallel to each other except for infinitesimal rotations.

The metrology bases A and B vector on each other, on (g) and on (p) to generate position vectors $(\bar{p}/a)_A$, $(\bar{b}/a)_A$ and $(g/v)_B$ throughout the range of motions of tables I, II, III and point 8 of Fig. II.1. The range of these observations is contained in a rectangular parallel piped envelope whose volume is divided into a cubic lattice with a mesh size of about 20% of the smallest dimension of the envelope. Position vectors are recorded for all the nodes of this mesh field.

The N.B.S. calibration method aims to express the vector (\bar{p}/g) in the coordinates of the gage piece G. Employing the summation principle of EI.3b the required vector $(\bar{p}/g)_G$ would be synthesized from the measured vectors as in EII.2

$$(\bar{p}/g)_G = (\bar{p}/a)_G + (\bar{a}/b)_G + (\bar{b}/g)_G$$

$$\text{or } (\bar{p}/g)_G = (b/a)_G - (\bar{g}/b)_G \quad \text{EII.2}$$

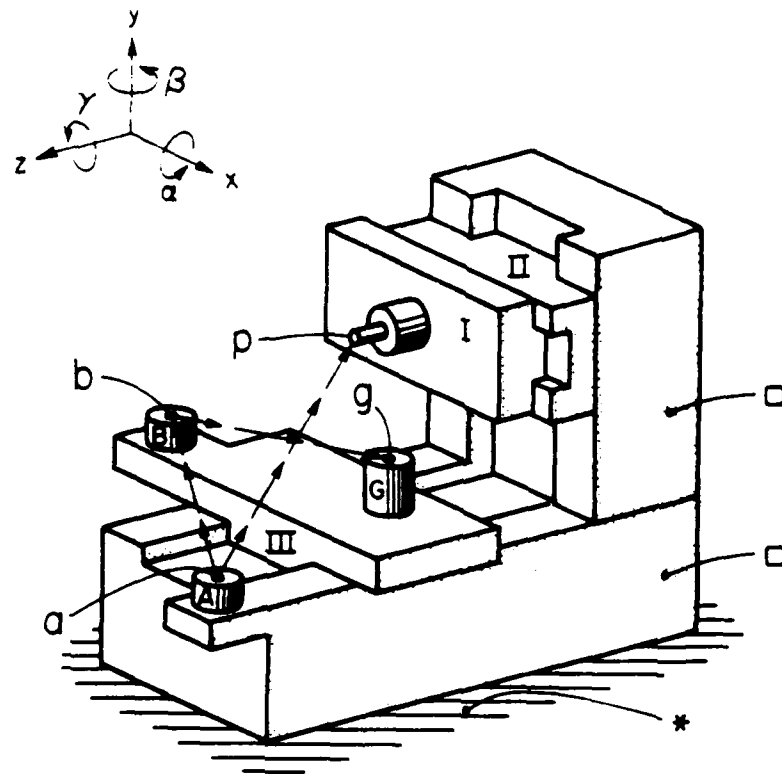


Fig. II.7 Machine of Fig. II.1 With Calibration Stations.

Because the coordinate axes of the three metrology bases are off-parallel from each other by minute rotations the measured vectors must be transformed to the base G as follows

$$\{\bar{p}/a\}_G = [C_{G,A}] \{p/a\}_A = [C_{G,B}] [C_{B,A}] \{p/a\}_A$$

$$\{b/a\}_G = [C_{G,A}] \{b/a\}_A = [C_{G,B}] [C_{B,A}] \{b/a\}_A$$

$$\{g/b\}_G = [C_{G,B}] \{g/b\}_B$$

Substituting these transformations into EII.2

$$(\bar{p}/g)_G = [C_{G,B}] [C_{B,A}] [(\bar{p}/a)_A - (\bar{b}/a)_A] - [C_{G,B}] (\bar{g}/b)_B \quad \text{EII.3}$$

where:

$$(\bar{p}/g)_G = \begin{bmatrix} X_{p/g} \\ Y_{p/g} \\ Z_{p/g} \end{bmatrix}_G, \quad (p/a)_A = \begin{bmatrix} X_{p/a} \\ Y_{p/a} \\ Z_{p/a} \end{bmatrix}_A,$$

$$(b/a)_A = \begin{bmatrix} X_{b/a} \\ Y_{b/a} \\ Z_{b/a} \end{bmatrix}_A, \quad (g/b)_B = \begin{bmatrix} X_{g/b} \\ Y_{g/b} \\ Z_{g/b} \end{bmatrix}_B$$

$$[C_{G,B}] = \begin{bmatrix} 1 & \dot{\gamma}_{G/B} & -\dot{\beta}_{G/B} \\ -\dot{\gamma}_{G/B} & 1 & \dot{\alpha}_{G/B} \\ \dot{\beta}_{G/B} & -\dot{\alpha}_{G/B} & 1 \end{bmatrix}$$

$$[C_{B,A}] = \begin{bmatrix} 1 & \dot{\gamma}_{B/A} & -\dot{\beta}_{B/A} \\ -\dot{\gamma}_{B/A} & 1 & \dot{\alpha}_{B/A} \\ \dot{\beta}_{B/A} & -\dot{\alpha}_{B/A} & 1 \end{bmatrix}$$

Equation EII.3 implemented with the data from metrology posts A and B yields the coordinates of the probe point p (or tool point 7) relative to a reference point in the gage G (or a reference point in work piece W). This information is in the coordinates of the work piece. These data are stored with corresponding machine measurements of the positions of tables I, II, and III. This record is then the calibration of the machine implicit in which are the actual built in errors described in Figs. II.2, 3 and equation EII.1. This calibration is then used to automatically compensate the machine controls during the production mode.

II. REFERENCES

1. Moore, Wayne R., "Foundations of Mechanical Accuracy", The Moore Special Tool Co., Bridgeport, Conn., 1970.
2. Hocken, R. et al, "Three Dimensional Metrology", Annals of C.I.R.P., Vol. 26, pp. 403-408, 1977.
3. Schultschick, R., "The Components of the Volumetric Accuracy", Annals of C.I.R.P., Vol. 26, pp. 223-228, 1977.
4. Love, W. J. and Scarr, A. J., "The Determination of the Volumetric Accuracy of Multi Axes Machines", MTDC.
5. Busch, K., Kunzmain, H., and Waldele, F., "Calibration of Coordinate Measuring Machines", Precision Engineering, Vol. 7, No. 3, July 1985.
6. Portman, V. T., "A Universal Method for Calculating the Accuracy of Machine Devices", Soviet Engineering Research, Vol. 1, No. 7, 1981.

III. FRICTION OF THIN FILM SLIDEWAYS

Precision guideways lapped with box-straight edges described earlier Fig. II.5 can be made straight to within a .001mm camber in a 0.4 m length⁽¹⁾. This then sets a standard by which operating distortions to guideways may be judged. Thermal distortions, structural flexibility back lash and wear are the most serious detractors from precise straight line guidance. As an example of the magnitude of distortion attributable to thermal gradients consider the case of a cast iron guideway represented by a prismatic bar 100 mm deep. Assume that along the length of this bar there is a portion 0.4 m long in which there is a temperature drop of 1°C from the top to bottom surfaces. Such a thermal gradient will have produced a 1.8 μ m camber in the .4 m length and a slope of 18 μ rad on each end (Appendix A.III). That is the 1°C temperature difference introduced errors 1.8 x the geometric errors inherent in the fabricated guideway.

A potent direct and or indirect source of such thermal distortions is the frictional drag of sliding surfaces. Not only does friction cause local temperature gradients in the sliding surfaces but it is also reflected in the power demands on the driver which in turn becomes a source of heat contributing to the thermal distortion of the structure. Vibration related to friction dynamics is another error generating phenomenon. Patently the mechanics of friction must be understood for rational design and diagnostics of precision mechanisms.

The mechanics of drag between two bodies depends on the details of the interfacial zone between them. Excluding macro electro-mechanical effects, five interface

structures are normally referred to in the study of sliding surfaces. Figs. III.1a - e show these basic structures and the coefficients of friction roughly associated with them.

Friction Model (a); Fig. III.1

The identification DRY for this model implies that there is no deliberate effort to provide a fluid lubricant to the interface. This is also the most rudimentary model of the five cases given. Its simplicity gives promise of lowest first cost and maximum support rigidity. On the other hand it suffers by comparison because it is associated with the highest expected friction and wear. While the purest form of model (a) is not a promising basis for precision guides, the friction mechanics involved is worth examining because it exists at times, to a degree, in all the other models of Fig. III.1 as well.

Many theories explaining friction between pairs of metal surfaces prevade past and current literature. The earliest concept, credited to Amontons (1699), pictures drag resulting from interlocking asperities of the mating surfaces. Later when instruments were developed capable of measuring the microscopic topography of smooth surfaces the results gave apparent support to the interlocking concept. Even the finest finishes magnified show roughness as in Fig. III.2b. Such apparent serrations certainly suggest interlock resistance to relative motion of the mating elements. On the other hand Fig. III.2b is somewhat misleading because this form of record is usually based on unequal scales. The horizontal scale is often shown as 1% of the vertical scale. Fig. III.2c shows the same profile with equal scales. The true surface contour of a well finished guideway now appears in the microscopic view as a gently rolling meadow. Rather than breaking through a barrier of slender bristles it would now seem more plausible

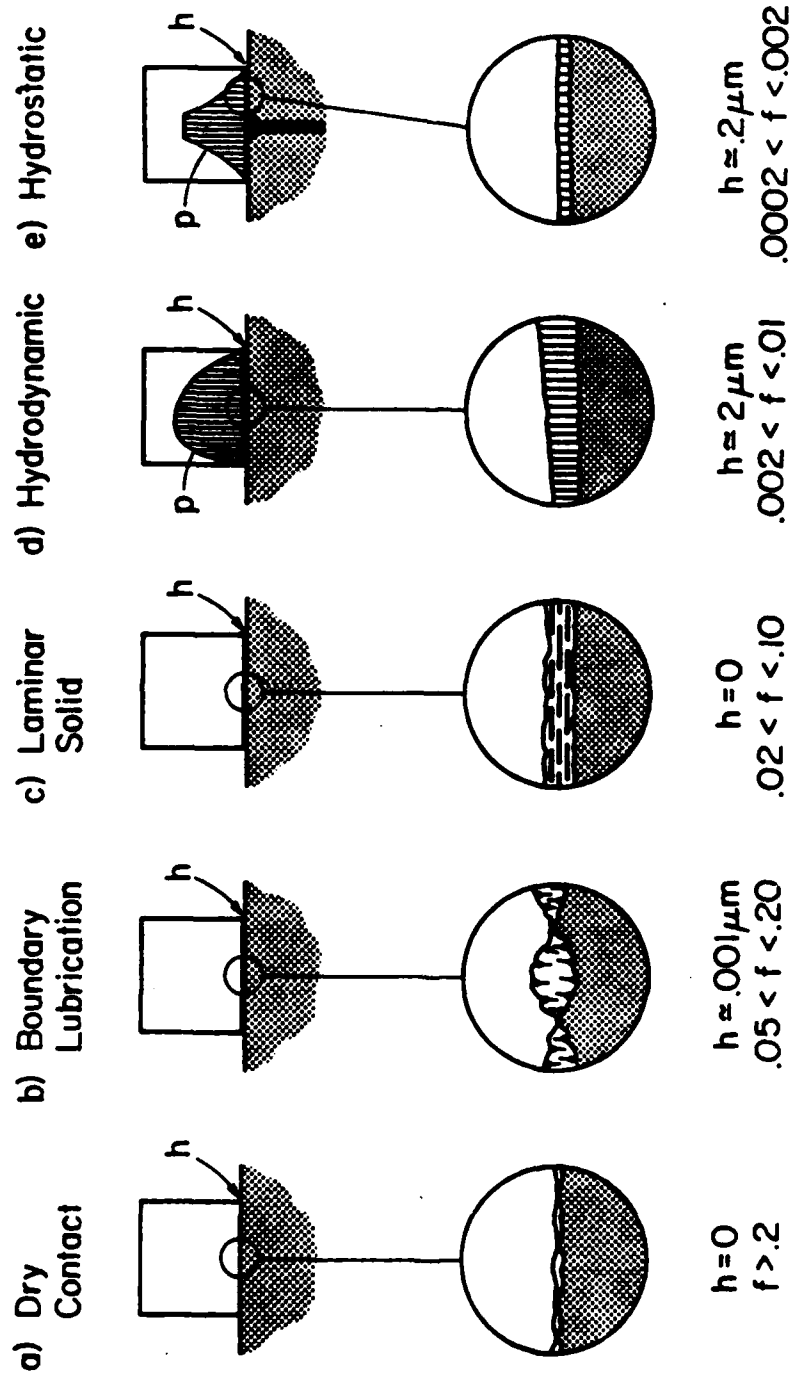


Fig. III.1 Classes of Lubrication by Interface Structures.

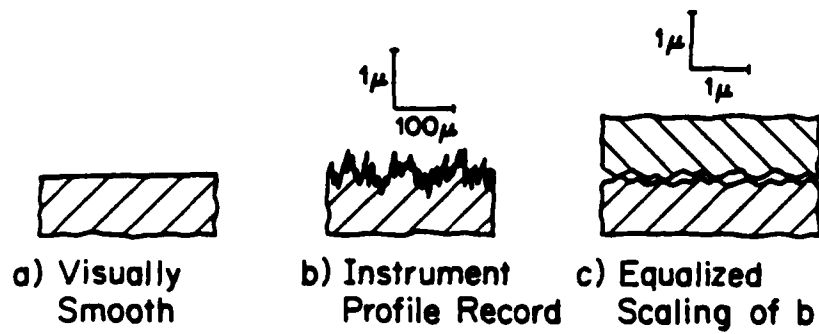


Fig. III.2 Effect of Choice of Scales on Comprehension of Surface Roughness.

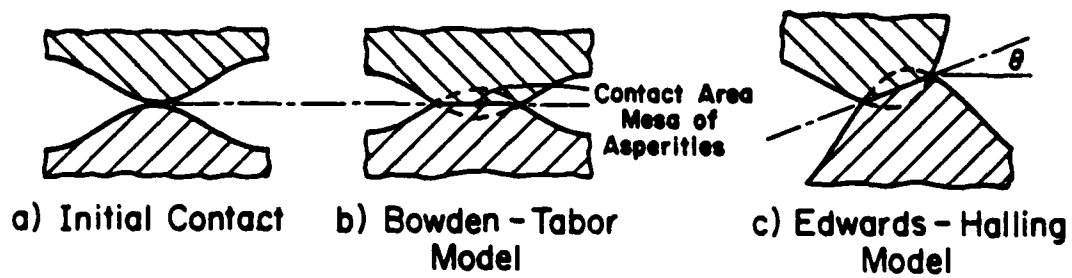


Fig. III.3 Asperity Contact Geometry.

that motion between mating surfaces could be accommodated by a hill climbing and dropping action. Such motion is however energy conservative, whereas friction decidedly a nonconservative action. An alternate concept of friction, motivated by the picture of stubby asperities, is the adhesion model advanced by Bowden and Tabor⁽²⁾. The B & T model is the basis on which are built current analytical refinements to the theoretical mechanics of friction between sliding solids.

Adhesion Mechanics of Friction

When two flat visually smooth surfaces are pressed together the nominal pressure p_a equals N/A_a where N is the compressing load and A_a is the apparent contact area of the bodies involved. In reality the load is supported on a multitude of peaks as depicted in Fig. III.3b. If A' is the area of contact of a typical asperity pair and n is the number of such contacting pairs then the real total area of contact is $A_r = n A'$. It follows then that $N = p A_r$ where p is the mean pressure, acting on the n contact areas, sufficient to sustain load N . As the load N is increased the existing contact points soon reach plastic flow conditions. Having reached their load carrying limit, the junction points offer no further resistance to deformation. Further overall deformation caused by an increase in N brings new asperities into load sharing contact. There is an increase to the total real area in proportion to the increase in load. This hypothesis and analogous electrical conductivity tests⁽³⁾ on pairs of flat plates, indicate that the total real area A_r increases in proportion to the increase in applied force N and is independent of the apparent area A_a . Furthermore the actual total contact area at a typical full load never reaches more than a minute fraction of the apparent area.

That is maximum $A_r \simeq \frac{1}{400} A_a$.

Bowden-Tabor First Analytical Approximations

In this initial analytical approximation to the coefficient of friction it is assumed that the stress distribution within the asperity is one dimensional, essentially a simple bar in compression. Hence

$N = p_c A_r$ $p_c =$ Critical stress observed in compression
loading of a simple bar.

$N =$ Compressive load normal to plane of the
interface between the bearing surfaces.

$T = s_c A_r$ $s_c =$ Failure shear stress of a bar in simple
tension, $s_c = 0.5 \sigma_c$. Where σ_c is the
tensile stress in a bar undergoing large
plastic flow due to simple tensile loading.

$T =$ Traction force applied along the plane of the
interface i.e., a shearing load.

$$\text{But } p_c \simeq 3 \sigma_c, s_c = 1/2 \sigma_c = \frac{1}{2} \times \frac{1}{3} p_c$$

$$\text{Since } f = \frac{T}{N} \text{ then } f = \frac{s_c A_r}{p_c A_r} = \frac{1}{6}.$$

It seems that a simplified analysis leads to a coefficient of friction $f = 1/6$. Actual tests of friction in dry metal pairs indicate coefficients ranging from $f = 0.5$ to $f = 1.5$. Apparently this mathematical model based on simple compression needs refinement.

Combined Stress Model, Junction Growth and Surface Contamination Effects.

If a shear stress is indeed applied across the junction area the combined stress pattern is now such that the pressure component available to sustain load N is actually reduced. This suggests that a compensatory increase in contact area will take place. This area growth increases the required shear load T to be associated with sliding. This alone will increase the coefficient of friction from the earlier estimate of $1/6$ towards values more like those experienced in practice. Bowden and Tabor⁽²⁾ observed in the laboratory that two similar and thoroughly decontaminated metals will exhibit coefficients of friction $f > 100$. This behavior was attributed to local welding. Sliding motion creates high temperature at the contacting asperity peaks. This speculation is reinforced by laboratory tests during which sparks (incandescent temperatures) were observed under a microscope. At these temperatures pure materials will spot weld. The welds offer shear resistance with almost negligible call for a squeeze load N , hence the observed coefficient of friction approaches infinity in some cases.

As in normal welding, the micro-welding described above is diminished by contaminants especially oxides and moisture which are ever present in normal sliding conditions. The analytical influence of less than clean conditions can be approximated by calling up equation EIII.1 which is a reduced plastic failure criterion for the case of combined stresses.

$$p^2 + \alpha^2 s_f^2 = \alpha^2 s_c^2 \quad \text{EIII.1}$$

$$\text{where } p = \frac{N}{A} \quad s_f = \frac{T}{A} \quad \alpha^2 \simeq 10$$

s_c = critical bulk shear stress of the weaker material.

s_f = apparent shear failure stress of contaminated bearing surface.

$s_f = c s_c$ c = cleanliness coefficient $0 < c < 1$

$$f = \frac{T}{N} = \frac{s_f A_r}{p A_r} = \frac{s_f}{p}$$

Substituting these equivalents into Eqtn. III.1 leads to

$$f = \frac{c}{\alpha(1-c^2)^{1/2}} \quad \text{EIII.2}$$

If the surfaces are perfectly clean, $c = 1$, equation. EIII.2 indicates a theoretical $f \simeq \infty$. If $c = .85$, then $f = .51$ and if $c = .50$, $f = .18$. Dry metal pairs under normal atmospheric conditions should be oxidized sufficiently to expect a cleanliness quotient c of about .85 which would lead from EIII.2 to a f expectation of about 0.5.

Equation EIII.2 implies that a completely oxidized surface ($c = 0$) should enjoy a coefficient of friction $f = 0$. No such conclusion can be gleaned from any test results. This conflict between expectation and reality is more easily resolved if c were termed an adhesion coefficient. What seems to take place is that the protective oxide being very brittle cracks easily. Under the high local pressures of the asperities, the virgin metals diffuse through the fissures in the cracked oxide film to meet each other to form welds. Since the fissure conduit area is a fraction of asperity area A' the apparent traction strength is less than a perfectly decontaminated surface but more than a completely oxide protected surface.

A Refinement to the Adhesion Theory

Edwards and Halling^{(4),(5)} invoke the asperity interlock concept and interpose it on the Bowden-Tabor model. In this case the supporting mesa, is on the average inclined

at some mean angle θ to the horizontal as in Fig. III.3c as contrasted to $\theta = 0$ of Fig. III.3b.

Moving against the buttress, defined by θ , increases the resistance to gross motion. The coefficient of friction is now defined as

$$f_{EH} = \frac{f_{BT} + \phi}{(1 - \phi f_{BT})^{1/2}} = \text{coefficient of friction by Edwards \& Halling}^{(4)}. \quad \text{EIII.3}$$

where ϕ is a function of θ and work hardening effects on the junction areas. At $\theta = 0$, $\phi = 0$.

$$f_{BT} = \frac{c}{c(1-c^2)^{1/2}} = \text{coefficient of friction calculated by the Bowden-Tabor model where } \theta = 0 \text{ ie, equation EIII.2.}$$

To gather a sense of the influence of asperity interlocking consider a case of $\theta = 10^\circ$ and $f_{BT} \simeq .3$ the Edwards Halling formula yields $f_{EH} = .45$ or a 50% increase in the coefficient of friction because the effect of interlocking.

If dissimilar metals are run dry on each other welding is resisted somewhat better. Phosphor bronze, brass or cast iron running dry against steel are the better bearing combinations with dry friction coefficients of about 0.4. While this figure verges on being acceptable for guideways the problem remains, namely dry metal-metal friction is not smooth or steady enough for precision systems. There are however non-metallic solids which not only have a somewhat lower to very low values of f and behave much more smoothly and are less prone to seizure. These dry solids interposed between the metal surfaces add lubricity to the interface. Resulting coefficients can vary between .03 and .35. Solid lubricants come in inorganic and organic forms. The two

classifications have entirely different mechanisms to arrive at their dry lubricity.

Inorganic Solid Lubricants

Fig. III.1c symbolizes solid dry lubrication as a process whereby flakes of a solid slide easily on each other. Graphite is the original solid lubricant. Its lubricity comes from its natural laminar structure. It is a crystalline form of carbon whose atoms are arranged in regular layers. While these layers possess high bending and breaking strengths the bonds between them are very weak. The evident low friction is a manifestation of this weakness which allows the layers to slide on each other rather easily with the result that $.05 < f < 0.15$. The lower limit of f occurs at high pressures and the upper limit at low pressures. This performance is maintained up to 200°C. The sliding is smooth and steady. Graphite adheres well to metal surfaces and also embeds well into carrier materials such as polymers.

Graphite has some idiosyncrasies which must be recognized however. Low friction and low wear are realized only in the presence of water vapor. Graphite does not work well in vacuum and dehydrated conditions. Furthermore the edges of the graphite crystal planes are abrasive hence it is important to orient the crystals parallel to the bearing surface. Fortunately such orientation is enhanced by the lamellar structure which encourages the formation of flat flakes with a strong tendency to stick to flat surfaces in the desired fashion. The problem with explicitly introducing a form of solid lubricant such as graphite between metal surfaces is that the thin film is eventually lost by wearing away. Fortunately, unlike wear of metals, the debris from solid lubricants such as graphite and other successful solids does not cause rapid wear until the surface is rubbed down to raw metal. Nevertheless the life of the film is an

engineering concern which currently is assessed in terms of its limiting PV factor (apparent pressure x sliding velocity). This term if augmented with an appropriate coefficient of friction suggests power dissipation per unit area of the bearing. This connection in turn suggests that the local temperature generated is strongly related to the level of PV at which the bearing is operating. These connections are oversimplified but a relationship between the dynamic strength of the film at particular temperatures is roughly integrated into limiting PV values observed in life tests. Ideally more complete data on solid lubricant would include limiting pressure recommendations and thermal conductivity of the film. Graphite, having a superior thermal conductivity, enjoys one of the higher allowable PV ratios among the list of viable dry solid lubricants.

Molybdenum disulfide, MoS_2 , powder is the other important inorganic lubricant. It is normally assumed to be a later discovery than graphite but it might have been in use as long as graphite but not recognized as such since it was confused to be a special graphite form. Again low friction results from failure along the cleavage faces this time between MoS_2 layers. This weak bond, parallel to the sliding plane, mated with great strength normal to the sliding plane is the basis for low coefficients of friction ($.03 < f < .2$ depending on load). Unlike graphite, MoS_2 does not need water vapor or oxidation to serve its purpose hence it is an excellent alternative to graphite in such environments. MoS_2 has a PV limit 5 x better than graphite. Furthermore MoS_2 has even better adherence to metals than graphite and a load carrying capacity 28 x better than graphite. Graphite does have a distinct superiority if electrical and thermal conductivity is desirable. Except for the latter operating condition, MoS_2 films will be superior to graphite films for dry precision guideways.

Molybdenum films can be deposited on metal surfaces by spraying a mist of MoS_2 in a volatile fluid carrier. After the carrier has evaporated from the surface MoS_2 remains. The surface is then rubbed with an appropriate cloth burnishing the MoS_2 into the metal. The resulting film has a very low coefficient of friction and a thickness of only $0.1\mu m$ which insures dimensional control so necessary to a precision guideway. Increased durability can be achieved by increasing the film thickness up to $10\mu m$ through repetitions of the process described above. The larger film thickness does detract from the quality of a guideway precision. Sputtering is an alternative process for laying down very thin yet very durable films for precision guides. Another convenient method for laying down a film is to spray MoS_2 in a resin carrier onto the metallic surface. The carrier again is allowed to evaporate and then the film is cured at a specific temperature to give a hard varnish like finish. Such a film has a very good life but the resulting thickness is many times greater than that converted with a burnishing or sputtering method. Again the thickness of resin bonded films might not be compatible with precision guideways.

Organic Solid Lubricants

The other approach to dry film lubrication is by way of polymers. The two most successful are Nylon and PTFE (polytetrafluoroethylene) commercially known as Teflon, Fluon etc.. PTFE is the more interesting polymer because its coefficient of friction can be as low as .03. Its properties and mechanics of sliding are unlike other materials. A very low coefficient of friction, chemical inertness and a high melting point are the characteristics which have made PTFE such a desirable and popular material. But there are prominent negative characteristics that have been difficult

barriers to bearing applications. Its normal form is acquired by moulding but it is not easily machined because of excessive thermal distortion created by machining. Finally the very nature of its low friction is due to its poor mechanical strength. The attractiveness of the low coefficient of friction and its stability at high and low temperatures (300°C to -200°C) has been a motivator for development of methods to overcome the stubbornly negative qualities.

For reasons that are not clear, despite chemical inertness and poor mechanical strength PTFE forms good smooth strongly adhering films to metal surfaces. Good smooth films can be produced by a transfer process. Solid PTFE is made to slide under pressure on a clean, dry metal surface and so transfer itself to the metal. But the film so created has insufficient wear resistance for bearings.

PTFE in solid form in addition to poor mechanical strength also suffers from creep under load and poor wear resistance. To help circumvent these deficiencies, PTFE is currently impregnated into a reinforcing matrix of such materials as glass fibers, carbon fibers, MoS_2 and porous lead-bronze. The reinforcing carriers add strength and increase the modulus which in turn reduces the deformation. Finally wear rate is improved 10,000 fold. But the coefficient of friction of the composite is raised to approximately 0.25 from the promise of $f = .03$. Several commercially available composites offer PTFE incorporated in the pores of a sintered bronze strip which itself is bonded to a steel backing strip. Another widely used commercial composite with PTFE is in the form of fibers interwoven with glass fiber. The weave is impregnated with a phenolic resin the whole bonded to a steel back strip. These composites can sustain maximum PV values of 100,000 psi x ft/in. The stability of PTFE composite reinforcements have good prospects for guides especially those which must operate in non-fluid

and vacuum environments.

Nylon (Dupont) is another polymer with considerable utility in mechanical systems. Its mechanical strength and resistance to creep is superior to that of PTFE. Nevertheless like PTFE to acquire sufficient strength and stability, Nylon must also be composited for satisfactory guideways. Because of growth due to moisture absorption Nylon at present is probably inadequate for precision guides.

Delrin (Dupont) is an acetal resin filled with PTFE. The acetal resin lends its high strength, low creep and stiffness to the composite while the PTFE provides the low friction. The static and kinetic coefficients of Delrin 500 AF are .08 and .14 respectively.

Boundary Lubrication, Fig. III.2b

The coefficient of friction and wear life of dry bearing surfaces can be improved considerably by wetting the interface of the solids with an oily fluid. The mechanics of the easy sliding is identified as Boundary Lubrication. Although the introduction of a fluid might lead one to expect the phenomenon of friction to be vastly different than that described in the previous sections the fact is that the principles are remarkably similar that is:

- a) A contaminant impairing the welding of asperity junctions is introduced.
- b) The contaminant reduces the shear strength of the asperity junctions.
- c) Finally the contaminant increases the ratio of crushing strength to shear strength of the thin film involved.

The oily film involved in boundary lubrication goes beyond the obvious role of a

weld impairing contaminant. Hardy⁽⁶⁾ provided the earliest fuller explanation of the part that certain liquids play in boundary lubrication. Bowden and Tabor⁽²⁾ built on Hardy's concepts to develop a model of the mechanics of boundary lubrication. Hardy observed that successful fluid lubricants possess a long chain highly polarized molecular structure. The polar head of such molecules induce a strong physical adsorption to the bearing surfaces. The long chain molecules standing on end with heads adhering to the metal surfaces appeared somewhat like brush bristles which would separate the surfaces yet allow the bearing surfaces to move laterally on each other by elastically flexing to the displacement and snapping back into a supporting mode. The interfering asperities concept is not present in Hardy's model. The inconsistencies between the mechanistic model and observed behavior caused Bowden and Tabor to modify Hardy's model.

The B and T model is depicted in Fig. III.3b. The concept of squeeze load supporting asperities is retained but now this load is shared by Hardy's bristle like oily molecules filling the voids between asperities. The real area of support is increased from A_r described in the early sections to A of Fig. III.4. The asperity function area is a fraction, α , of A . The area supported by the molecules introduced by the oil is the remaining fraction $1-\alpha$. Because of this cooperative support of the load the asperity junction area is much reduced and of course the presence of the fluid essentially eliminates asperity welding.

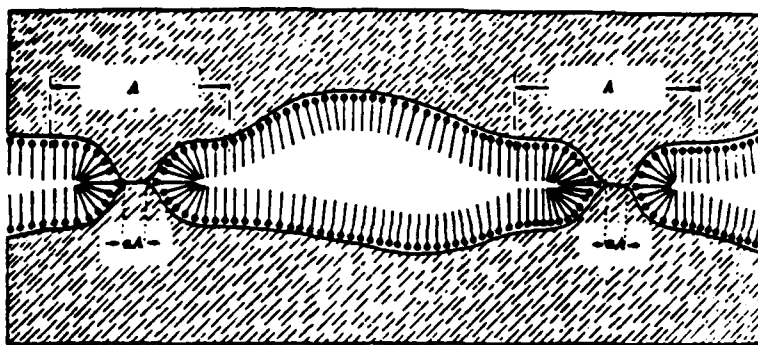


Fig. III.4 Long Molecule Support of Sliding Bodies.

It has been known a long time that animal fats and vegetable oils make good boundary layer lubricants while mineral oils and alcohols are poor lubricants. Some key ingredients responsible for good boundary lubrication are stearic acid (animal fats) or palmitic acid (cotton seed and palm oil) or oleic acid (olive oil). Such ingredients are instrumental in creating strong adherence of the fluid molecules to the metal surface. It is poor adherence to the working surfaces that marks pure mineral oils as poor lubricants. On the other hand if only 1 to 5% by volume of stearic acid is added to mineral oil it is converted into a good lubricant. Strangely stearic acid and the other favorable acids by themselves are not good lubricants but rather play a chemical role. The presence of these acids causes a chemical reaction with the oxides of some of the more reactive bearing materials. The result of this reaction is the creation of a new substance, a metallic soap film chemically bound to the bearing metal. Copper, zinc, tin, etc. are good reactive materials for boundary lubrication. Boundary lubrication is poor on the noble metals because their chemical inertness giving witness to the observation that it is the chemical attack of the favorable oils that makes for good boundary lubrication. Typically reactive metals will yield a coefficient of friction $f = 0.1$ whereas with unreactive metals $.3 < f < .7$.

The metallic soap under high pressure becomes a solid lubricant sharing the load with the asperities. Under favorable boundary lubrication conditions the asperity junction area of Fig. III.4 is very small compared to the area supported by the metallic soap (α is small). Therefore the friction is predominantly that of the metallic soap. If wear is defined as the breaking off of the tips of the asperity junctions, the reduced junction area of Fig. III.4 makes for smaller wear particles. In this way the support contributed by the metallic soap results in lower wear rates.

Boundary lubrication is normally discussed in terms of a thin oil film between sliding metal surfaces as was the case above. Applications of oil to organic solids is beneficial although the chemical generation of soaps is more problematical in such cases. Denton⁽⁶⁾ studied the efficacy of two commercial types of PTFE composites operating with liquid lubricants. The composites were in the form of .060 inch skived tapes intended as bearing surface overlays for linear slideways of machine tools. Sliding tests were conducted with bearing loads generating an apparent pressure of 200 psi. Kinetic coefficients of friction and wear were observed under $p v = 3333$ psi x ft/m operating conditions. Static coefficients of friction were measured at the termination of each sliding run. By way of a control identical tests were conducted with lubricated cast iron slideways surfaces. TABLE III.1 is of an abstract of test results pertinent to this discussion. Friction coefficients are given for sliding on freshly ground hardened steel surfaces. Initially the readings are given for a very short run ($D < 1.0$ "). Run-in operations are represented by the results observed after a sliding passage of 10^5 inches. The short run tests with the two PTFE composites types show kinetic coefficients of friction $f_k = .035$ and $f_k = .031$. These values are essentially equal to the kinetic coefficient for bulk PTFE on steel. On the other hand after a

run-in period, $D = 10^5$ inches, the friction coefficients have increased substantially to $f_k = .131$ and $f_k = .097$ for the two PTFE types. This pattern of results suggests that at the onset of run-in the contacting asperities are predominantly PTFE against steel but as the run-in progresses the soft PTFE asperities are worn down exposing more of the filler to the hardened steel mating surface. The coefficient of friction at the end of the run-in period is the resultant of PTFE and filler contributions to friction. Near the end of the run-in ($D = 10^5$ inches) the coefficient of friction for the mineral filler composite has risen to $f_k = .131$ while the bronze filler composite has risen to $f_k = .097$ or a coefficient of friction 35% less than that of the mineral filler model. Apparently, since bronze is favorably reactive to the lubricating oil, good boundary lubrication occurs on and around the bronze asperities. On the other hand the mineral asperities not being reactive to the lubricant do not develop beneficial boundary lubrication. It could be said then that the presence of a lubricant does very little to reduce friction of PTFE composites unless the filler is a 'good' bearing metal that is one that is associated with effective boundary lubrication. It should be remembered however that a liquid lubricant also serves as a coolant and anti-corrodent so that at higher sliding velocities the PTFE mineral composite could enjoy some benefit from these secondary roles of lubricants in bearing systems.

The cast-iron tests show performance to be much more independent of length of run-in distance. This could be because the surface of cast-iron can be ground smoother than is possible for PTFE composites. In a way cast iron is also a composite, being a distribution of graphite in the body of iron. Wearing down of a cast iron surface merely exposes new graphite spots so that coefficients of friction remain fairly constant from the onset of sliding through run-in, as indicated in TABLE III.1.

Meanwhile the exposed iron being reactive to the oil lubricant, boundary lubrication prevails as well.

The ratio of f_s/f_k is a rough indicator of stick-slip (chatter) tendencies of a pair of bearing surfaces. If this ratio, called the "stick-slip coefficient"⁽⁶⁾, is equal to or greater than unity there is risk of chatter. From TABLE III.1 after run-in ($D = 10^5$ in.) the PTFE mineral composite is running dangerously close to chattering, while the PTFE-bronze composite and the cast iron have almost identical safe f_s/f_k ratios. Once again the existence of boundary lubrication shows its beneficial hand.

TABLE III.1

D		Surfaces and Lubricants		
		1*	2*	3*
0-1 in	f_s	.027	.027	.110
	f_k	.035	.031	.126
	f_s/f_k	.77	.87	.87
10^5 in	f_s	.128	.084	.112
	f_k	.131	.097	.127
	f_s/f_k	.98	.87	.88
10^2 in	K wet	5804	1757	1916
	K dry	11220	30400	---
10^5 in	K wet	30	39	13
	K dry	37	138	---

- 1* Mineral filled PTFE, Compound Way oil against steel.
- 2* Bronze filled PTFE, Compound Way oil against steel.
- 3* Cast iron, Compound Way oil against steel.

f_s : static coeff. of friction

f_k : kinetic coefficient of friction

f_s/f_k : stick slip coefficient.

$K (10^2)$: $(\text{in.}^3 \text{ min./ft. lb. hr.}) \times 10^{-10}$ after 10^2 units of travel.

$K (10^5)$: $(\text{in.}^3 \text{ min./ft. lb. hr.}) \times 10^{-10}$ after 10^5 units of travel.

\dot{D} : Sliding distance traveled at observed data.

Summary

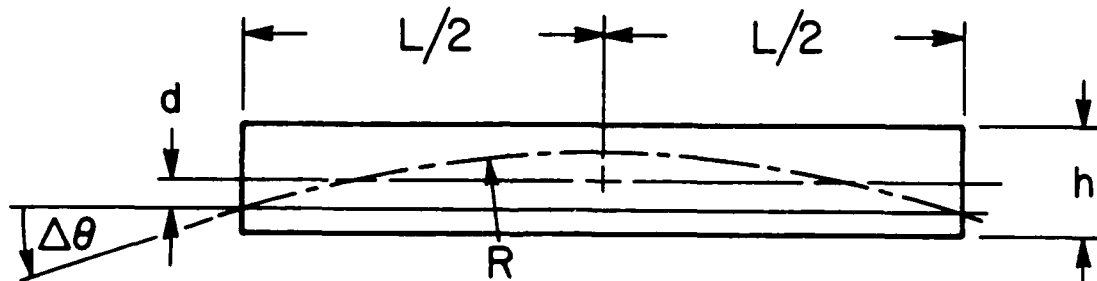
Table III.1 demonstrates that PTFE composite surfaces could work on ordinary machine tool slideways but the wear rate and geometrical instability, due to moisture absorption, makes them poor candidates at this point of development for precision guideways. Dimensional growth of almost 10% due to moisture absorption as not compatible with precision tolerances of less than $1\mu\text{m}$. A wear rate 3 - 4 x more rapid than a lubricated cast iron surface can be accommodated by frequent replacement of the composite tapes. While this is an acceptable procedure for reconditioning an ordinary machine tool it is not so for precision surfaces since each replacement will introduce errors well beyond that tolerated for precision systems. The same assesment could be made of MoS_2 composites. The synthetics are at present not likely substitutes for lubricated cast iron precision slideways.

III. References

- [1] Wayne, R. Moore, "Foundations of Mechanical Accuracy; The Moore Special Tool Company", (1970).
- [2] F. P. Bowden, D. Tabor, "The Friction and Lubrication of Solids", Pt. II. Oxford University Press, (1964).
- [3] R. Holm, "Electrical Contacts Handbook", Springer-Verlag, Berlin 1958.
- [4] C. M. Edwards, J. Halling, "An Analysis of the Plastic Interaction of Surface Asperities and its Relevance to the Value of the Coefficient of Friction", J. Mech. Engng. Sci. 10, (1968), 101.
- [5] J. Halling, "Principles of Tribology", The MacMillan Press Ltd. 1975.
- [6] J. E. Denton, "Friction and Wear of Cast Iron and Polytetrafluoroethylene Materials Lubricated with Water Based Fluids", MS Thesis, Univ. of Cincinnati 1983.

APPENDIX AIII

Given a lapped guideway with a residual error in straightness described as a .001 mm camber in a sector 400 mm long. Assume that the curved path is part of a circle then the given path geometry can be expressed as a radius of curvature R and slope $\Delta\theta$, Fig. AIII.1.



Thermal Distortion, 1°C
Variation from Top to Bottom

Fig. AIII.1 Geometry of Curved Path

$$\text{Camber } d = .001 \text{ mm} \quad \text{where } d = \frac{1}{2} R \Delta\theta^2$$

$$\text{Sector length } L = 400 \text{ mm} \quad \text{and} \quad \frac{L}{2} = R \Delta\theta$$

$$\text{Slope } \Delta\theta < .01 \text{ rad.}$$

$$\text{Hence } R = \frac{L^2}{8d} = \frac{400^2}{8 \times .001} = 2 \times 10^7 \text{ mm}$$

$$\Delta\theta = \frac{L}{2R} = \frac{400}{2 \times 2 \times 10^7} = 20 \mu \text{ rad}$$

Thermal-Bowing of a Straight Guideway

Given a guide rail in the form of a prismatic bar of depth h . Along the length of the rail there is a sector L units long wherein the difference in temperature between the upper and lower surfaces is ΔT . The strains developed by this temperature gra-

dent will cause the rail to bow as in Fig. AIII.1 to a curvature of radius R' and a slope $\Delta\theta'$ at each end of the thermal sector. The thermal strains e at the upper and bottom surfaces are

$$e = \frac{\alpha \Delta T}{2} ; \quad \alpha = \text{coefficient of thermal expansion for the rail.}$$

$$\text{Furthermore } e = \frac{h}{2R'} \quad \text{or} \quad R' = \frac{h}{\alpha \Delta T}$$

Given R' , the corresponding camber d' and slope $\Delta\theta'$ are determined by the geometrical transformations given earlier i.e.

$$d' = \frac{L^2}{8R'} = \frac{1}{8} \frac{L^2}{h} \alpha \Delta T$$

$$\Delta\theta' = \frac{L}{2R'} = \frac{L}{2h} \alpha \Delta T$$

For purposes of illustration consider a cast iron guideway with the following specifications:

$$\alpha = 9 \times 10^{-6}, \quad L = 400 \text{ mm}, \quad \Delta T = 1^\circ\text{C}$$

It follows then that:

$$d' = \frac{L}{8} \times \frac{400^2 \times (9 \times 10^{-6}) \times 1.0}{100} = 1.8 \text{ } \mu\text{m}$$

$$\Delta\theta' = \frac{400}{2 \times 100} (9 \times 10^{-6}) \times 1.0 = 1.8 \text{ } \mu \text{ rad}$$

IV. THICK-FLUID FILM LUBRICATION

The preceding chapter dealt with two bodies wherein sliding on each other was eased by a solid protective film as little as .005 microns thin. The friction and wear of these thin films are not negligible but in the light of the simplicity of such bearing systems they do provide effective lubrication for many commercial applications. On the other hand aside from metal to metal boundary lubrication wear, friction and dimensional instability of these thin films are not acceptable for precision systems especially at the higher rubbing speeds. An alternative strategy for bearing systems is to create a fluid film which is pressurized sufficiently to push the bearing surfaces apart so that surface asperities do not contact or interlock on each other. When this separation is accomplished wear is completely eliminated and friction is reduced to viscous shearing of the fluid film. Such attractive behavior is indeed realized in externally and self pressurized (EX.P & S.P.) bearings wherein the friction is less than 10% of the best thin film experience. While the fluid space separating the metal surfaces in these bearings is very small (less than $2.5 \mu\text{m}$ in some instances) it is nevertheless hundreds of times thicker than that of solid films discussed in section III. Hence by contrast these bearings are referred to as thick film bearings. Alternatively since the friction experienced is so much less, this form of lubrication is sometimes referred to as perfect lubrication. The friction and wear characteristics of the thin films of section III were a consequence of the rheological (mechanical) properties of the film generated. On the other hand the viscosity of the fluid is the property dictating thick fluid film lubrication.

EX.P and S.P. lubrication is essentially a process whereby fluid inertia and viscosity forces generate hydraulic pressures capable of lifting one surface off its mate. The analytical mechanics describing this action is based on the fundamental Navier-Stokes Equations of Appendix AIV.1. A completely rigorous solution of the N-S equations is a formidable challenge even with the fastest computers. Fortunately there are reasonably realistic engineering approximations appropriate to bearings which can reduce the N-S equations to tractable forms. Stripped of the less effective terms as is done in Appendix AIV.1 the remaining key elements clarify the physics of pressure generation and distribution. These simplifications lead to useful quantitative determinations.

Appendix AIV.1 demonstrates the process of reducing the N-S equations to the partial differential equations of EX.P. or S.P. lubrication. The fundamental simplifying assumption stems from the observation that the film thickness of practical fluid film bearings is infinitesimal compared to the other two flow path dimensions. It is therefore further assumed that pressure, viscosity, and density variations across the film are negligible compared to these variations along the other two flow paths. The slit like geometry of the flow path also encourages the assumption that the Reynolds number in most practice will be sub-critical. That is the inertia forces of the N-S equations are negligible compared to the dissipative (viscous) forces. These initial relaxations of the complete N-S equations lead to lubrication equation EIV.1. This equation will be referred to here as the generalized Reynolds equation.

$$\frac{\partial}{\partial x} \left(\frac{h^3}{\mu} \rho \frac{dp}{dx} \right) + \frac{\partial}{\partial y} \left(\frac{h^3}{\mu} \rho \frac{dp}{dy} \right) = 12(\text{r.h.s.}) \quad \text{EIV.1}$$

where: $h(x,y)$ = fluid film thickness
 $\mu(x,y)$ = fluid viscosity
 $\rho(x,y)$ = mass density of fluid
 $p(x,y)$ = fluid pressure of the film

$$\text{r.h.s.} = \rho \left\{ u_I \left(\frac{\partial z}{\partial x} \right)_I - u_{II} \left(\frac{\partial z}{\partial x} \right)_{II} + v_I \left(\frac{\partial z}{\partial y} \right)_I - v_{II} \left(\frac{\partial z}{\partial y} \right)_{II} \right\} +$$

$$\frac{\partial}{\partial x}(\rho h u) + \frac{\partial}{\partial y}(\rho h v) +$$

$$\frac{\partial(\rho h)}{\partial t} - (\Phi_{II,f} + \Phi_{I,f})$$

where: u and $v = \frac{(\dot{x}_{(II/0)} + \dot{x}_{(I/0)})}{2}$ and $\frac{(\dot{y}_{(II/0)} + \dot{y}_{(I/0)})}{2}$

Subscripts II, I, and 0 refer to points on the upper surface,
lower surface and stationary reference point.

$\Phi_{II,f}$ and $\Phi_{I,f}$ = fluid mass flux rate into interface clearance film through
surface II and I respectively.

Furthermore additional reductions are allowed if the following observations are also applicable

1. Bearing surfaces are not porous. That is there is no fluid flow through the bearing surfaces $\Phi_{II,f} = \Phi_{I,f} = 0$.
2. Fluid is incompressible that is density is invariant ($\frac{\partial \rho}{\partial t} = 0$).
3. Viscosity is constant throughout the film.

4. Only surface II is moving and that only along the x axis.

5. Surfaces do not pulsate ($\frac{\partial h}{\partial t} = 0 = \frac{\partial z}{\partial t}$).

6. Surfaces are not stretchable, $\frac{\partial U_{II}}{\partial x} = 0$.

7. Surface I lies in the x, y plane ie ($\frac{\partial z}{\partial x}$)_I = ($\frac{\partial z}{\partial y}$)_I = 0.

These further reductions to the N.S. equations lead to the familiar lubrication equation EIV.2a.

$$\frac{\partial}{\partial x} (h^3 \frac{\partial p}{\partial x}) + \frac{\partial}{\partial y} (h^3 \frac{\partial p}{\partial y}) = -6 \mu U \frac{\partial h}{\partial x} \dots \quad \text{EIV.2a}$$

where: $U = \dot{x}_{(II/0)}$

Even before equation EIV.1 is actually solved for $p(x,y)$ it does convey the roles played by the parameters of the physical model. The right hand side (r.h.s.) identifies the terms responsible for the fluid flow (pumping) sources within the clearance between the bearing surfaces. The left hand side (l.h.s.) of EIV.1 not only contains the pressures one would seek from a solution but also the resistivity to the flow through the clearance $h(x,y)$. Referring to the rudimentary model and its equation EIV.2a the r.h.s. indicates that for self generation of flows to occur, the product $\dot{x}_{(II/0)} \cdot \frac{\partial h}{\partial x}$ must exist in most regions of the film domain. That is one surface must have a sliding velocity and the clearance h must vary in places i.e. a hydraulic wedge or step must occupy some portion of the film domain. In the case of a linear slideway $\dot{x}_{(II/0)}$ does occur. If one surface were allowed to rock relative to its mate $\partial h / \partial x$ would also occur but such cyclic rocking is not acceptable for precision systems. In precision slideways

$\frac{\partial h}{\partial x} \simeq 0$ except for errors in the guiding surfaces hence the r.h.s. of EIV.2a is essentially zero and the lubrication equation becomes EIV.2b

$$\frac{\partial}{\partial x} \left(h^3 \frac{\partial p}{\partial x} \right) + \frac{\partial}{\partial y} \left(h^3 \frac{\partial p}{\partial y} \right) = 0 \dots \quad \text{EIV.2b}$$

If atmospheric gauge pressure, $p = 0$, prevails as the sole boundary condition to EIV.2b there will be no pressure generated in the film. Thick film lubrication therefore fails to develop in this model. The bearing system retreats to the thin film of boundary lubrication described in section III.

It is sometimes argued that hand scraping of linear guideways creates pockets with sloped sides such that local $\frac{dh}{dx} \neq 0$ and therefore the r.h.s. of EIV.2a could exist in spots throughout the film domain. But pockets due to scraping or error undulations in the surfaces produce a surface profile of odd symmetry. The resulting pressures generated will also be in odd symmetry throughout the film domain. Hence the sum total of the localized self generated lifts is zero. This neutralizing symmetry could be destroyed if the sliding velocity $\dot{x}_{(II/0)}$, were sufficiently high to cause cavitation on the trailing side of each pocket. The velocity needed to incur cavitation however is well beyond the sliding velocities of linear guides. Finally since stop-go motion is the usual mode of action for linear guides, the sliding velocity near each end of travel decays causing the r.h.s. of the Reynolds equation to decay as well even if an average $\frac{dh}{dx}$ did exist. In short it could be said that self pressurized (S.P.) lifting of the surfaces is not a realistic expectation for precision linear guideways. Unless external pressurization (EX.P.) is provided precision linear guideways will operate on only the thin film of boundary lubrication.

Externally Pressurized Guideway (The Hydrostatic Bearing)

If the r.h.s. of EIV.2a is negligible, as argued above with respect to linear precision guideways, this equation can be reduced to the homogeneous form EIV.2b. If further one considers a flat linear guideway ($\frac{\partial h}{\partial x} = \frac{\partial h}{\partial y} = \frac{\partial h}{\partial z} = 0$) this equation can be reduced further to the Laplacian form EIV.3.

$$\frac{\partial^2 p}{\partial x^2} + \frac{\partial^2 p}{\partial y^2} = 0 \quad \text{EIV.3}$$

The determination of the pressure $p(x,y)$ distribution from EIV.3 depends on the x,y plan view of the domain D occupied by the working fluid and the pressures, p_B , existing at the boundaries of the domain. A trivial solution of EIV.3 occurs when p_B is constant all along the boundaries. Then by observation $p(x,y) = p_B = \text{a constant}$. If only ambient gauge pressure ($p_B = 0$) acts on the boundaries domain pressure $p(x,y)$ will also disappear. Hence there is no lift force as was already suggested in the earlier discussion of EIV.2a. To generate a working pressure inside the domain it is necessary that the boundary pressures impressed vary around the boundaries of the lifting domain. Such is the condition which prevails in EX.P flat bearings. Fig. IV.1 is an effective model of a basic hydrostatic linear guideway. The upper sliding member II is a precision ground surface with a series of pockets machined into the surface Fig. IV.1a,b. The pressure distribution working on the sliding member II at sample sections A-A and B-B is also illustrated. The integral of the pressures at such sections becomes the generated lift W . If laminar flow is assumed for the model of Fig. IV.1a,b there is an analogous electrical resistance net work (see Appendix I for analogs). Hence the established iconics and terminology of electrical net works can be transferred to the

fluid system to advantage as in Fig. IV.1c.

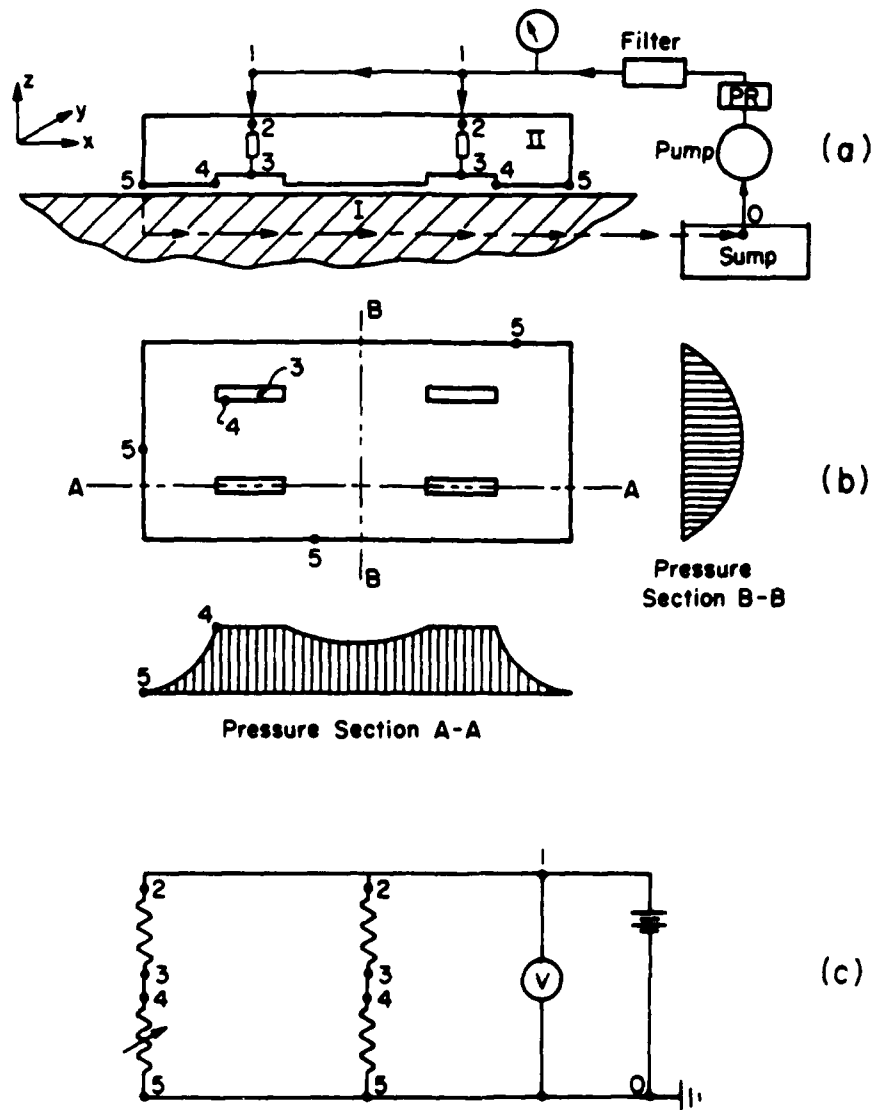


Fig. IV.1 Basic Hydrostatic Slideway

Mechanics of an Elementary Hydrostatic Bearing.

The pump between terminals 0 (sump) and 1 (pump outlet) of the hydraulic system Fig IV1.a, raises the pressure by $p_{1/0}$. The pressurized oil continues through the manifold from 1 to 2 with a negligible pressure drop hence $p_{2/0} \simeq p_{1/0}$. Between stations 2 and 3 there is a fluidic resistor causing the pressure drop $p_{2/3}$. The fluid continues into the pocket identified by the boundary contour 4. As will be explained later the pocket pressure drop $p_{3/4} \simeq 0$. The fluid continues from boundary 4 through the bearing clearance domain to the exit boundary 5. From 5 the fluid continues by gravity feed back to the sump 0. The flow through the domain bounded by contours 4 and 5 is through a passage with parallel flat surfaces separated by a film thickness h of the order of $50 \mu\text{m}$. This surface domain throughout which the clearance h defines the lubricating film is alternatively referred to as the clearance zone or as the land of the bearing. The viscous resistance to this flow and the flow from 2 to 3 are the controlling resistances (R_{4-5} and R_{2-3}) to the total flow.

The starting point to the quantitative analysis is the determination of the lift force W generated by the surface with boundaries defined by the contours 4 and 5. The pocket areas yield a lift $W_p = p_{3/0} \times \text{pocket area}$. The pressure at terminal 0 is the ambient pressure. Further it may be assumed that there is a negligible pressure drop from 3 to 4 across the pocket. The land domain (4-5) contributes a lift W_l based on the integration of pressure over the area of this region. Solution of EIV.3 will provide $p(x,y)$ for this integration. Solving this equation for a domain even as simple as that shown in Fig. IV.1 however involves complex techniques. For exposition's sake consider initially the simpler hydrostatic bearing of Fig. IV.2 rather than the model of

Fig.IV.1. This substitution will serve to high light the role of physical parameters without the blurring effects of analytical complexity.

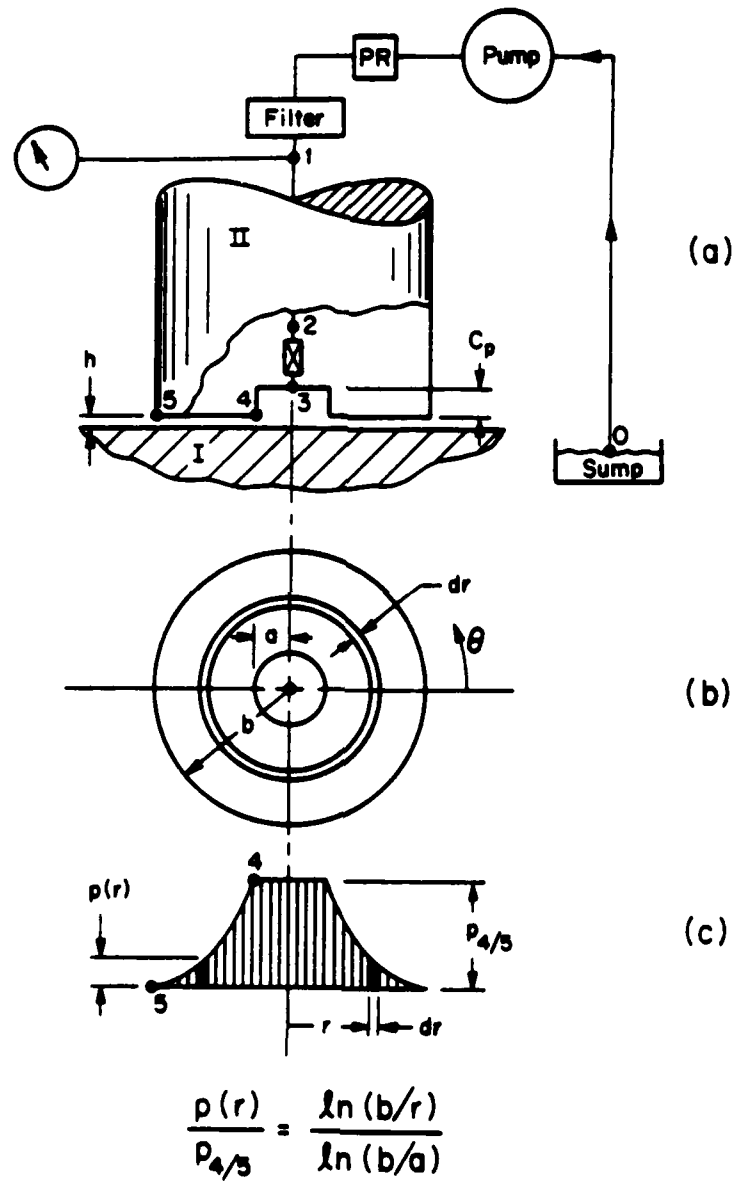


Fig. IV.2 Circular Hydrostatic Bearing

The Laplace partial differential equation EIV.3 prevails for the fields of Fig. IV.2 but polar coordinates are more convenient for the case of a circular domain. A transformation such as described in the complex variable reference⁽¹⁾ yields the equivalent harmonic equation EIV.4a

$$r^2 \frac{\partial^2 p}{\partial r^2} + r \frac{\partial p}{\partial r} + \frac{\partial^2 p}{\partial \theta^2} = 0 \quad \text{EIV.4a}$$

From symmetry of the pressure map about axis there will be no tangential variation in p i.e.

$$\frac{\partial p}{\partial \theta} = \frac{\partial^2 p}{\partial \theta^2} = 0$$

Hence the coordinate θ disappears as a variable. The partial differential equation above now becomes the ordinary differential equation EIV.4b

$$r^2 \frac{d^2 p}{dr^2} + r \frac{dp}{dr} = 0 \quad \text{EIV.4b}$$

From Appendix A.IV.2 the solution to EIV.4b for the specific case of Fig. IV.2 is

$$\frac{p(r)}{p_{4/0}} = \frac{L_n(b/r)}{L_n(b/a)} \quad \text{EIV.5a}$$

Lifting Capacity of Hydrostatic Bearings

The pressure solution integrated over the land area 4-5 yields the lift W_l . The lift contributed by the pocket area is $W_p = \pi a^2 p_{3/0}$. The total lift $W = W_l + W_p$ is given by EIV5.b (Appendix AIV.2).

$$W = p_{3/0} \cdot \pi b^2 \cdot K_w \text{ where } K_w = \frac{1-(a/b)^2}{L_n(b/a)^2} \quad \text{EIV.5b}$$

The lift force W for other bearing plan views will also be expressed as EIV.5b but of course with K_w taking on a form reflecting the actual geometry in point.

Most practical land and pocket geometries do not lend themselves to closed form solutions as was done for the case of Fig. IV.2 in the illustrative derivation. Conformal mapping⁽¹⁾ could be used to analyze a few more plan view patterns. Electrical conducting sheet analog tests is an experimental alternate to conformal mapping. Reference⁽²⁾ contains a directory of various bearing land plan views for which $p(x,y)$ were determined from electrical resistance sheet analogs. W_c was subsequently determined by numerical integration. Specific load coefficients K_w could be abstracted from the appropriate performance figures of reference⁽²⁾.

The analog method used for reference⁽²⁾ as well conformal mapping are limited to the solution of the Laplace equation. These methods have been largely superseded by numerical approximation methods. The Finite Difference, Finite Element and the Boundary Element Methods not only readily solve the more general Reynolds equation but also compute various related subsidiary data. A simplification of the Finite Element Method well suited to the lubrication equation is described in Appendix AIV.3. At this point however it is expedient to continue with the special case of the circular hydrostatic bearing to explore some of the general behavior characteristics of EX.P bearings.

Flow Rate Through the Bearing

The volumetric flow rate Q_{4-5} through the clearance domain 4-5 and the corresponding pressure drop due to laminar flow appears from Appendix AIV.2 as a fluidic equivalent of Ohm's law namely

$$p_{4/5} = \frac{6\mu L_n(b/a)}{\pi h^3} Q_{4.5}$$

which takes on the more familiar Ohm's law form

$$p_{4/5} = R_{4-5} Q_{4.5} \quad \text{EIV.5c}$$

where R_{4-5} = fluidic resistance to flow from contour 4 to contour 5. The resistance can be written as

$$R_{4-5} = \frac{6\mu}{h^3} \cdot S_r \quad \text{EIV.5d}$$

S_r is a function of the shape of domain 4-5. In the case of Fig. IV.2 S_r is easily calculated to be $\frac{L_n(b/a)}{\pi}$. For the general case it would be computed as a part of the numerical analysis. Reference (2) plots conductances for other land geometries from which specific S_r could be evaluated.

The important observation to be made here is that in general the clearance resistances are proportional to h^{-3} and viscosity μ and that S_r is function of geometric proportions and not the actual size of the clearance domain.

The cubic form of the clearance is a significant factor in the attractive behavior of bearings. The h^3 term also explains the earlier assumptions that the pressure drop across the pocket 3-4 is negligible. Consider a normal situation where h in region 4-5

is about 50 μm and the depth of the pocket is 10 x larger ($c = .5 \text{ mm}$) then the resistance R_{4-5} is 10^3 x larger than R_{3-4} . Hence the pressure drop within the pocket domain 3-4 is insignificant by comparison with the pressure drop in domain 4-5.

Static Stiffness k_s of Linearly Sliding Hydrostatic Bearings

Let k_s be the stiffness resisting changes in the nominal film thickness h due to changes in nominal bearing load W . Then

$$k_s = -\frac{dW}{dh} \text{ or } k_s = \frac{d}{dh}(Ap_{3/0}K_w) = -W \frac{p'_{3/0}}{P_{3/0}} \quad \text{EIV.6}$$

$$\text{where } p'_{3/0} = \frac{dp_{3/0}}{dh}$$

The nature of the pressure $p_{3/0}$ is defined by the details of the circulating system. The most common circulating system for EX.P. bearings is based on a constant pressure source. The pressure regulator P.R. maintains $p_{1/0}$ at a constant value while the flow rate is left to vary with variations in h . A less common system is based on a constant flow source without restrictor 2-3. In this case $p_{1/0}$ is left to vary with variations in h . The constant flow source will be discussed later. With a constant pressure source an intermediate restrictor 2-3 is necessary if the stiffness k_s is not to vanish.

Gauge pressure $p_{3/0}$ is related to the pressures at the other terminals by the loop equation for an across variable defined in Section I. Applied to the specifics of Fig. IV.1, the loop equation is $p_{3/0} = p_{3/2} + p_{2/1} + p_{1/0}$. Since $p_{2/1} \approx 0$ the preceding equation becomes $p_{3/0} = p_{3/2} + p_{1/0}$.

$$\text{Let: } \phi = \frac{P_{2/3}}{P_{3/0}} \text{ or } \frac{P_{2/3}}{P_{4/5}} \text{ or } \frac{P_{2/3}}{P_{4/0}}$$

It follows that $P_{4/5} = P_{1/0} \frac{1}{1+\phi}$. From Appendix AIV.2 lift W of EIV.6 can now be written, in terms of the fixed supply pressure $P_{1/0}$ as $W = A P_{1/0} \left(\frac{1}{\phi+1} \right) K_w$ where $\phi = \frac{R_{2-3}}{R_{4-5}}$.

The flow restrictor 2-3 acts as a resistor $R_{2/3}$ to create the pressure drop $P_{2/3}$. There are three types of passive restrictors in common use for hydrostatic bearings i.e.

- a. Laminar Flow Restrictor with a fixed resistance R_{2-3} . The most usual form is that of a capillary tube of length L_c and an ID of d_c .

$$\text{The constitutive equation in that case is } Q_{2,3} = \frac{\pi d_c^4}{128 \mu L_c} \cdot P_{2/3}$$

- b. Orifice Restrictor in the form of Fig. IV.3a below. The orifice discharge freely into the pocket domain 3-4. The flow pressure relationship is the basic orifice equation of incompressible flow.

$$Q_{2,3} = C_D \frac{\pi d_o^2}{4} \sqrt{\frac{2}{\rho} (P_{2/3})} \text{ where}$$

C_D = coefficient of discharge

d_o = orifice diameter

ρ = mass density of fluid

- c. Inherently Compensated Restrictor or the name preferred here Proximity Restrictor. This is a variation on the simple Orifice Restrictor as in the Fig. IV.3b below. The orifice is placed so close to the opposing bearing surface that the restricting area to flow is not the orifice

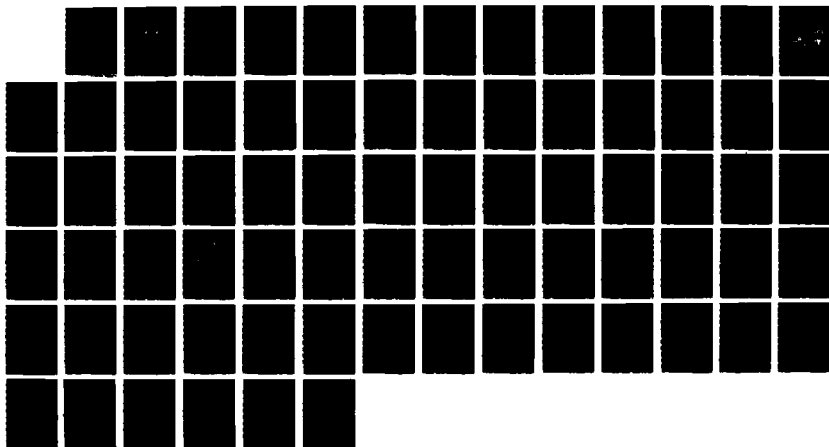
AD-A181 836

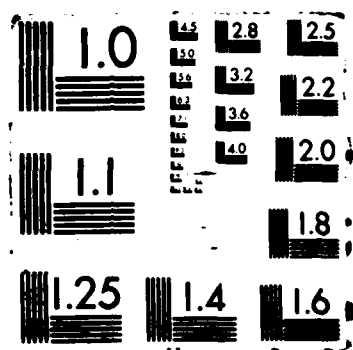
THE SCIENCE OF AND ADVANCED TECHNOLOGY FOR
COST-EFFECTIVE MANUFACTURE OF (U) PURDUE UNIV
LAFAYETTE IN SCHOOL OF INDUSTRIAL ENGINEERING J MODREV
DEC 86 N00014-83-K-0385 F/G 13/8

2/2

UNCLASSIFIED

NL





area $\frac{\pi d_o^2}{4}$ but rather the area $\pi d_2 h$ as shown because $\pi d_2 h \ll \frac{\pi d_o^2}{4}$

ie $\frac{d_o}{4} \gg d_2 h$.

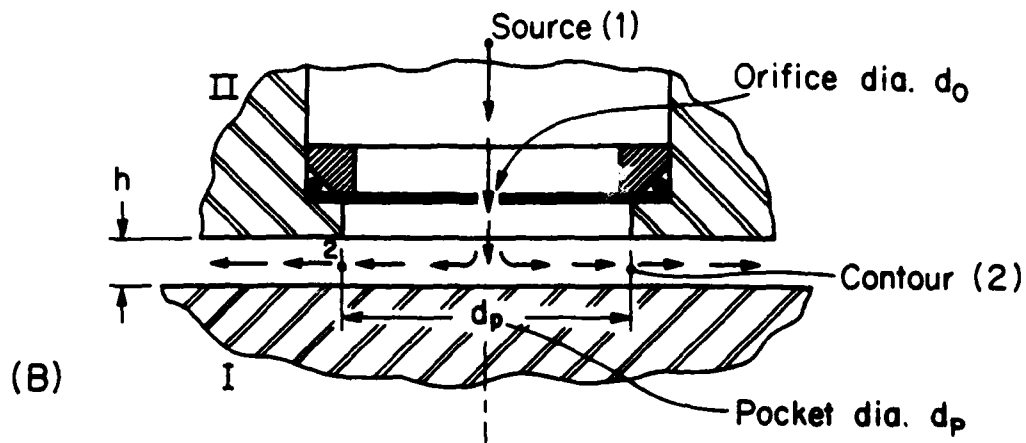


Fig. IV.3a Orifice Restrictor

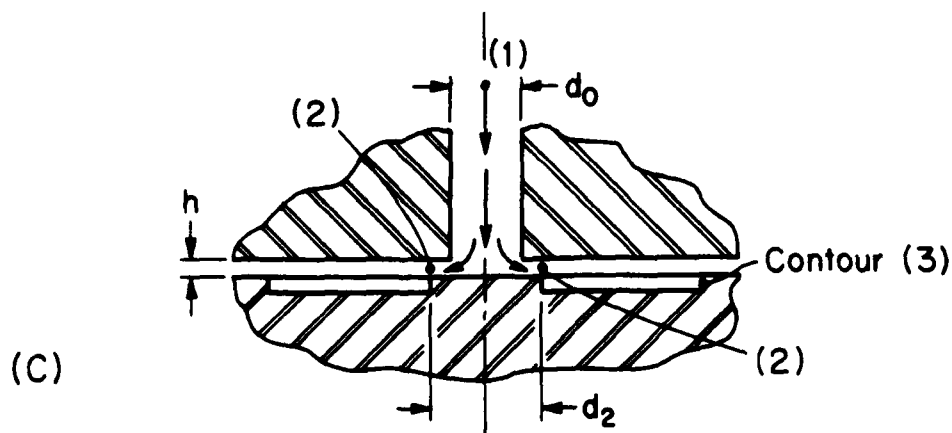


Fig. IV.3b Inherently Compensated (Proximity) Restrictor

The constitutive equation now is

$$Q_{2.3} = C_d \pi d_o h \sqrt{\frac{2}{\rho} p_{2/3}}$$

The various restrictors might be said to be represented by the generalized constitutive equation

$$Q_{2.3} = C_{2-3} h^\alpha p_{2/3}^\beta \quad \text{EIV.7}$$

where the exponent α assumes values of 1, $\frac{1}{2}$, $\frac{1}{2}$ respectively for the restrictors defined above.

From the series arrangement of resistances of Fig. IV.2,

$$Q_{4.5} = Q_{2.3} \text{ hence } K_{4-5} \cdot p_{4/5} = C_{2-3} \cdot h^\alpha \cdot p_{2/3}^\beta$$

where $K_{4-5} = (R_{4-5})^{-1} \dots$ Conductance

Differentiating the above two sides w. r. to h

$$\frac{d}{dh} (K_{4-5} \cdot p_{4/5}) = C_{2-3} h^\alpha \left(\frac{\alpha}{h} (p_{2/3})^\beta + \beta (p_{2/3})^{\beta-1} \cdot (p_{2/3})' \right)$$

$$\text{or } Q_{4.5} \left[3/h + \frac{p'_{4/5}}{p_{4/5}} \right] = Q_{2.3} \left[-\frac{\alpha}{h} - \beta \frac{p'_{2/3}}{p_{2/3}} \right]$$

Since $p_{2/3} = p_{2/1} + p_{1/0} + p_{0/5} + p_{5/4} + p_{4/3}$ or

$$p_{2/3} = 0 + p_{1/0} + 0 + p_{5/4} + 0$$

$$p'_{2/3} = 0 + 0 + 0 - p'_{4/5}$$

which when substituted into the r.h.s of the above equilibrium equation yields.

$$-3/h + \frac{p'_{4/5}}{p_{4/5}} = -\frac{\alpha}{h} - \frac{\beta p'_{4/5}}{\phi p_{4/5}}$$

hence

$$\frac{p'_{4/5}}{p_{4/5}} \left(1 + \frac{\beta}{\phi}\right) + \frac{1}{h} (3 - \alpha) = 0$$

Applying EIV.6

$$k_s = -W \frac{p'_{4/5}}{p_{4/5}} = -\frac{W}{h} \left[\frac{3 - \alpha}{1 + \beta/\phi} \right] \text{ or}$$

$$k_s = -\frac{W}{h} \cdot (3 - \alpha) \cdot \left[\frac{\phi}{\phi + \beta} \right] \quad \text{EIV.8}$$

Optimizing k_s w.r. to choice of $\phi = \frac{p_{2/3}}{p_{4/5}}$

This optimum occurs at $\frac{dk_s}{d\phi} = 0$. Hence

$$\frac{dk_s}{d\phi} = \frac{-d}{d\phi} \left(W \cdot (3 - \alpha) \cdot \frac{\phi}{\phi + \beta} \right) = -(3 - \alpha) \left[\frac{dW}{d\phi} \cdot \left(\frac{\phi}{\phi + \beta} \right) + \frac{W}{\phi + \beta} - \frac{W\phi}{(\phi + \beta)^2} \right]$$

$$\text{where: } \frac{dW}{d\phi} = \frac{d}{d\phi} \left(Ak_u \cdot p_{4/5} \right) = \frac{d}{d\phi} \left(Ak_w p_{4/0} \frac{1}{(1 + \phi)} \right)$$

$$\therefore \frac{dW}{d\phi} = Ak_w p_{1/0} \left(-\frac{1}{(1 + \phi)^2} \right) = -W \frac{1}{(1 + \phi)}$$

Substituting $dW/d\phi$ into the previous equation for $\frac{dk_s}{d\phi}$.

$$\frac{dk_s}{d\phi} = \frac{-(3 - \alpha)W}{\phi + \beta} \left[\frac{-\phi}{1 + \phi} + 1 - \frac{\phi}{\phi + \beta} \right]$$

$$\text{for } \frac{dk_s}{d\phi} = 0 = 1 - \phi \left(\frac{1}{1 + \phi} + \frac{1}{\phi + \beta} \right) = 0 \quad \text{Hence } \phi^2 = \beta \quad \phi_{\text{opt}} = \beta^{1/2}$$

The final tabulation of stiffnesses associated with the three types of upstream res-

trictors is given by TABLE II.

TABLE II
Performance Characteristics by Restrictor, R_{2-3} Types

Restrictor 2-3	C_{2-3}	α	β	k_s	ϕ_{opt}	$k_{s,max}$
a. Capillary	$\frac{\pi d_c^4}{128\mu L_c}$	0	1	$\frac{-W}{h} \cdot 3 \cdot \frac{\phi}{\phi+1}$	1	$-1.5 \frac{W}{h}$
b. Orifice	$C_D \frac{\pi d_o^2}{4} \sqrt{\frac{2}{\rho}}$	0	1/2	$\frac{-W}{h} \cdot 3 \cdot \frac{\phi}{\phi+\frac{1}{2}}$	$\beta^{\frac{1}{2}}$	$-1.757 \frac{W}{h}$
c. Proximity *	$C_D \pi d_o \sqrt{\frac{2}{\rho}}$	1	1/2	$\frac{-W}{h} \cdot 2 \cdot \frac{\phi}{\phi+\frac{1}{2}}$	$\beta^{\frac{1}{2}}$	$-1.171 \frac{W}{h}$

$$\phi = \frac{P_{2/3}}{P_{4/5}}, \quad W = A \cdot P_{1/0} \cdot \frac{1}{1+\phi}, \quad k_s = -\frac{W}{h} \cdot (3-\alpha) \cdot \frac{\phi}{(\phi+\beta)}, \quad Q = C_{2-3} h^n P_{2/3}^d$$

* Inherently compensated restrictor.

Quantitative Performance of a Sample EX.P. Bearing.

Given the nondimensional load coefficient K_w and the flow resistance shape factor S_r , the quantitative performance figures are readily generated as demonstrated in the Appendix AIV.2. As mentioned earlier K_w and S_r however must come from a numerical solution of EIV.3 for each EX.P. bearing plan view. To continue a study of the magnitudes of performance the analysis of AIV.2 borrows the K_w and S_r for a circular bearing. Other plan views will have their own characteristic values but most likely practical plan views will have K_w and S_r coefficients differing by less than 60% from the sample circular model. This difference can not be ignored for practical design but for the time being the circular model is taken in AIV.2.

The bearing chosen for the demonstration was that of Fig. IV.2 with the following specification:

Diameter of contour 5 = 100 mm

Diameter of contour 4 = 50 mm

Viscosity $\mu = .07 \text{ Ns/m}^2$ (light oil)

Clearance $h = 40 \text{ }\mu\text{m}$

Restrictor 2-3 a capillary with $\phi = 1$

Supply pressure, $p_{1/0} = 3.45 \times 10^5$ pascals

Sliding speed = 0.2 m/s

From these given data the following performance figures were determined:

- 1) Load carrying capacity $W = 731\text{N}$
- 2) Oil flow rate $Q = 1.19 \times 10^{-7} \text{ m}^3/\text{s}$
- 3) Pump power required. Power = 0.164 watts
- 4) Restrictor 2-3 is a capillary tube 0.75 mm ID and length of 164 mm
- 5) Static stiffness = $27.4 \times 10^6 \text{ N/m}$
- 6) Coefficient of friction = .0028
- 7) Reynolds Number at the inner edge of the 4-5 field was 3.8

The data above such as the coefficient of friction, low power requirements etc. speak adequately for themselves. But one must compare the bearing stiffness to the flexural rigidity of a cast iron beam to adequately appreciate the stiffness of a hydrostatic bearing. The stiffness k_s reported ($27.4 \times 10^6 \text{ N/m}$) is identical to that of a cast iron box beam 100 mm x 100 mm x 1000 mm with a wall thickness of 10 mm and centrally loaded in bending. The major dimension of the bearing, its diameter, is no more

than the width of the cast iron beam used for comparison.

Lateral Guidance and Bidirectional Bearing Performance.

So far the bearing was presented as a device for supporting unidirectional vertical loads. Guideways on the other hand must restrain in transverse as well as vertical directions. Hydrostatic bearings can be applied to all four faces as in Fig. IV.4 to do just that. Along the transverse direction (x axis) the opposite bearing faces balance each other hydrostatically. However external disturbances acting to cause displacements along the x axis will be resisted by a hydraulic stiffness. This arises from an extension of the analysis made for Fig. IV.2 of the stiffness in the z direction. Earlier the stiffness of a single hydrostatic bearing film was described as $k_s = -\frac{W}{h} \cdot 3 \left(\frac{\phi}{\phi + \beta} \right)$ or $k_s = 3 \frac{P_{1/0}}{h} AK_w \left(\frac{\phi}{\phi + \beta} \right)$. If two faces oppose each other they combine to double the stiffness ie $k_s = 2 \times 3 \left(\frac{P_{1/0}}{h_0} AK_w \left(\frac{\phi}{\phi + \beta} \right) \right)$

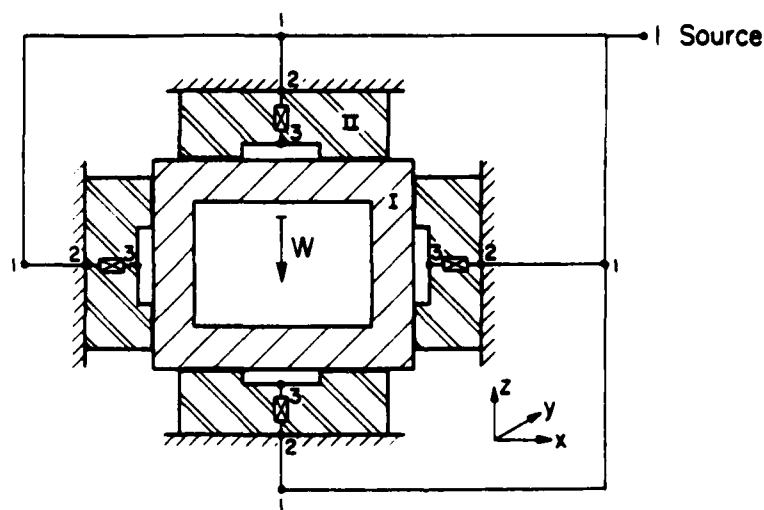


Fig. IV.4 Hydrostatic Guideway Two Dimensional Translatory Restraint.

For the case of the unidirectional bearing of Fig. IV.2 the supply pressure was related to the applied load W . For bidirectional bearing arrangements $p_{1/0}$ may be arbitrarily set to any higher value. The higher the supply pressure the greater the static stiffness attained. For instance in the quantitative example given earlier a unidirectional bearing called for $p_{1/0} = 3.45 \times 10^5$ pascals to support a load of 731N and yielded a stiffness $k_s = 27.4 \times 10^6$ N/m. With the double acting system of Fig. IV.4 not only is the stiffness automatically double in the x direction but also if the supply pressure $p_{1/0}$ is increased four fold the overall stiffness in the x direction is now $k_s = 2 \times 4 \times 27.4 \times 10^6 = 219.2 \times 10^6$ N/m. If this eight fold increase in stiffness were matched again by a cast iron beam it would be a 168 mm x 168 mm x 1000 mm box beam, while the bearing geometry retains its original diameter.

If the transverse constraint was by boundary lubricated surfaces, sideways play would be inevitable even if mitigated by gibs as in Fig. II.4a. With hydrostatic bearings on these surfaces there is a sideways restraint equivalent to an enormously stiff hydraulic spring with negligible imposed drag.

The resistance by the upper and lower bearings to z directed deflections is slightly stronger because of the static load W carried by this pair. As the static load W is applied the upper clearance increases from h_0 , its zero load value, while the lower bearing clearance decreases by the same amount. The two stiffnesses combine to produce

$$k_s = 3 \times p_{1/0} AK_w \left(\frac{\phi}{\phi + \beta} \right) \left(\frac{1}{h_o + \Delta h} + \frac{1}{h_o - \Delta h} \right)$$

$$\text{or } k_s = 3 \times p_{1/0} AK_w \left(\frac{\phi}{\phi + \beta} \right) \frac{2}{h_o \left(1 - \left(\frac{\Delta h}{h_o} \right)^2 \right)}$$

where:

$h_o =$ Bearing clearance no load situation.

$\Delta h =$ Change in bearing clearance due to the imposition of a load W .

Pitching and Yawing Restraint

The vertical and horizontal guidance as described above is very effective. But a bearing with a single source and single pocket 3-4 in a symmetrical field 3-4-5 will develop almost no resistance to pitch, yaw and roll. However two bearings side by side as in Fig. IV.5 will use their moment arms and kinematics to generate moment stiffness. If the bearing faces I and II are exactly parallel to each other ($\beta = 0$ Fig. IV.5a) both bearings will show the clearance h_o . With a pitch angle (b) β the clearance is now wedge like and unequal in the two bearings. For the left hand bearing the clearance is squeezed down and therefore the flow resistance $R_{4'-5'}$ increases over the neutral case of $\beta = 0$. Because of this increased resistance the flow rates $Q_{4'5'}$ and $Q_{2'3'}$ decrease. Pressure drop $p_{2'3'}$ will correspondingly reduce. That is the pressure level $p_{3'/0}$ will increase beyond the neutral level $p_{3/0}$ Fig. IV.5c. This means that the lift force W' of the left hand bearing will grow as the clearance h' is depressed. On the r.h.s. the action on surface 3"-4"-5" is the converse to that of the l.h.s. The two bearings together then create a correcting moment to opposing rotation β . A repeat of this

argument with another pair of bearings in the transverse direction will provide yawing restraint. These same effects are realized by a bearing with multiple sources as in Fig. IV.1.

To compute the pitching stiffness k_j , one must solve the Laplace equation EIV.2b. A simple solution is no longer available for any plan form including the circular plan exploited earlier for its simplicity. Numerical analysis is practically the sole tool for quantitative evaluation of angular stiffness.

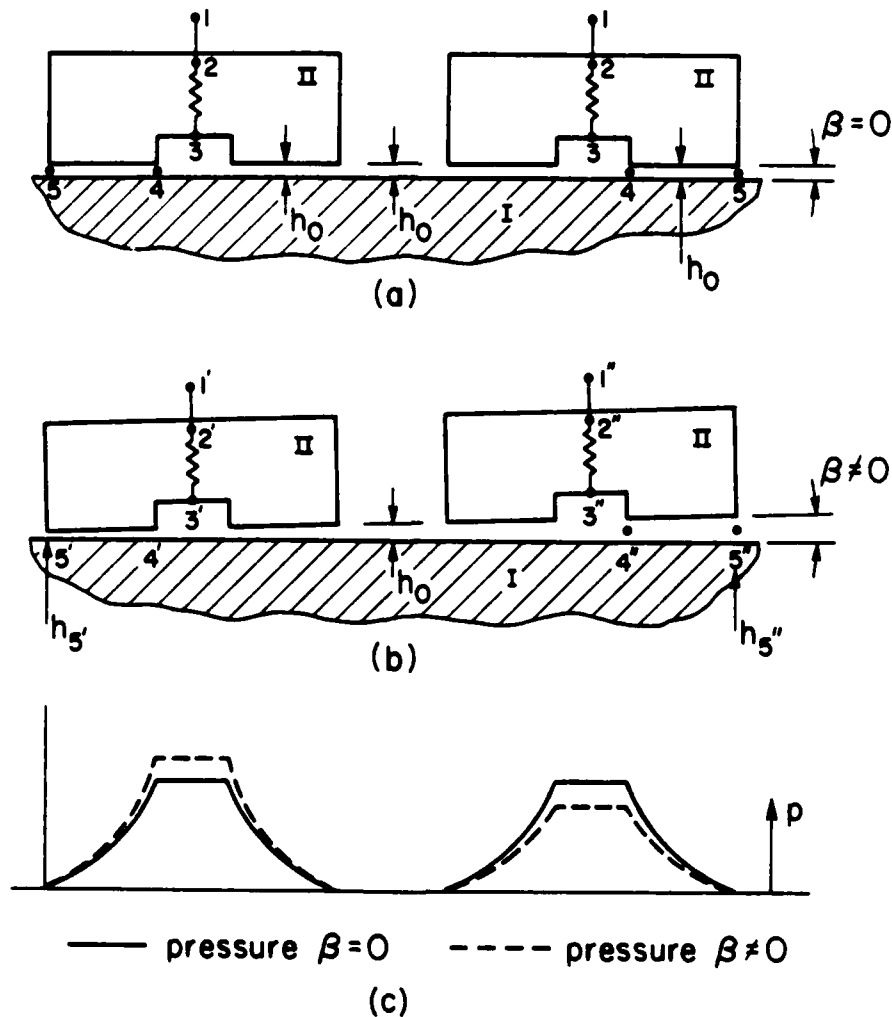


Fig. IV.5 Mechanics of Pitching Restraint.

Constant Flow Source

The constant pressure source described above is the dominant choice for EX.P. systems. A constant flow source is an alternative occasionally preferred because this yields a bearing of somewhat superior stiffness. For a unidirectional EX.P. bearing with a fixed flow rate the stiffness $k_s = 3 \frac{W}{h}$ rather than $k_s = \frac{3}{2} \frac{W}{h}$ which is the best that the fixed pressure source can offer. With a constant flow source there is no control restrictor 2-3 hence some simplification is gained on this score. On the other hand a regulator capable of maintaining a fixed flow rate, despite pressure variations, is a more complex mechanism than a combination of pressure regulator and any of the 2-3 resistors described earlier. Furthermore with a fixed pressure source several bearings can be fed from a single point. On the other hand if a fixed flow source system is chosen each bearing must have its own constant flow regulator. This adds considerably to the complexity of the system.

Adaptive Control of Hydrostatic Slideways

Increasing expectations for precision guidance puts evermore emphasis on support stiffness for slideways and more error free guideways. A double acting guideway as in Fig. IV.4 is preferred for the sake of stiffness over the single acting hydrostatic models of Fig. IV 1,2. However guideway precision is still limited by the geometric errors of a large complex structural element such as a conventional guideway. An adaptive control whereby the slider is positioned to a more precise reference line can generate stiffness and precision performance beyond the inherent limitations of a structural guideway. No other system of sliding or rolling support is better suited to adaptive

control than the hydrostatic floating principle because the support pressure is so easily manipulated.

Reference 6 and Fig. IV.6 from that reference represent a basic adaptive control system applied to the hydrostatic double acting guideway principle. The passive control restrictors 1-2 of Figs. IV 1,2,4 are now replaced with a differential control valve (D.C.V.) which is activated by reference to a precision straight edge (SE). Tuning throttles (TT_u and TT_l) replace the flow conserving and pressure generating resistances of the thin films of Figs. IV 1,2,4. The tuning throttles are essentially miniature hydrostatic pads, surrogates for the 4-5 zone of Figs. IV 1,2,4.

The operation of the adaptive control system is as follows. The tuning throttles TT have their clearances h_T (upper) and h_T (lower) initially set so that, at the expected nominal load W carried by the slider II, the upper and lower valve opening gaps (G_u , G_l) of the DCV Fig. IV.6b are equal. That is the valve is in neutral position at nominal load W . If operating conditions add a dynamic increment in load, δw , slider II will depress δz relative to the reference straight edge SE. The upper gap G_u of the DCV will increase by δ_z so increasing the upper valve flow rate. Simultaneously the lower gap G_l will decrease reducing the lower valve flow rate. The upper DCV flow feeds into the lower junction J_l and onto TT_l . The increased flow rate due to δz will cause an increase in back pressure at J_l hence the lifting force of the lower pocket will increase to counter the δw imposed. Similarly the lower valve gap feeds flow into J_u and thence through TT_u . The reduced flow from the lower valve allows the back pressure on TT_u to decrease. Hence δz causes a decrease in upper pocket pressure adding to the lift force countering δw . The push-pull pressure variations on slider II causes it to stabilize near the neutral level. With the pockets sealed around their

peripheries there is essentially zero flow rate from junctions J to the pockets. Hence the pocket depths play no role in positioning control. It then follows that errors in the geometry of these pockets have no effect on positioning precision. Fidelity is determined by the precision straight edge SE. It is claimed⁽⁶⁾ that, when this system was set for a nominal load of 1176 N, a variation of ± 980 N altered the static position no

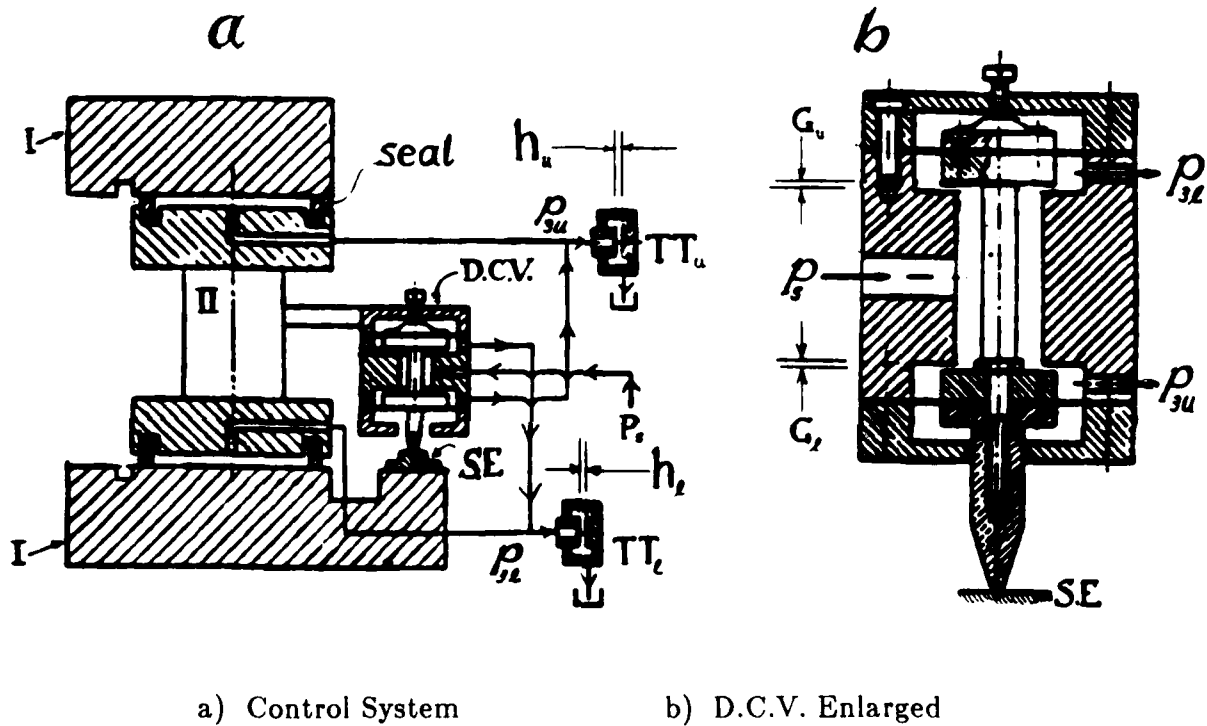


Fig. IV.6 Adaptive Control of Hydrostatic Guideway. Ref. 6.

References IV

1. R. Churchill, "Introduction to Complex Variables and Applications", McGraw Hill.
2. H. C. Rippel, "Cast Bronze Hydrostatic Bearing Design Manual", Cast Bronze Bearing Institute 1975.
3. Shih-I, Pai, "Viscous Flow Theory - I Laminar Flow", D. Van Nostrand Inc.
4. H. Schlichting, "Boundary Layer Theory", McGraw Hill Book Co.
5. A Cameron, "Principles of Lubrication", John Wiley & Sons.
6. C. V. Fikin, A. N. Pivouarov, "Study of Non-Flow Two Sided Hydrostatic Support", STANK I. INSTRUMENT, V. 46, Issue 3, 1975.
7. S. H. Crandall, "Engineering Analysis", McGraw Hill Book Co.
8. K. H. Huebner, "The Finite Element Method for Engineers", John Wiley & Sons.
9. Becker, Carey and Oden, "Finite Elements", Prentice Hall, V. 1, 1981.
10. Zienkiewicz, "The F.E.M. in Structural and Continuum Mechanics", McGraw Hill, 1967.

APPENDIX: AIV.1

Reduction of Navier-Stokes Equations

The analytics of specific problems of fluid flow have their origins in the general equations of Navier-Stokes^{3,4,5}. This set of equations is based on the equilibrium of forces acting on the faces of an infinitesimally small fluidic cube. The N-S implicitly include all of the stress terms involved in the equilibrium. This total rigour results in equations that defy closed form solutions for the most general case. Specific problems however allow order-of-magnitude comparison of terms in the N-S equations and a subsequent reduction of these equations to more tractable forms. Such is the case with the lubrication problem where reductions described here lead to the Reynolds p.d.e., EIV.1.

The foundation of the N-S structure is the equilibrium of intensive forces $\overline{\mathcal{F}}$ (N/m³) acting on cubic element dx, dy, dz. Using the notation of Section I this equation is

$$\overline{\mathcal{F}}_{e,e} = \overline{\mathcal{F}}_{E,e} + \overline{\mathcal{F}}_{S,e}$$

where: $\overline{\mathcal{F}}_{*,e}$ = inertial intensive force acting on the cube e.

$\overline{\mathcal{F}}_{E,e}$ = Intensive force that earth exerts on cube e. That is the gravitational body force acting on e.

$\overline{\mathcal{F}}_{S,e}$ = Intensive force that medium S contacting the cube e exerts on it.

Force $\overline{\mathcal{F}}_{S,e}$ is compounded of contributions from the normal stress (pressure p) and parallel stress (shear τ). The latter stress arises from the viscous drag on the faces of e hence

$$\overline{\mathcal{F}}_{S,e} = \overline{\mathcal{F}}_{p,e} + \overline{\mathcal{F}}_{\tau,e}$$

The complete intensive force equation becomes E.AIV.1a

$$\overline{\mathcal{F}}_{e,e} = \overline{\mathcal{F}}_{E,e} + \overline{\mathcal{F}}_{p,e} + \overline{\mathcal{F}}_{\mu,e} \quad \text{E.AIV.1a}$$

The necessary Continuity Equation for the cube e is

$$\frac{d\rho}{dt} + \nabla \cdot (\rho \bar{u}) = \dot{\phi}_{e,s} \quad \text{E.AIV.1b}$$

ρ = mass density of fluid

\bar{u} = velocity vector of fluid at the cube e

$$= u \hat{i} + v \hat{j} + w \hat{k}$$

$\dot{\phi}_{e,s}$ = mass leakage rate from e to a sink s (per m^3 of element e).

The Through terms of E.AIV.1a and the Across terms of E.AIV.1b are related by the appropriate Constitutive Laws E.AIV.1c, c', c''.

$$\overline{\mathcal{F}}_{e,e} = \rho \frac{D\bar{u}}{Dt} = \rho \left[\frac{\partial \bar{u}}{\partial t} + (\bar{u} \cdot \nabla) \bar{u} \right] \quad \text{E.AIV.1c}$$

$$\text{where } \bar{u} \cdot \nabla = u \frac{\partial}{\partial x} + v \frac{\partial}{\partial y} + w \frac{\partial}{\partial z}$$

$$\overline{\mathcal{F}}_{E,e} = \rho g \hat{E}/e \quad \text{E.AIV.1c'}$$

$$\overline{\mathcal{F}}_{p,e} = \nabla p = \frac{\partial p}{\partial x} \hat{i} + \frac{\partial p}{\partial y} \hat{j} + \frac{\partial p}{\partial z} \hat{k}. \quad \text{E.AIV.1c''}$$

The fourth term $\overline{\mathcal{F}}_{\mu,e}$ has an associated constitutive law which does not lend itself to abbreviated expressions as those above. It is now expedient to represent $\overline{\mathcal{F}}_{\mu,e}$ as the matrix E.AIV.1d the elements of which are taken from references^{3,4,5}.

$$\overline{\mathcal{F}}_{\mu,e} = \begin{bmatrix} (a_1 + a_2 + a_3) \\ (b_1 + b_2 + b_3) \\ (c_1 + c_2 + c_3) \end{bmatrix} \quad \text{E.AIV.1d}$$

$$\begin{aligned} a_1 &= \frac{\partial}{\partial x} \left[\mu \left(2 \frac{\partial u}{\partial x} - \frac{2}{3} \nabla \cdot \bar{U} \right) \right] \\ b_1 &= \frac{\partial}{\partial y} \left[\mu \left(2 \frac{\partial v}{\partial y} - \frac{2}{3} \nabla \cdot \bar{U} \right) \right] \\ c_1 &= \frac{\partial}{\partial z} \left[\mu \left(2 \frac{\partial w}{\partial z} - \frac{2}{3} \nabla \cdot \bar{U} \right) \right] \end{aligned} \quad \text{E.AIV.1d'}$$

$$\nabla \cdot \bar{U} = \frac{\partial u}{\partial x} + \frac{\partial v}{\partial y} + \frac{\partial w}{\partial z}$$

$$\begin{aligned} a_2 &= \frac{\partial}{\partial y} \left[\mu \left(\frac{\partial u}{\partial y} + \frac{\partial v}{\partial x} \right) \right] ; a_3 = \frac{\partial}{\partial z} \left[\mu \left(\frac{\partial w}{\partial x} + \frac{\partial u}{\partial z} \right) \right] \\ b_2 &= \frac{\partial}{\partial z} \left[\mu \left(\frac{\partial v}{\partial z} + \frac{\partial w}{\partial y} \right) \right] ; b_3 = \frac{\partial}{\partial x} \left[\mu \left(\frac{\partial u}{\partial y} + \frac{\partial v}{\partial x} \right) \right] \\ c_2 &= \frac{\partial}{\partial v} \left[\mu \left(\frac{\partial w}{\partial x} + \frac{\partial u}{\partial z} \right) \right] ; c_3 = \frac{\partial}{\partial y} \left[\mu \left(\frac{\partial v}{\partial z} + \frac{\partial w}{\partial y} \right) \right] \end{aligned} \quad \text{E.AIV.1d''}$$

Simplification by Orders of Magnitude Deletions

Equation E.AIV.1d is a major hurdle to meaningful analysis. The operating dimensions and materials for lubricating systems allow the following simplifications.

1. The film thickness h (z axis) at any point of bearing is about three orders of magnitude smaller than the transverse flow path length that the fluid will traverse. It follows then that the velocity gradients relate as

$$\begin{aligned} \frac{\partial u}{\partial z} &\ggg \frac{\partial u}{\partial x} , \frac{\partial u}{\partial y} \\ \frac{\partial v}{\partial z} &\ggg \frac{\partial v}{\partial x} , \frac{\partial v}{\partial y} \\ \frac{\partial w}{\partial z} &\lll \frac{\partial u}{\partial z} , \frac{\partial v}{\partial z} \end{aligned}$$

Hence: $\nabla \cdot \bar{u} \lll \frac{\partial u}{\partial z}, \frac{\partial v}{\partial z}$

and: $a_2 \lll a_3$

$b_2 \ggg b_3$

Furthermore any mixed second derivative is orders of magnitude smaller than

$$\frac{\partial^2 u}{\partial z^2} \text{ or } \frac{\partial^2 v}{\partial z^2}$$

Deleting the higher order of magnitude terms reduces E.AIV.1d to E.AIV.1e

$$\overline{\mathcal{F}}_{u,e} = \begin{bmatrix} \frac{\partial}{\partial z} \left(\mu \frac{\partial u}{\partial z} \right) \\ \frac{\partial}{\partial z} \left(\mu \frac{\partial v}{\partial z} \right) \\ 0 \end{bmatrix} \quad \text{E.AIV.1e}$$

2. $\overline{\mathcal{F}}_{E,e} \lll \overline{\mathcal{F}}_{\mu,e}$ because the weight of a thin (h) element of lubricant is negligibly small compared to the viscous terms.
3. Referring back to $\overline{\mathcal{F}}_{e,e}$, the flow in the thin film is essentially laminar so that kinetic effects are small. Except for unusual systems the inertial stresses are negligible compared to shear stresses arising from viscous drag i.e. $\overline{\mathcal{F}}_{e,e} \lll \overline{\mathcal{F}}_{\mu,e}$.
4. Finally $\partial p / \partial z \lll \partial p / \partial x$ hence also $\frac{\partial}{\partial z} \left(\mu \frac{\partial}{\partial z} \right)$ terms.

Hence the N-S equations for purposes of more lubrication situations is

$$\begin{bmatrix} 0 \\ 0 \\ 0 \end{bmatrix} = - \begin{bmatrix} \partial p / \partial x \\ \partial p / \partial y \\ 0 \end{bmatrix} + \begin{bmatrix} 0 \\ 0 \\ 0 \end{bmatrix} + \begin{bmatrix} \frac{\partial}{\partial z} (\mu \frac{\partial u}{\partial z}) \\ \frac{\partial}{\partial z} (\mu \frac{\partial v}{\partial z}) \\ 0 \end{bmatrix} \quad \text{E.AIV.1f}$$

Derivation of the Reynolds Equations for Thin Film Lubrication

The generalized Reynolds Equation E.IV.1 is based on continuity of flows in and out of the sample volume, Fig. AIV.1. Surfaces I and II represent the two bodies of a bearing separated at points $x_{I/0}$, $y_{I/0}$ by the distance $h = z_{II/I}$. Let $\mathcal{M}_{\alpha,f}$ be the mass flow rate from face α into the control volume f using the subscript notation rules of Section I. The conservation law described in Section I becomes in this specific case

$$\mathcal{M}_{w,f} + \mathcal{M}_{e,f} + \mathcal{M}_{s,f} + \mathcal{M}_{n,f} + \mathcal{M}_{II,f} + \mathcal{M}_{I,f} + \dot{\psi}_{I,f} + \dot{\psi}_{II,f} = 0 \quad \text{E.AIV.1g}$$

$$\text{but } \mathcal{M}_{w,f} + \mathcal{M}_{e,f} = \mathcal{M}_{w,f} - \mathcal{M}_{f,e} = - \frac{\partial}{\partial x} \mathcal{M}_{w-e} dx$$

$$\text{and } \mathcal{M}_{s,f} + \mathcal{M}_{n,f} = - \frac{\partial}{\partial y} \mathcal{M}_{s-n} dy$$

$$\mathcal{M}_{II,f} = -\rho w_{II} dx dy + \rho u_{II} dy \left(\frac{\partial z}{\partial x} \right)_{II} dx + \rho v_{II} dx \left(\frac{\partial z}{\partial y} \right)_{II} dy$$

$$\text{where: } u_{II} = \dot{x}_{II/0}, v_{II} = \dot{y}_{II/0}, w_{II} = \dot{z}_{II/0}$$

$\rho w_{II} dx dy =$ Mass flow out of f due to the velocity of element $dx dy$ at II moving away from f .

$\rho v_{II} dy \left(\frac{\partial z}{\partial x} \right)_{II} dx =$ Mass flow rate into volume f due to the element $dx dy$ at II traveling into f at a velocity $u_{II} \left(\frac{\partial z}{\partial x} \right)_{II}$. The latter being a component of u_{II}

along the outer normal to the surface at point II.

$\rho v_{II} dx (\frac{\partial z}{\partial y})_{II} dx$ Same general mechanics as above.

$$\mathcal{M}_{1f} = -\rho w_I dx dy - \rho u_I (\frac{\partial z}{\partial x})_I dx dy - \rho v_I (\frac{\partial z}{\partial y})_I dx dy$$

$$u_I = \dot{x}_{I/0} \quad v_I = \dot{y}_{I/0} \quad w_I = \dot{z}_{I/0}$$

$\dot{\phi}_{1f}$ = Mass flux rate through the skin (pores) at point I into the control volume f.

$\dot{\phi}_{II,f}$ = Mass flux rate through the skin at point II into the control volume f.

$$\mathcal{M}_{p,f} = -h \frac{\partial p}{\partial t} dx dy$$

Entering these definitions into E.AIV.1g produces continuity equation E.AIV.1h

$$\begin{aligned} \frac{\partial \mathcal{M}}{\partial x} dx + \frac{\partial \mathcal{M}}{\partial y} dy = \rho \left[-w_{II/I} + u_{II} \left(\frac{\partial z}{\partial x} \right)_{II} - u_I \left(\frac{\partial z}{\partial x} \right)_I + \dots \right. \\ \left. \dots + v_{II} \left(\frac{\partial z}{\partial y} \right)_{II} - v_I \left(\frac{\partial z}{\partial y} \right)_I \right] dx dy + \dots \\ \dots + [\dot{\phi}_{II,f} + \dot{\phi}_{1f} - h \frac{\partial \rho}{\partial t}] dx dy \end{aligned} \quad \text{E.AIV.1h}$$

$$\frac{\partial \mathcal{M}}{\partial x} dx = dx dy \left[\frac{\partial}{\partial x} \int_0^b \rho u dz \right] \quad \text{E.AIV.1i}$$

$$\text{From E.AIV.1f } \frac{\partial p}{\partial x} = \frac{\partial}{\partial z} \mu \frac{\partial u}{\partial z}$$

Integrating twice with b.c at $z = 0$, $u = u_I$, at $z = h$, $u = u_{II}$ yields

$$u = -\frac{\partial p / \partial x}{\partial \mu} (h^2 - z^2) + (z/h) u_{II/I} + u_I$$

Integrating and differentiating as per E.AIV.i yields

$$\frac{\partial \mathcal{A}}{\partial x} dx = dx dy \left[-\frac{1}{12} \frac{\partial}{\partial x} \left(\frac{\rho h^3}{\mu} \right) \frac{\partial p}{\partial x} + \frac{1}{2} \frac{\partial}{\partial x} \rho h (u_I + u_{II}) \right]$$

In a similar fashion

$$\frac{\partial \mathcal{A}}{\partial y} dy = dy dx \left[-\frac{1}{12} \frac{\partial}{\partial y} \left(\frac{\rho h^3}{\mu} \right) \frac{\partial p}{\partial y} + \frac{1}{2} \frac{\partial}{\partial y} \rho h (v_I + v_{II}) \right]$$

Substituting these definitions into E. AIV.1h and recognizing that

$$w_{II}/\rho + h \partial p / \partial t = \frac{\partial(\rho h)}{\partial t}$$

$$\begin{aligned} \frac{\partial}{\partial x} K \frac{\partial p}{\partial x} + \frac{\partial}{\partial y} K \frac{\partial p}{\partial y} &= \rho \left[u_I \left(\frac{\partial z}{\partial x} \right)_I - u_{II} \left(\frac{\partial z}{\partial x} \right)_{II} + v_I \left(\frac{\partial z}{\partial y} \right)_I - v_{II} \left(\frac{\partial z}{\partial y} \right)_{II} \right] + \dots \\ &\dots + \left[\frac{\partial}{\partial x} (\rho h U) + \frac{\partial}{\partial y} (\rho h V) \right] + \left[\frac{\partial \rho h}{\partial t} - (\dot{\phi}_{II,I} + \dot{\phi}_{II,I}) \right] \quad \text{E.IV.1} \end{aligned}$$

$$\text{where:} \quad K = \frac{\rho h^3}{12\mu} \quad U = \frac{u_I + u_{II}}{2} \quad V = \frac{v_I + v_{II}}{2}$$

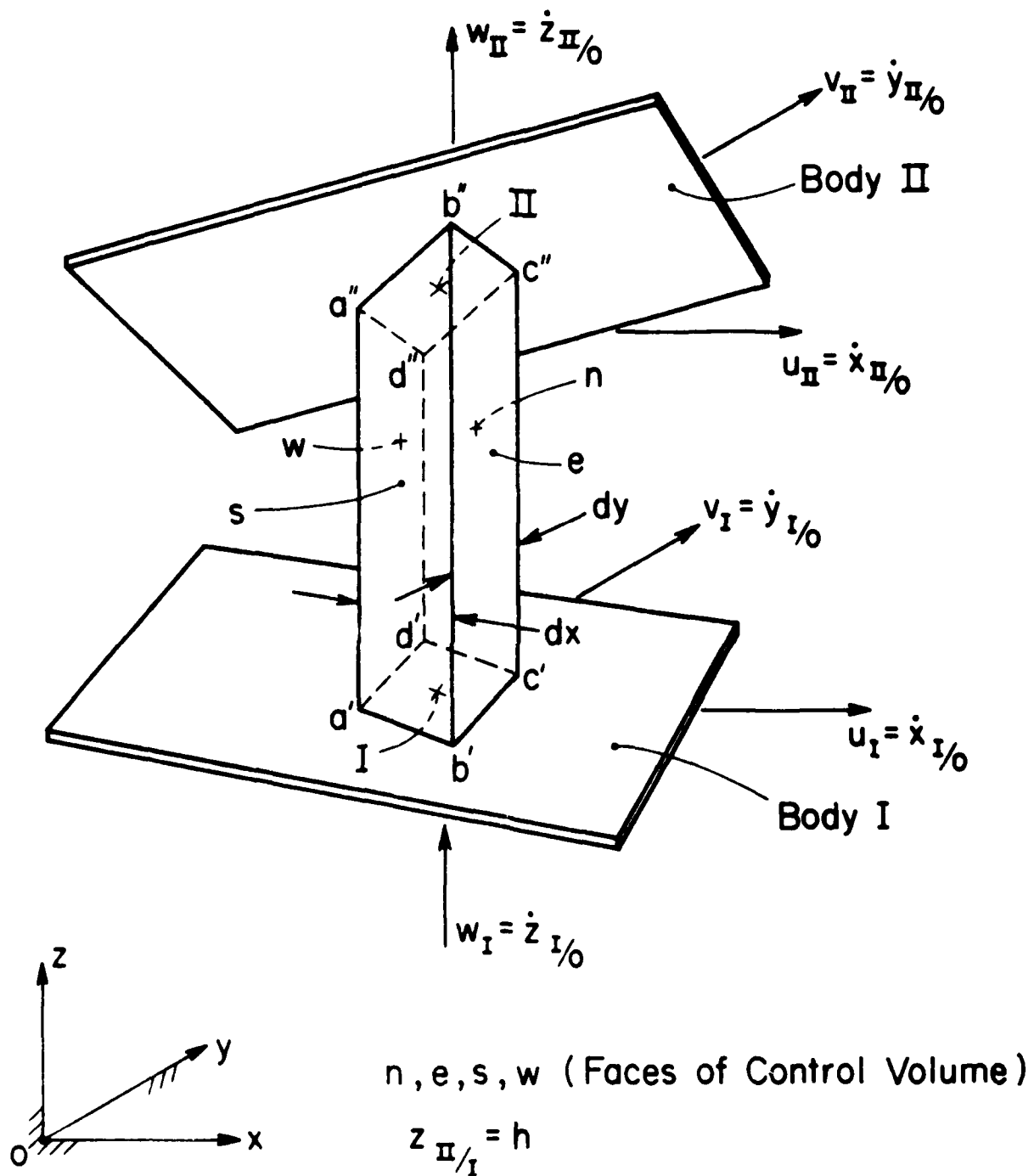


Fig. AIV.1 Element of Thick Film Between Moving Surfaces I & II.

APPENDIX: AIV.2

Pressure Distribution in Clearance Zone 4-5 Fig. IV.5

Differential equation for zone 4-5 is

$$r^2 \frac{d^2 p}{dr^2} + r \frac{dp}{dr} = 0 \quad \text{EIV.4b}$$

Let $S = \frac{dp}{dr}$ then equation EIV.4b becomes $r^2 \frac{dS}{dr} + rS = 0$. Which in turn yields

$$S = \frac{-C_1}{r} = \frac{dp}{dr} \text{ and finally } p = -C_1 L_n(r) + C_2. \text{ Assuming b.c. at } r = a, p = p_{4/0}$$

and at $r = b, p_{5/0} = 0$ the coefficients C become:

$$C_1 = \frac{p_{4/0}}{L_n(b/a)} ; C_2 = C_1 L_n(b)$$

Applying these coefficients the solution for the gradient $\frac{dp}{dr}$ and the pressure of the circular pad bearing are:

$$\frac{dp}{dr} = -\frac{p_{4/0}}{r} \cdot \frac{1}{L_n(b/a)} \quad \frac{p}{p_{4/0}} = \frac{L_n(b/r)}{L_n(b/a)} \quad \text{EIV.5a}$$

Lifting forces W_p, W_ℓ and W

W_p : lift contributed by pocket bordered by contours 3 & 4.

$$W_p = p_{3/0} \cdot \pi a^2 \text{ assuming } p_{3/4} \simeq 0$$

W_ℓ : lift contributed by clearance domain 4-5.

$$W_\ell = \int_4^5 p dA = \frac{p_{4/0}}{L_n(\frac{b}{a})} 2\pi \int L_n(\frac{b}{r}) r dr$$

Let $(\frac{r}{b})^2 = q$ and $(\frac{a}{b})^2 = q_a$ then

$$W_c = \frac{\pi p_{4/0} b^2}{-L_n(q_a)} \int_{q_a}^1 -L_n(q) dq \text{ hence}$$

$$W_c = \frac{\pi p_{4/0} b^2}{L_n(q_a)} (1 - q_a L_n(q_a) - q_a)$$

Let $W = W_p + W_c$ (total lift)

$$W = p_{3/0} \pi a^2 + \frac{\pi p_{4/0} b^2}{L_n(q_a)} (1 - q_a L_n(q_a) - q_a)$$

Recall that: $p_{3/0} = p_{4/0}$ and $a^2 = b^2 q$ equation above becomes

$$W = p_{3/0} \pi b^2 q_a + p_{3/0} \pi \left(\frac{1}{L_n(q_a)} - q_a - \frac{q_a}{L_n q_a} \right) \text{ or}$$

$$W = p_{3/0} \pi b^2 \frac{[1 - (a/b)^2]}{L_n(b/a)^2} \quad \text{EIV.5b}$$

Therefore $W = p_{3/0} \cdot A \cdot K_w$; K_w is the lift coefficient for the wetted field 3-4-5 of Fig.

IV.3

$$K_w = \frac{1 - (a/b)^2}{L_n(\frac{b}{a})^2}$$

Other plan views with there own shaped contours 3-4-5 will have their own dimensionless expressions for K_w . These coefficients in most part must be computed by numerical analysis.

Flow rate $Q_{4.5}$ through the flow field 4-5

The flow entering border contour 4 and exiting the border contour 5 is $Q_{4.5}$ using the subscript notation and polarity rules for through variables of Section I. Flow rate $Q_{4.5}$ is related to $p_{4/5}$ with a constitutive law appropriate for the domain 4-5. The constitutive law can be borrowed from electrical mechanics by way of the analog relating one dimensional laminar flow Q to electrical current flow I . The current flow along a conductor t units thick, B units wide and a material conductivity k is described by the constitute equation $I = -ktB \frac{de}{dx}$.

Consider the sample element of the film in the clearance field between r and $r + dr$ of Fig. IV.3. The fluidic constitutive equation can be generated by the following analog transformations:

$$I \rightarrow Q, E \rightarrow p, dx \rightarrow dr, B \rightarrow 2\pi r, k \rightarrow c_f$$

The analogous constitutive equation becomes

$$Q_{r,(r+dr)} = -c_f h 2\pi r \frac{dp}{dr} \quad \text{where } c_f = \frac{h^2}{12\mu} \quad \mu = \text{viscosity}$$

A note on c_f : Traditional fluid mechanics does not explicitly designate a property c_f named here "fluidic conductivity". This term is introduced here, however, because it provides a necessary link in analysis by analog. It is the property of the fluid lamina bounded by the parallel walls of the clearance field.

The final form for the constitutive equation of the circular field 4-5 becomes

$$Q_{4.5} = \frac{-h^3}{6\mu} r \cdot \frac{dp}{dr}$$

Earlier the gradient of p was shown to be $\frac{dp}{dr} = \frac{-C_1}{r}$ with $C_1 = \frac{p_{4/0}}{L_n(\frac{b}{a})}$. Furth-

ermore for this illustration $p_{4/5}$ may be substituted for $p_{4/0}$ since $p_{5/0} = 0$.

Hence:

$$Q_r(r + dr) = Q_{4.5} = \frac{+h^3\pi}{6\mu} \frac{p_{4/5}}{L_n(\frac{b}{a})} \text{ or in the format of a fluidic "Ohm's Law". That}$$

is $Q_{4.5} = \frac{1}{R_{4-5}} p_{4/5}$ where resistance $= R_{4-5} = \frac{6\mu}{\pi h^3} L_n(b/a)$. For other shaped clear-

ance fields with uniform clearance h , $R_{4-5} = \frac{6\mu}{h^3} S_r$ where S_r is a resistance shape factor usually determined by numerical computation.

$$\text{Coefficient of Friction } f = \frac{D}{W}$$

Let $\bar{D}_{I,II}$ be the apparent drag force vector that surface I exerts on surface II. This force is actually that exerted by the fluid in the clearance on surface II. As such it is created by the fluid shear and pressure stresses acting on surface II that is

$$\bar{D}_{I,II} = \int \tau_{II} dA + \int p(r, \theta) \cdot \frac{dh}{dr} \cdot dA \text{ from contour 4 to contour 5.}$$

$$\tau_{II} = \text{shear stress on surface II} = \frac{dv}{dz}(II) \times \mu$$

The fluid velocity pattern within the clearance h is a composite of two parts (Fig.

$$\text{AIV.2-1) } \frac{dv}{dz} = \frac{dv'}{dz} + \frac{dv''}{dz}.$$

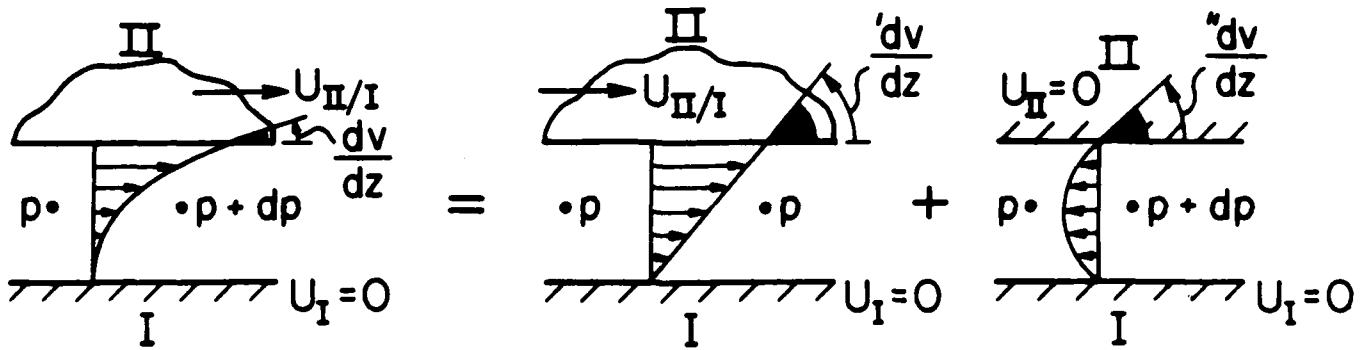


Fig. AIV.2-1 Thin Bearing Film Kinematics

$$\text{Therefore: } \int \tau(\text{II}) dA = \mu U_{\text{II/I}} \int \frac{1}{h} dA + \frac{1}{2} \int h \cdot \frac{dp}{dr} \cdot dA$$

$$\text{Hence: } D_{\text{I,II}} = \mu U_{\text{II/I}} \int \frac{1}{h} dA + \frac{1}{2} \int h \frac{dp}{dr} \cdot dA + \int \frac{dh}{dr} \cdot p \cdot dA$$

$$dA \approx r d\theta dr$$

The sliding velocity is taken to be constant in magnitude and oriented in a fixed direction. The pressure gradient $\frac{dp}{dr}$ on the other hand is assumed to vary with r and θ . If h and the plan view of the domains 3-4 and 4-5 are symmetrical about the z axis, the last two integrals disappear. Furthermore if the clearance h is constant as is the usual case for sliding tables the frictional drag reduces to

$$\bar{D}_{\text{I,II}} = \mu \bar{U}_{\text{II/I}} \left[\frac{A_{3-4}}{h_{3-4}} + \frac{A_{4-5}}{h_{4-5}} \right] \quad \text{E.AIV.2a}$$

Equation E.AIV.2a prevails for all symmetrical plan views not just the circular plan illustrated.

Quantitative evaluation of hydrostatic bearing performance.

Example:

Given: A circular pad bearing with the following specifications.

Light oil employed with a viscosity: $\mu = .07 \text{ Ns/m}^2$

Table sliding velocity: $U_{II/I} = .2 \text{ m/s}$

$a = 50 \text{ mm}$, $b = 100 \text{ mm}$, $\phi = 1$

Pump pressure: $p_{1/0} = 3.45 \times 10^5 \text{ pascals (N/m}^2\text{)}$

$h = 40 \text{ }\mu\text{m}$ Pocket depth = 2.0 mm

Find: Flow rate: Q

Coefficient of Friction: f

Size of capillary restrictor

Pumping power required: Power_p

Static stiffness: k_s

Lifting load capability: W

Solution:

Geometric properties:

$$A_{3-4} = \frac{\pi}{4} \times 50^2 = .1963 \times 10^4 \text{ mm}^2 = .196 \times 10^{-2} \text{ m}^2$$

$$A_{3-5} = \frac{\pi}{4} \times 100^2 = .785 \times 10^4 \text{ mm}^2 = .785 \times 10^{-2} \text{ m}^2$$

$$A_{4-5} = A_{3-5} - A_{3-4} = (.785 \times 10^{-2} - .196 \times 10^{-2}) = .589 \times 10^{-2} \text{ m}^2$$

$$W = p_{1/0} \cdot \frac{1}{1+\phi} \cdot A_{3-5} \cdot k_w \quad K_w = \frac{1 + \left(\frac{a}{b}\right)^2}{L_n(b/a)^2} = 0.54$$

$$W = 3.45 \times 10^5 \cdot \frac{1}{1+1} \cdot 0.54 \quad W = 731 \text{ N (164 lbs)}$$

Static Stiffness:

$$k_s = \frac{731 \cdot 3/2}{40 \times 10^{-6}} \quad k_s = 27.4 \times 10^6 \text{ N/m (156,000 lbs/in)}$$

This is identical to the flexural stiffness of a 1 m long cast iron ($E = 117 \times 10^9 \text{ N/m}^2$) box beam centrally loaded. The dimensions of the beam being 100 mm x 100 mm x 1000 m with a 10 mm wall thickness.

Viscous Table Drag:

$$D_{I,II} = \mu U_{II/I} \left\{ \frac{A_{3-4}}{h_{3-4}} + \frac{A_{4-5}}{h_{4-5}} \right\} \quad \text{E.AIV.2a}$$

$$D_{I,II} = .07 \times 0.2 \left\{ \frac{.196 \times 10^{-2}}{2 \times 10^{-3}} + \frac{.589 \times 10^{-2}}{40 \times 10^{-6}} \right\}$$

$$D_{I,II} = 2.06 \text{ N}$$

$$(0.46 \text{ lbs})$$

Coefficient of Friction:

$$f = \frac{D_{I,II}}{W} = \frac{2.06}{731} \quad f = .0028$$

Flow Rate: $Q_{4.5}$

$$Q_{4.5} = \frac{P_{4/5}}{R_{4-5}}, \quad P_{4/5} = \frac{P_{1/0}}{1 + \phi} = \frac{3.45 \times 10^5}{2} = 1.73 \times 10^5 \text{ pascals}$$

$$R_{4.5} = \frac{6\mu}{h^3} \frac{L_n(b/a)}{\pi} = \frac{6 \times .07}{(40 \times 10^{-6})^3} \cdot \frac{L_n(2)}{\pi}$$

$$R_{4-5} = \frac{1}{68} \times 10^{14} \text{ Ns/m}^5$$

$$Q_{4.5} = 1.725 \times 10^5 \times 68 \times 10^{-14}$$

$$Q_{4.5} = 119 \times 10^{-9} \text{ m}^3/\text{s}$$

$$(.436 \text{ in}^3/\text{min})$$

Pump Power:

$$\text{Power}_P \quad Q_{1.0} \times P_{1/0} = Q_{4.5} \times P_{1/0}$$

$$\text{Power}_P = 119 \times 10^{-9} \times 3.45 \times 10^5 = .041 \text{ Watts}$$

$$(5.5 \times 10^{-5} \text{ H.P.})$$

Assume that the combined efficiency of motor and pump is about $0.5 \times 0.5 = .25$ then:

Net Power dissipation = .164 watts

$$(.22 \times 10^{-3} \text{ H.P.})$$

Appropriate Resistor 2-3.

The choice of resistor ratio $\phi = 1.0$ anticipates a capillary type of controlling R_{2-3} . This might be a capillary tube with an inside diameter d_c . Considering the probabilities of clogging it would be desirable to keep d_c to more than 0.5 mm I.D. From Table

If the conductance of a capillary tube is $C_{2-3} = \frac{\pi d_c^4}{128 \mu \ell_c}$. The conductance of the

clearance field 4-5 is $C_{4-5} = \frac{h^3}{6\mu} \cdot \frac{1}{S_r}$. For the specific case of Fig. IV.2 $S_r = \frac{L_n(b/a)}{\pi}$.

From continuity $Q_{2,3} = Q_{4,5}$, or $C_{2-3} = C_{4-5}$ if $\phi = 1.0$ as given hence

$$\frac{\pi d_c^4}{128\mu \ell_c} = \frac{h^3}{6\mu} \frac{\pi}{L_n(b/a)} \quad \text{therefore}$$

$$\ell_c = \frac{d_c^4}{h^3} \times \frac{6}{128} L_n(b/a) \quad \text{where } d_c = .5 \times 10^{-3} \text{ m}$$

$$h = 40 \times 10^{-6} \text{ m}$$

$$b/a = 2.0$$

Yielding $\ell_c = .032 \text{ m} = 32 \text{ mm} (1.25 \text{ in})$

If a more prudent capillary ID was chosen such that $d_c = .75 \text{ mm}$ then $\ell_c = 32$
 $(\frac{.75}{.50})^4 = 162 \text{ mm} (6.3 \text{ in}).$

While the capillary tube is the common choice for laminar restrictors the above illustration does suggest some limits on performance. It would not be unreasonable to expect precision systems to run with clearances $h = 20 \mu\text{m}$ in the interest of increasing stiffness k_s . This halving of h will call for an eight fold increase in ℓ_c . Given a $d_c = 0.75 \text{ mm}$ the corresponding ℓ_d will now be $8 \times 163 \text{ mm}$ or $1.296 \text{ m} (51 \text{ in})$ a length which could be awkward to fit into assemblies or even to fabricate. There is however an alternate not often recognized.

Earlier in Section IV it was observed that the flow resistance R_{4-5} was independent of the actual size of the plan view so that another bearing geometrically similar but of a different scale will have the same resistance providing the fluid viscosity and clearance h were similar. This recognition suggests that a scaled down facsimile (except for h) of field 4-5 will be exactly what would be needed for the restrictor 2-3.

Calculations above are predicated on the flow in the clearance h being laminar. That is Reynolds Number < 2000 . For the passage formed by contour 4 of the pockets the Reynolds Number could be defined as

$$R_e^{\#} = \frac{Q_{4.5}/L_4}{\nu}$$

Where: L_4 = developed length of contour 4

ν = kinematic viscosity μ/ρ

(oil with $\mu = .07$, $\nu \approx 10^{-7}$)

For the illustrated bearing $L_4 = 2 \pi a = 2 \pi 50 \text{ mm}$, $Q_{4.5} = 119 \times 10^{-9}$ and $\nu = 10^{-7}$ (m,s) or

$$R_e^{\#} = \frac{119 \times 10^{-9}}{2\pi \cdot 50 \times 10^{-3}} \times \frac{1}{10^{-7}} = 3.8$$

Using a $\frac{1}{4}$ size facsimile for the restrictor 2-3 increases the $R_e^{\#}$ four fold to a value of 15.2.

APPENDIX: AIV.3

Linear Triangular Finite Element Method

The conductance and convection of currents through and out of a thin electrical conducting plate is described by the p.d.e. E.AIV.3a.

$$\frac{\partial}{\partial x} \left(kt \frac{\partial e}{\partial x} \right) + \frac{\partial}{\partial y} \left(kt \frac{\partial e}{\partial y} \right) - Ce = q(x,y) \quad \text{E.AIV.3a}$$

where: e = potential

$k(x,y)$ = conductivity of the plate material

$t(x,y)$ = plate thickness at point x,y

$q(x,y)$ = current flux from the surface to an external sink

$C(x,y)$ = coefficient of convection from surface to external sink.

This type of p.d.e. prevades much of physics and engineering. The Reynolds equation is obviously from this family where pressure p replaced voltage e and $\frac{\rho h^3}{12\mu}$ replaces kt . By this substitution where h is equivalent to t we can now define the fluidic conductivity of a thin film as being $\frac{\rho h^2}{12\mu} = k$.

Reduction of E.AIV.3a to algebraic form by the finite difference method is equivalent to setting up a rectangular network of conductors as in Fig. AIV.3a. The current flow from w to c actually takes place through the shaded band of Fig. AIV.3a. In the F.D. model the shaded band is represented by the discrete conductor $K_{w-c} =$

$$\left(\frac{k_w t_w + k_c t_c}{2} \right) \frac{dy}{dx}. \text{ In the same way } K_{s-c} \text{ would be shown to be } \left(\frac{k_s t_s + k_c t_c}{2} \right) \frac{dx}{dy},$$

$$K_{e-c} = \left(\frac{k_e t_e + k_c t_c}{2} \right) \frac{dy}{dx} \quad \text{and} \quad K_{n-c} = \left(\frac{k_n t_n + k_c t_c}{2} \right) \frac{dx}{dy}.$$

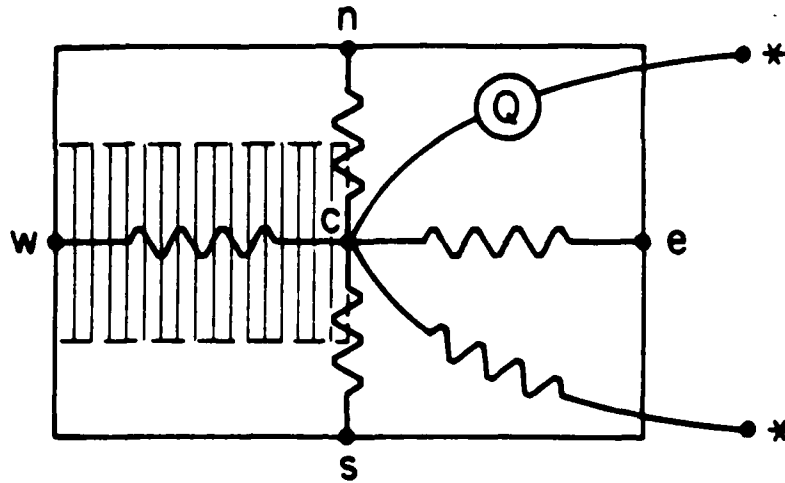


Fig. AIV.3a Finite Difference Model

From the conservation principle $I_{w-c} + I_{e-c} + I_{s-c} + I_{n-c} + I_{c-} = q_c \cdot dx \cdot dy$. Applying constitutive laws (Ohm's law in this illustration).

$$K_{w-c} e_{w/c} + K_{e-c} e_{e/c} + K_{s-c} e_{s/c} + K_{n-c} e_{n/c} + K_{c-} e_{-/c} = q_c \cdot dx \cdot dy \quad \text{hence}$$

$$K_{w-c} e_w + K_{e-c} e_e - [K_{w-c} + K_{e-c} + K_{s-c} + K_{n-c} + K_{c-}] e_c + \dots$$

$$\dots + K_{s-c} e_s + K_{n-c} e_n = q_c \cdot dx \cdot dy$$

In the rectangular network each of the nodes plays the role of the center node of five nodes. Thus a field with N interior nodes will yield N simultaneous equations represented by E.AIV.3b.

$$[K] \{e_c\} = dx \cdot dy \{q_c\} \quad \text{E.AIV.3b}$$

For the Reynolds equation p_c replaces e_c and the r.h.s. of EIV.1 replaces q_c . Equation E.AIV.3b is solved for e_c , that is p_c which integrated over the field yields the lift

W for the bearing field.

The Linear Triangular Element

A network of uniform rectangles, on which the F.D.M. is based, is not the best representation if the rectangular mesh does not conform well to the borders of the field and/or if the potential gradients are such as to suggest variable mesh spacings. A mosaic of assorted triangular tiles (finite elements) can be made to conform more successfully to the actual geometry. As in the net for the rectangular mesh it is desirable to establish conductors for the network lines between each node of triangular elements as indicated by Fig. AIV.3b.

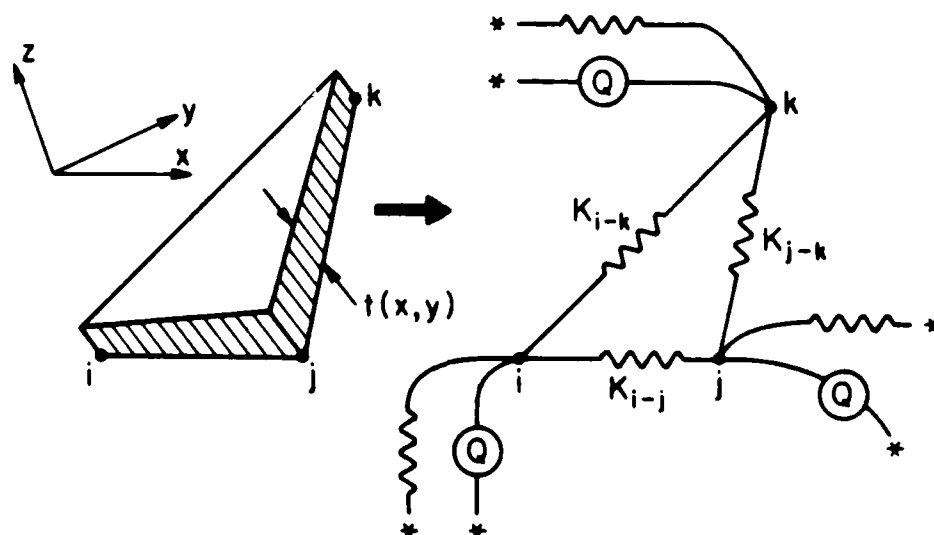


Fig. AIV.3b Linear Triangular Finite Element.

Derivation of the values of K_{i-j} , K_{i-k} , K_{j-k}

The equivalent discrete conductor for the F.D. model was easily evaluated from the conduction through the shaded portion of the rectangular mesh. The triangular mesh

can not be so directly analyzed. An energy principle of mechanics however will serve to establish equivalent conductors. This is the principle of Minimum Co-content⁷ (watts) which is an extension of the Minimum Potential Energy⁷ principle (joules). We shall here abstract from the principle of minimum Co-content a relationship which is sufficient for the purposes of establishing the discrete conductors equivalent to the linear continuum of the triangular element. That is, for any arbitrary combination of the potentials at nodes i, j, k the Co-content, \mathcal{C} , of the equivalent system of discrete conductors must be identical to the Co-content of the triangular element with a linear distribution of the potentials interior to it.

The determination of Co-content, \mathcal{C} , through the triangular element with linear potential distribution, Fig. AIV.3c, can be expedited if that figure is disassembled into component figures. Fig. AIV.3 ci, cj, ck. The Co-content for each component is a simpler analysis for which we shall use the figure ci for a sample derivation. Fig. AIV.3d is the plan view of the ci model. The strips parallel to the edge $i-j$ are lines of constant potential.

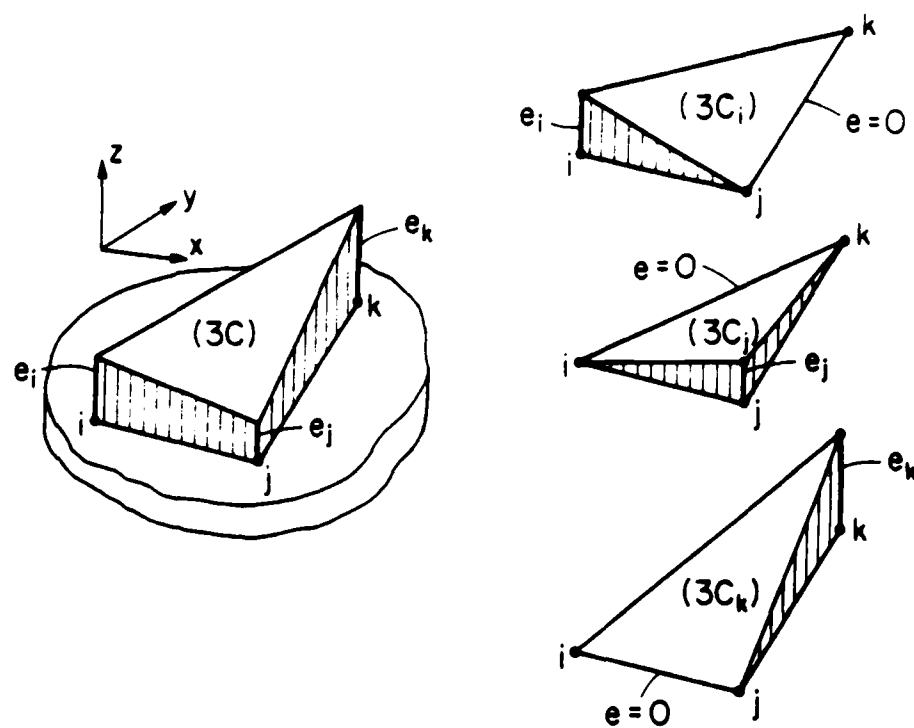


Fig. AIV.3c Linear Potential Field

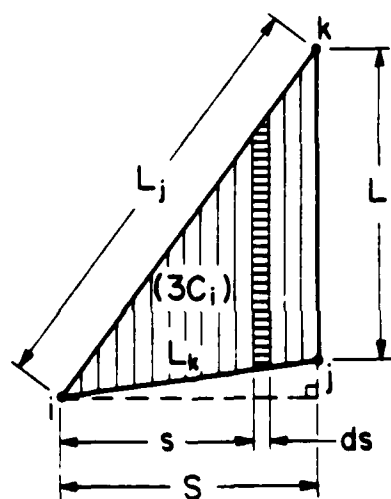


Fig. AIV.3d Plan View Model ci With Power \mathcal{E}_i

The contribution to the full Co-content, \mathcal{C}_i , is $d\mathcal{C}_i$ of the shaded strip of Fig. AIV.3d that is

$$d\mathcal{C}_i = I(s) \cdot de = kt\ell_s \frac{de}{ds} \cdot ds \quad (\text{watts})$$

$$\text{where} \quad \ell_s = s \frac{L_i}{S}, \quad \frac{de}{ds} = -\frac{e_i}{S}$$

$$\text{Hence} \quad d\mathcal{C}_i = kt \frac{sL_i}{S} \left(\frac{-e_i}{S}\right)^2 ds$$

$$\text{Then} \quad \mathcal{C}_i = \frac{L_i e_i^2}{S} \int_0^1 (kt) z dz, \quad z = \frac{s}{S}$$

If the variable kt is approximated as linearly varying from the corner values $(kt)_i$, $(kt)_j$ and $(kt)_k$ the kt of the shaded strip of Fig. AIV.3d is $(kt)_i (1-z) + \frac{z}{2} (kt)_j + \frac{z}{2} (kt)_k$ hence

$$\int_0^1 (kt) z dz = 1/2 (kt)_{av}, \quad (kt)_{av} = \frac{(kt)_i + (kt)_j + (kt)_k}{3}$$

So that integration above yields:

$$\mathcal{C}_i = \frac{kt L_i e_i^2}{2S} \quad \text{but} \quad \frac{SL_i}{2} = \Delta \text{ (area of the triangle)} = \frac{1}{2} \begin{vmatrix} 1 & x_i & y_i \\ 1 & x_j & y_j \\ 1 & x_k & y_k \end{vmatrix}$$

$$\text{Finally:} \quad \mathcal{C}_i = \left(\frac{kt}{4\Delta} \right) L_i^2 e_i^2 \quad \text{watts}$$

By a similar process the power expressions for the c_j and c_k figures are

$$\mathcal{C}_j = \left(\frac{kt}{4\Delta} \right) L_j^2 e_j^2 \quad , \quad \mathcal{C}_k = \left(\frac{kt}{4\Delta} \right) L_k^2 e_k^2$$

Invoking the strategy mentioned earlier that the Co-content of the discrete conductors must be equal to the Co-content of the triangular element

$$K_{i-k} e_i^2 + K_{i-j} e_i^2 = \mathcal{C}_i = \left(\frac{kt}{4\Delta} \right) L_i^2 e_i^2$$

$$K_{j-k} e_j^2 + K_{i-j} e_j^2 = \mathcal{C}_j = \left(\frac{kt}{4\Delta} \right) L_j^2 e_j^2$$

$$K_{k-i} e_k^2 + K_{k-j} e_k^2 = \mathcal{C}_k = \left(\frac{kt}{4\Delta} \right) L_k^2 e_k^2$$

Solving the above simultaneous equations for the three K values yields.

$$K_{i-j} = \frac{kt}{8\Delta} \left[L_i^2 + L_j^2 - L_k^2 \right]$$

$$K_{j-k} = \frac{kt}{8\Delta} \left[L_j^2 + L_k^2 - L_i^2 \right]$$

$$K_{i-k} = \frac{kt}{8\Delta} \left[L_k^2 + L_i^2 - L_j^2 \right]$$

$$\text{but } L_i^2 = (x_{k/i})^2 + (y_{k/j})^2$$

$$L_j^2 = (x_{k/i})^2 + (y_{k/L})^2$$

$$L_k^2 = (x_{j/i})^2 + (y_{j/i})^2$$

$$L_i^2 + L_j^2 - L_k^2 = (x_{k/j})^2 + (x_{k/i})^2 - (x_{j/i})^2 + \dots + \text{similar y terms}$$

$$\text{but } (x_{j/i}) = x_{j/k} + x_{k/i}$$

$$\text{and } (x_{j/i})^2 = x_{j/k}^2 + 2x_{j/k} x_{k/i} + x_{k/i}^2$$

$$\text{Hence } L_i^2 + L_j^2 - L_k^2 = -2(x_{j/k} \cdot x_{k/i} + y_{j/k} \cdot y_{k/i})$$

Finally $K_{i-j} = -\frac{kt}{4\Delta} (x_{j/k} \cdot x_{k/i} + y_{j/k} \cdot y_{k/i})$ or

$$K_{i-j} = +\frac{kt}{4\Delta} (x_{j/k} x_{i/k} + y_{j/k} y_{i/k}) \text{ similarly} \quad \text{E.AIV.3c'}$$

$$K_{j-k} = +\frac{kt}{4\Delta} (x_{j/i} \cdot x_{k/i} + y_{j/i} \cdot y_{k/i}) \quad \text{E.AIV.3c''}$$

$$K_{k-i} = +\frac{kt}{4\Delta} (x_{k/j} \cdot x_{i/j} + y_{k/j} \cdot y_{i/j}) \quad \text{E.AIV.3c'''}$$

Equations E.AIV.3c then are the equivalent conductances connecting the corners of the linear triangular element of Fig. AIV.3b. It remains to establish the branches simulating the convection and external source flows.

Equivalent Lumped Convective Conductors For Element i, j, k, With a Fixed Convective Coefficient C In Its Field

Let $Q_{i,\infty}$, $Q_{j,\infty}$, $Q_{k,\infty}$ be the equivalent lumped flows convected out of nodes i, j and k towards the ambient sink ∞ .

Let \mathcal{M}_{i-j} be the moment of $Q_{i,\infty}$ around the edge j-k of Fig. AIV.3d. \mathcal{M}_{i-j} is also the moment of convected flux integrated about the edge j-k.

$$\mathcal{M}_{j-k} = Q_{i,\infty} \mathcal{S} = C \int e \ell \, ds (1 - \frac{s}{S}) \cdot S \quad \text{where } \ell = Li \frac{s}{S}$$

$$\text{Let } s/S = u, \text{ then } Q_{i,\infty} S = S^2 C Li \int e_{i/\infty} (1-u)^2 u + \frac{(e_{j/\infty} + e_{k/\infty})}{2} u^2 (1-u) du$$

$$\text{Hence: } Q_{i,\infty} = \frac{C\Delta}{12} (2e_{i/\infty} + e_{j/\infty} + e_{k/\infty}) \quad \text{E.AIV.3d'}$$

$$Q_{j,\infty} = \frac{C\Delta}{12} (e_{j/\infty} + 2e_{j/\infty} + e_{k/\infty}) \quad \text{E.AIV.3d''}$$

$$Q_{k,\infty} = \frac{C\Delta}{12} (e_{i/\infty} + e_{j/\infty} + 2e_{k/\infty}) \quad \text{E.AIV.3d'''}$$

Alternately the above equations can be stated as

$$Q_{i,\infty} = C\Delta \left(\frac{e_{i/\infty}}{3} + \frac{e_{j/i}}{12} + \frac{e_{k/i}}{12} \right) \quad \text{E.AIV.3e'}$$

$$Q_{j,\infty} = C\Delta \left(\frac{e_{j/\infty}}{3} + \frac{e_{i/j}}{12} + \frac{e_{k/j}}{12} \right) \quad \text{E.AIV.3e''}$$

$$Q_{k,\infty} = C\Delta \left(\frac{e_{k/\infty}}{3} + \frac{e_{i/k}}{12} + \frac{e_{j/k}}{12} \right) \quad \text{E.AIV.3e'''}$$

The latter equations allow a pictorial representation of - Ce of E.AIV.3a by Fig. AIV.3e.

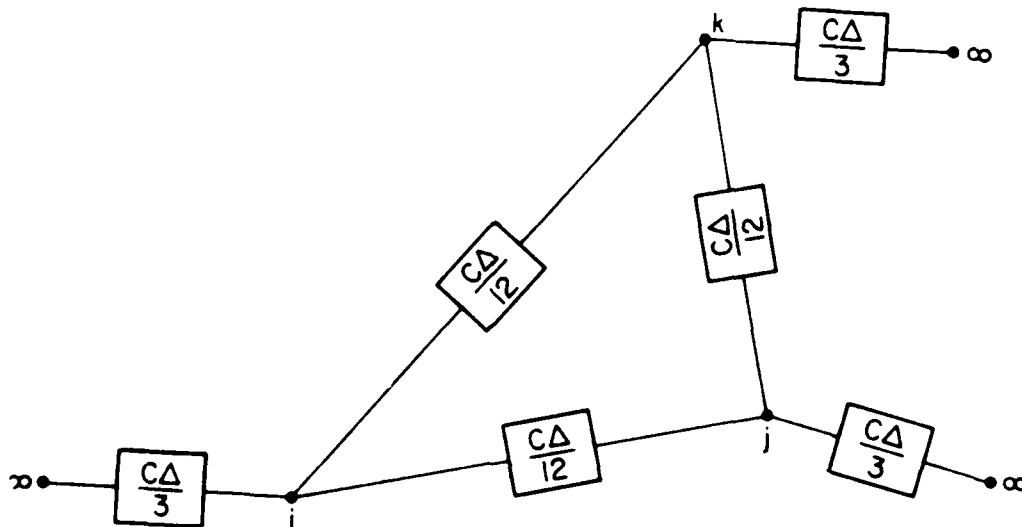


Fig. A.IV.3e Network Representation of Convective Equations E.AIV.3e.

Equivalent Lumped Flow Sources for Element i, j, k Given a Linear Flux Field q.

Let Q_i^* , Q_j^* , Q_k^* be the equivalent concentrated source flows at nodes i, j and k.
Let \mathcal{M}_{j-k} be the moment of Q_i^* about edge j-k as well as the integrated moment of flow q about edge j-k.

$\mathcal{M}_{j-k} = Q_i^* S = \int q \ell (1-s/S) S ds$. This equation is the same form as \mathcal{M}_{j-k} for convected flows but with a linear q distribution rather than e distributions hence

$$Q_i^* = \frac{\Delta}{12} (2q_i + q_j + q_k) \quad \text{E.AIV.3f'}$$

$$Q_j^* = \frac{\Delta}{12} (q_i + 2q_j + q_k) \quad \text{E.AIV.3f''}$$

$$Q_k^* = \frac{\Delta}{12} (q_i + q_j + 2q_k) \quad \text{E.AIV.3f'''}$$

Fig. AIV.3f is total representation of E.AIV.3a applied to the finite element i-j-k. The total flow towards node i can be expressed by reference to the subnetwork of Fig. AIV.3f.

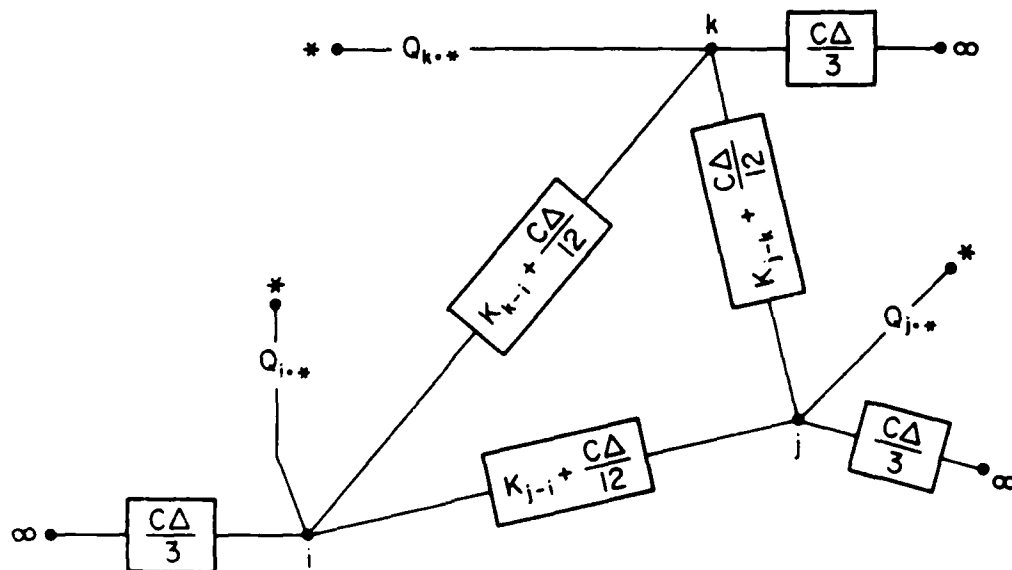


Fig. A.IV.3f Linear Element Network Representing E.AIV.3a On Element i,j,k.

Conservation of Flows Into The Central Node of a Cluster of Elements

Figure AIV.3g(a) shows a field of linear triangles laid out to solve E.IV.a. Figure AIV.3g(b) is a subassembly of n triangular elements such as discussed above. The elements (in this case $n=6$) share a common node g . Each element of the cluster has its own properties (Δ , k , t , c , q). To identify a property with a particular element, it will be subscripted by the addresses of the nodes making up the corners of the element. As an example $(C\Delta)_{g,m,m+1}$ combines C and Δ of the Element $(g, m, m+1)$. When the n elements are assembled the contiguous edges of Fig. AIV.3g(b) and nodes of neighboring elements coalesce their conductances and sources into the star network of Fig. AIV.3g(c) where

$$\tilde{Q}_g = Q_g \cdot (g,1,2) + Q_g \cdot (g,2,3) \dots + Q_g \cdot (g,m,m+1) \dots + Q_g \cdot (g,n,1) \quad \text{E.AIV.3g'}$$

$$\text{and } Q_g \cdot (g,m,m+1) = \frac{\Delta}{12} (2q_g + q_m + q_{m+1})$$

$$\tilde{K}_{g,\infty} = \left(\frac{C\Delta}{3}\right)(g,1,2) + \left(\frac{C\Delta}{3}\right)(g,2,3) \dots \left(\frac{C\Delta}{3}\right)(g,m,m+1) \dots + \frac{C\Delta}{3}(g,n,1) \quad \text{E.AIV.3g''}$$

Elements EL $(g, m-1, m)$ and EL $(g, m, m+1)$ share a common edge $g-m$. Hence the equivalent conductors along branch $g-m$ combine to K_{g-m} of E.AIV.3h.

$$K_{g-m} = \left[K_{g-m} + \frac{C\Delta}{12} \right]_{g,m-1,m} + \left(K_{g-m} + \frac{C\Delta}{12} \right)_{g,m,m+1} \quad \text{E.AIV.3h}$$

$$\text{From E.AIV.3 } \left[K_{g-m} \right]_{g,m-1,m} = \left[\frac{kt}{4\Delta} \right]_{g,m-1,m} \cdot (x_{g/m-1}x_{m/m-1} + y_{g/m-1}y_{m/m-1})$$

A similar cycling of subscripts will generate $(K_{g-m})_{g,m,m+1}$. Finally applying the conservation principle to the cluster at g , using E.AIV.3f,g,h, yields E.AIV.3i.

$$-\tilde{Q}_g - \tilde{K}_{(g-\infty)}e_{g/\infty} + \sum_{\substack{m=1 \\ m \neq g}}^n (K_{g-m}e_{m/g}) = 0 \quad \text{or}$$

$$\sum_{\substack{m=1 \\ m \neq g}}^n K_{g-m} e_m - \left[\sum_{\substack{m=1 \\ m \neq g}}^n (K_{g-m}) + \tilde{K}_{g-\infty} \right] e_g = \tilde{Q}_g, \quad \text{E.AIV.3i}$$

Where $e_m = e_{m/\infty}$, $e_g = e_{g/\infty}$ and m are the global addresses of the modes surrounding the central node g . There are N unknown values e_g in the entire field of Fig. A.IV.3g(a) hence there are N equations of the form E.AIV.3i to be solved simultaneously either by direct methods or by such iterative methods as successive over relaxations (SOR) of the Gauss-Seidel algorithm. Direct methods such as Gauss Elimination are faster than iterative methods but the latter are easier to program, adaptable to non-linear situations and require less storage.

Interest in the F.E.M. has generated a lot of references for handling more sophisticated field problems than posed by E.AIV.3a. The texts of Huebner⁽⁸⁾, Oden⁽⁹⁾, Zienkiewicz⁽¹⁰⁾ were referred to frequently to develop the simplified physical treatment described here.

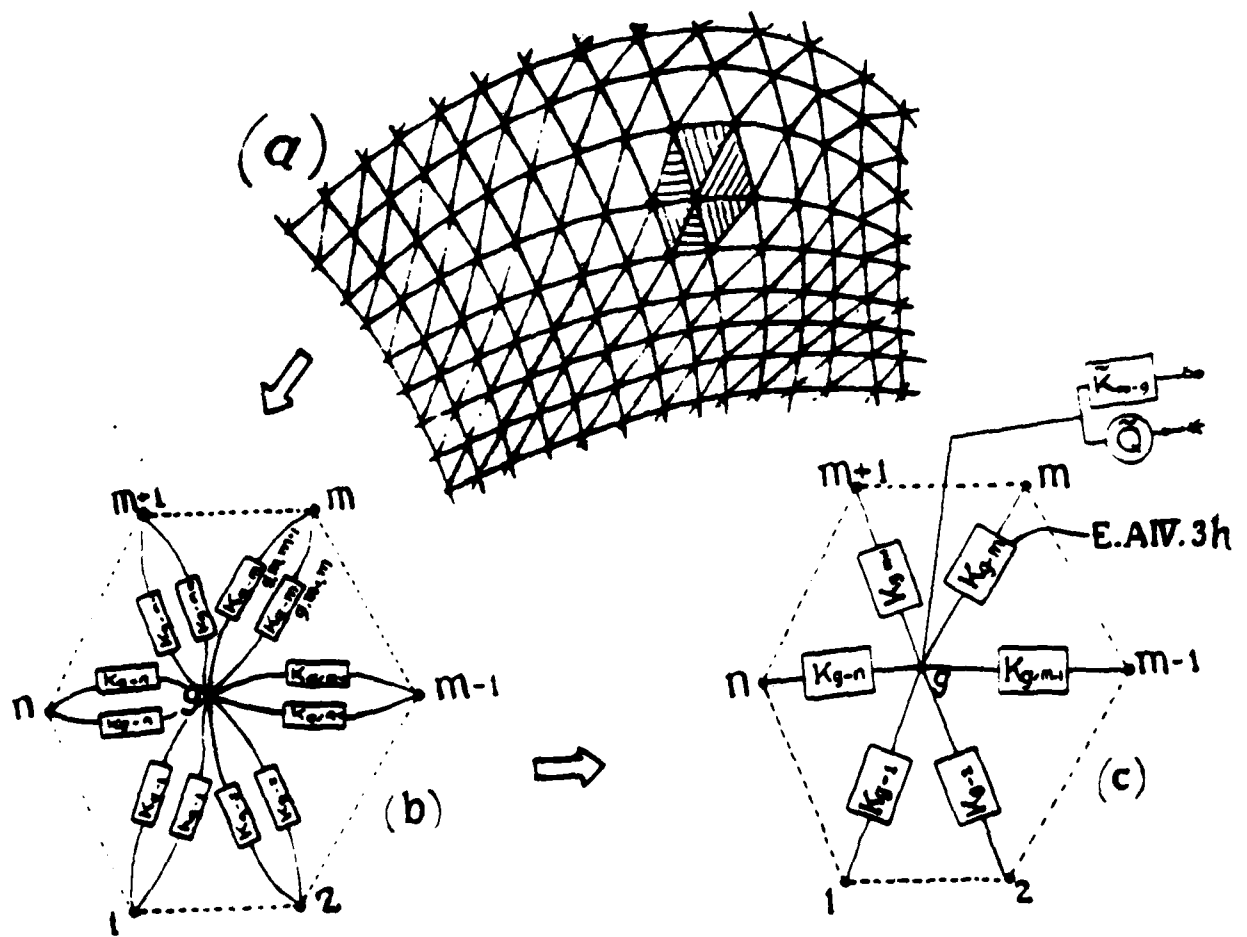


Fig. AIV.3g Node g Centered Cluster of Elements

V Aerostatic Bearing Guideways

An alternate to the liquid EX.P (hydrostatic) guideway is the gas EX.P (aerostatic) guideway. An obvious attraction of an air bearing is the ready availability of compressed shop air for the pressure source. But even more important is the elimination of an oil contaminated environment in which the metrology associated with precision systems would otherwise have to operate. The low viscosity of air ($\mu_{\text{air}}/\mu_{\text{oil}} \simeq 1/3000$) speaks for friction so low as to consider such bearings essentially frictionless. Not only is any suggestion of stick slip eliminated but also the frictionless operation enhances the precision of work piece positioning for numerically controlled machine tools. The mechanics of air bearings is closely related to the mechanics of precision air gages. The two principles joined provide a system capable controlling work piece positioning repetitively within $0.02 \mu\text{m}$. However the compressibility of gases in the supporting domains of the bearing introduces problems of increased response time to feedback controls and a susceptibility to self induced vibrations. Considering these hazards, the design of aerostatic bearings must be tuned more precisely than would be the case for the more forgiving hydrostatic bearing. That tighter tuning begins with a re-examination of EIV.1

Liquid bearings imply incompressibility hence the density term being constant is cancelled out of EIV.1. For gas bearings since the fluid is compressible the density variation must be reckoned with. From the thermodynamics of perfect gases at any instant or point in the system the pressure and density are related as $\rho(x, y, z, t) \propto p^{1/\gamma}$ where: γ is a polytropic constant. It is infinite for an incompressible fluid,

approximately 1.4 for adiabatic compression of air and equal to 1.0 for isothermal compression. Because the thermal mass of the guideways is overwhelming compared to that of the thermal mass of the gas coursing along the guiding surfaces, it may be usually assumed that the compression - expansion experienced by the film is isothermal, $\gamma = 1.0$. Equation EIV.1 therefore transforms to $\nabla \frac{h^3}{\mu} p \nabla p = 12 \text{ r.h.s.}$ (with absolute pressure p replacing ρ) or $\frac{1}{2} \nabla h^3 / \mu \nabla p^2 = 12 \text{ r.h.s.}$. If a flat EX.P guideway is considered with constant h and r.h.s. set to zero the gas bearing equation reduces to $\frac{\partial^2 p^2}{\partial x^2} + \frac{\partial^2 p^2}{\partial y^2} = 0$. If p^2 is replaced by Ψ then the flat EX.P gas bearing equation becomes

$$\frac{\partial^2 \Psi}{\partial x^2} + \frac{\partial^2 \Psi}{\partial y^2} = 0 \quad \text{E.V.1}$$

This form is identical to the liquid EX.P equation EIV.3. The techniques discussed earlier for evaluating the pressure distribution are valid for evaluating Ψ . The working pressure is $\sqrt{\Psi}$ with the restriction that the pressure constituting Ψ must be defined as absolute whereas the pressure previously defined as the lifting pressure was loosely referred to as gage pressure. For given boundary pressures $p_{4/}$ and $p_{5/}$, the gas bearing will give slightly higher lift load W than the liquid bearing because of the expansion of the gas as it approaches the border contour 5. There will however be a much larger mass flow with a gas medium primarily due to the much lower viscosity of gases when compared to liquids.

Perhaps the most effective way to compare hydrostatic and aerostatic performances is by an analysis, as in A.IV.2, of the circular bearing Fig. IV.2 with air as the medium rather than oil.

The circular gas bearing equation is modified from EIV.4b to

$$r^2 \frac{d^2 \Psi}{dr^2} + r \frac{d\Psi}{dr} = 0$$

The solution follows exactly that given in AIV.2 so that

$$\frac{d\Psi}{dr} = -\frac{\Psi_{4/5}}{r} \frac{1}{\text{Ln}(b/a)} \quad , \quad \Psi_{4/5} = \Psi_{4/*} - \Psi_{5/*} = (p_{4/*})^2 - (p_{5/*})^2 \quad \text{E.V.2a}$$

Integrating this gradient with the boundary conditions to the 4-5 domain yields

$$\frac{\Psi_{r/5}}{\Psi_{4/5}} = \frac{\text{Ln}(b/r)}{\text{Ln}(b/a)} \quad , \quad \Psi_{r/5} = (p_{r/*})^2 - (p_{5/*})^2 \quad \text{E.V.2b}$$

Comparison of Mass Flow, \mathcal{M} Gas & Oil Bearing

Referring to Fig. IV.2 the mass flow from the contour 4 towards contour 5 is

$$\mathcal{M}_{4.5} = -\rho_4 \frac{h^3}{12\mu} \cdot 2\pi r \left(\frac{dp}{dr} \right)_4$$

Where: subscript 4 represent the state at contour 4,

subscript 5 represent the state at contour 5.

Let: subscript ∞ represent the ambient state,

Isothermal compressible flow: $\rho_4 = \frac{\rho_\infty}{p_{\infty/*}} \cdot p_{4/*}$ while incompressible flow: $\rho_4 = \rho_\infty$.

Let subscripts g and ℓ identify gaseous and liquid properties respectively hence

$$(\mathcal{M}_{4.5})_\ell = (\rho_\infty)_\ell \frac{h_\ell^3}{6\mu_\ell} \pi r \cdot \frac{p_{4/5}}{r} \frac{1}{\text{Ln}(b/a)}$$

$$(\mathcal{M}_{4.5})_g = \frac{(\rho_\infty)_g}{p_{\infty/*}} \frac{h_g^3}{12\mu_g} \pi r \frac{\Psi_{4/5}}{r} \cdot \frac{1}{\text{Ln}(b/a)}$$

$$\text{Hence } \frac{(\mathcal{M}_{4.5})_g}{(\mathcal{M}_{4.5})_\ell} = \frac{(\rho_\infty)_g}{(\rho_\infty)_\ell} \left(\frac{h_g}{h_\ell} \right)^3 \left(\frac{\mu_\ell}{\mu_g} \right) \cdot \frac{[(p_{4/*})^2 - (p_{5/*})^2]}{2p_{\infty/*}(p_{4/*} - p_{5/*})} \quad \text{E.V.3a}$$

$$\text{or } (\mathcal{M}_{4.5})_g = \frac{(\rho_\infty)_g}{(\rho_\infty)_\ell} \left(\frac{h_g}{h_\ell} \right)^3 \left(\frac{\mu_\ell}{\mu_g} \right) \frac{(p_{4/*} + p_{5/*})}{2p_{\infty/*}} \quad \text{E.V.3b}$$

Let $\mu_\ell = .07 \text{ Ns/m}^2$ as in original oil bearing example

$$\mu_g = \mu_{\text{air}} = .02 \times 10^{-3} \text{ Ns/m}^2$$

$$\frac{\mu_\ell}{\mu_g} = 3500 \quad \text{and} \quad \frac{(\rho_\infty)_\ell}{(\rho_\infty)_g} = 722$$

Let $p_{4/5} = 1.725 \times 10^5 \text{ N/m}^2$ as in original oil bearing example AIV.2.

Also let $p_{5/*} = p_{\infty/*} = 1.013 \times 10^5 \text{ N/m}^2$

$$\text{then } \frac{p_{4/*} + p_{5/*}}{2p_{\infty/*}} = \left(\frac{1.725 + 1.013 + 1.013}{2 \times 1.013} \right) = 1.85$$

$$\text{Finally } \frac{(\mathcal{M}_{4.5})_g}{(\mathcal{M}_{4.5})_\ell} = \frac{1}{722} \left(\frac{h_g}{h_\ell} \right)^3 (3500) \times 1.85 = 8.97 \left(\frac{h_g}{h_\ell} \right)^3$$

Because the kinematic viscosity of the oil is about 5 x greater than that of air at ambient conditions the overall mass flow of air will be 8.97 x that of the oil example for the same film clearance. It is therefore the practice to make gas bearing clearances considerably smaller to conserve on the mass flow amongst other things.

In the earlier example of the oil bearing it was shown that the volumetric flow was $Q_{4.5} = .436 \text{ in}^3/\text{min}$. It then follows that SCFM flow rate for the air bearing would be

$$\frac{(Q_{4.5})_g}{(Q_{4.5})_\ell} = \frac{\mathcal{M}_g}{\mathcal{M}_\ell} \times \left(\frac{\rho_\ell}{\rho_g} \right) = 8.97 \times 722 = 6476$$

Since $(Q_{4.5})_\ell = .436 \text{ in}^3/\text{min}$ from AIV.2 then $(Q_{4.5})_g = .436 \times 6476 = 2823.5 \text{ in}^3/\text{min}$ or

air flow = 1.63 SCFM

If the original film thickness of 40 μm is halved for the gas bearing the flow rate would be reduced eight fold to about 0.2 SCFM.

Friction Comparison

Equation E.AIV.2a defined the viscous drag of the slide bearing. For the same geometry and velocities the drag formulation is the same for oil or gas bearings only the difference in viscosity plays a role. The coefficient of friction for the oil bearing was .0028. With air as the lubricant the coefficient of friction would then be $.0028/3500 = 8 \times 10^{-7}$! The bearing would be essentially without friction. Actually a pressurized film tapered only 0.2 arc seconds would create more of a disturbance.

Lifting Capacity of the Gas Bearing

Lift contributed by the h region (4-5) is

$$W_{4-5} = \int_4^5 p_{r/\infty} \cdot 2\pi r \, dr \quad , \quad p_{r/\infty} = p_{r/s} - p_{\infty/s}$$

Applying E.V.2b $p_{r/s} = \left[[(p_{4/s})^2 - (p_{5/s})^2] \frac{\text{Ln}(b/r)}{\text{Ln}(b/a)} + (p_{5/s})^2 \right]^{1/2}$

$$W_{4-5} = \int_4^5 \left[[(p_{4/s})^2 - (p_{5/s})^2] \frac{\text{Ln}(b/r)}{\text{Ln}(b/a)} + (p_{5/s})^2 \right]^{1/2} 2\pi r \, dr - \int_4^5 2\pi r \, dr$$

Let $p_{5/s} = p_{\infty/s}$

from the fluid state at contour 4. The actual choice of designations is a matter of convenience imposed by a particular equation.

The dynamic behavior of this system is approximated by adding dynamic increments to the steady state conservation equation. For this purpose let:

$\dot{m} = \delta \dot{M}$, the perturbation from steady state mass flowrate.

$\zeta = \delta p$, the perturbation from the steady state pressure.

$w = \delta W$, the perturbation from the static lift of the bearing.

$z = \delta h$, the increment in the static film thickness.

$M_{II-} = \text{mass of the oscillating body} = M_{II}$.

The total mass flow equation focused on the pocket in the dynamic state becomes

$$(\dot{M}_{2.3} + \dot{m}_{2.3}) + (\dot{M}_{5.3} + \dot{m}_{5.3}) + \dot{m}_{*.3} + \dot{m}_{II.3} = 0$$

$$\text{or } \dot{m}_{2.3} + \dot{m}_{5.3} + \dot{m}_{*.3} + \dot{m}_{II.3} = 0 \quad \text{E.V.4}$$

From Section IV the flow through passive types of restrictors is in general related to pressure drop and orifice or capillary flow areas. Hence perturbations in these flows would be related to perturbations in these parameters so that

$$\dot{m}_{2.3} = d\dot{M}_{2.3} = \frac{\partial \dot{M}_{2.3}}{\partial p_{3/*}} \delta p_{3/*} + \frac{\partial \dot{M}_{2.3}}{\partial h} \cdot \delta h \quad \text{or}$$

$$\dot{m}_{2.3} = + \frac{\partial \dot{M}_{2.3}}{\partial p_{3/*}} \cdot \zeta_{3/*} + \frac{\partial \dot{M}_{2.3}}{\partial h} \cdot z$$

The steady state flow through the domain 5-4 and into the pocket envelop is $\dot{M}_{5.34} \propto \psi_{5/3}$ and h^3 . It follows then that

$$\dot{m}_{5.3} = \frac{\partial \mathcal{M}_{5.3}}{\partial p_{3/*}} \cdot \delta p_{3/*} + \frac{\partial \mathcal{M}_{5.3}}{\partial h} \delta h \text{ or}$$

$$\dot{m}_{5.3} = \frac{\partial \mathcal{M}_{3/*}}{\partial p_{3/*}} \cdot \zeta_3 + \frac{\partial \mathcal{M}_{5.3}}{\partial h} \cdot z$$

The l.h.s. of EIV.1 contains the expression $\frac{\partial \rho h}{\partial t}$ that is $h \frac{\partial \rho}{\partial t} + \rho \frac{\partial h}{\partial t}$. The first term refers to the compressibility of the fluid hence the capacitance of the film. Since the film h in domain 4-5 is extremely small this capacitance will be neglected initially. In the domain of the pocket its depth plays the role of a very large h hence the capacitance here must now be considered. From Appendix A.I Table A.I.c, the capacitance of a volume is $C_{3-*} = \left(\frac{m}{np} \right)_3$ ie. $\left(\frac{vol_3 \rho_3}{\gamma p_{3/*}} \right)$, $\gamma = 1$ assuming isothermal conditions.

$$\text{Hence } \dot{m}_{3} = (vol_3 \frac{\rho_3}{p_{3/*}}) \dot{p}_{3/*} = -C_{3-*} \dot{p}_{3/*} = -C_{3-*} \dot{\zeta}_3$$

The second part $\rho \frac{\partial h}{\partial t}$ of $\frac{\partial \rho h}{\partial t}$ above describes the contribution to mass flow by squeezing the surfaces II and I together. As far as contributing to the mass flow into the pocket 3 the squeeze effect is $\dot{m}_{II.3}$ where $\dot{m}_{II.3} \simeq -\dot{z} \rho_3 A_3$ with $A_3 =$ area of pocket + a portion of the area 4-5.

The perturbed mass flow equation E.V.4 becomes

$$\begin{aligned} + \frac{\partial \mathcal{M}_{2.3}}{\partial p_3} \zeta_3 + \frac{\partial \mathcal{M}_{2.3}}{\partial h} z + \frac{\partial \mathcal{M}_{5.3}}{\partial p_{3/*}} \zeta_{4/*} + \frac{\partial \mathcal{M}_{5.3}}{\partial h} z + \dots \\ \dots - C_{3-*} \dot{\zeta}_{3/*} - \rho_3 A_3 \dot{z} = 0 \end{aligned} \quad \text{E.V.5a}$$

The conservation of momentum for the bearing system is defined by

$$M_{II} \ddot{z} = w_{4-5} + w_{3-4} = \zeta_{3/\infty} A_{3-4} + \zeta_{4/5} S_w A_{4-5}$$

where A_{3-4} is the area of the pocket, A_{4-5} is the area of the domain 4-5 and S_w is the area shape lift function, $S_w = \frac{\int_4^5 p dA}{p_{4/5} A_{4-5}}$. Since $\zeta_{4/5} = \zeta_{4/\infty}$ and $\zeta_{4/3} = 0$ let $\zeta_{4/5} =$

$$\zeta_{3/\infty} \quad \text{then} \quad M_{II} \ddot{z} = \zeta_{3/\infty} [A_{3-4} + S_w A_{4-5}] \quad \text{E.V.5b}$$

Substituting E.V.5b into E.V.5a yields

$$a_0 \ddot{z} + a_1 \dot{z} + a_2 z + a_3 z = 0$$

$$\text{where: } a_0 = C_{3-} B \quad B = \frac{M_{II}}{[A_{3-4} + S_w A_{4-5}]}$$

$$a_1 = - \left(\frac{\partial \mathcal{M}_{2.3}}{\partial p_{3/*}} + \frac{\partial \mathcal{M}_{5.3}}{\partial p_{3/*}} \right) B$$

$$a_2 = \rho_3 A_3$$

$$a_3 = - \left(\frac{\partial \mathcal{M}_{5.3}}{\partial h} + \frac{\partial \mathcal{M}_{2.3}}{\partial h} \right)$$

From Appendix A.V

$$\frac{\partial \mathcal{M}_{2.3}}{\partial p_{3/*}} = \frac{\mathcal{M}_{2.3}}{p_{3/*}} \cdot \mathcal{F}_{2-3} \quad \mathcal{F}_{2-3} = \frac{\frac{2}{\gamma} \beta^{2/\gamma} - (1 + \frac{1}{\gamma}) \beta^{(1/\gamma+1)}}{\beta^{2/\gamma} - \beta^{(1/\gamma+1)}}$$

$$\frac{\partial \mathcal{M}_{5.3}}{\partial p_{3/*}} = - \frac{\mathcal{M}_{3.5}}{p_{3/*}} \mathcal{F}_{3-5} \quad \mathcal{F}_{3-5} = \frac{1}{1 - \left(\frac{p_{\infty/*}}{p_{3/*}} \right)^2}$$

$$\frac{\partial \mathcal{M}_{2.3}}{\partial h} = \frac{\mathcal{M}_{2.3}}{h}, \quad (\text{inherently compensated}) \text{ otherwise } = 0$$

$$\frac{\partial \mathcal{M}_{5.3}}{\partial h} = -\frac{\partial \mathcal{M}_{3.5}}{\partial h} = -\frac{3\mathcal{M}_{3.5}}{h}$$

Finally

$$a_0 = C_{3-} \cdot B \quad B = \frac{\mathcal{M}_{11}}{[A_{3-4} + S_w A_{4-5}]}$$

$$a_1 = + \left[-\mathcal{F}_{2-3} + \mathcal{F}_{3-5} \right] \frac{\mathcal{M}_{2.3}}{p_{3/}} \cdot B$$

$$a_2 = \rho_3 A_3$$

$$a_3 = - \left(-3 \frac{\mathcal{M}_{3.5}}{h} + \frac{\mathcal{M}_{2.3}}{h} \right) = + \frac{\mathcal{M}_{2.3}}{h} H_{2-3}$$

$H_{2-3} = 2$ Inherently compensated orifice
3 otherwise

From the Routh-Hurwitz test conditions, stability (no self induced hammering) is realized if all a_j coefficients are positive and $a_1 a_2 - a_0 a_3$ is positive, ($a_1 a_2 > a_0 a_3$). The term $\mathcal{F}_{3.5} - \mathcal{F}_{2.3}$ of a_1 could conceivably go negative but the tabulation of these terms in Appendix A.V indicates that this expression is always positive. The remaining test for stability is that $a_1 a_2 > a_0 a_3$ that is

$$(\mathcal{F}_{3.5} - \mathcal{F}_{2.3}) \frac{\mathcal{M}_{2.3}}{p_{3/}} B \rho_3 A_3 > ? C_{3-} \cdot B \frac{\mathcal{M}_{2.3}}{h} H_{2-3}$$

$$\text{or } (\mathcal{F}_{3.5} - \mathcal{F}_{2.3}) \left(\frac{\rho_3}{p_{3/}} \right) A_3 > ? C_{3-} \cdot \frac{H_{2-3}}{h}$$

$$\text{where: } C_{3-} \simeq \text{vol}_{3-4} \frac{\rho_3}{p_{3/}} \simeq (\Delta + h) \cdot A_{3-4} \frac{\rho_3}{p_{3/}}$$

$$\text{Hence } (\mathcal{F}_{3.5} - \mathcal{F}_{2.3}) A_3 > ? \frac{(\Delta + h)}{h} A_{3-4} H_{2-3}$$

E.V.6

Δ = pocket depth

$\mathcal{F}_{3-5} - \mathcal{F}_{2-3} \simeq 2$, $A_3 \simeq$ Total wetted lift area

A_{3-4} = pocket area, Say $A_{3-4} = fA_3$

E.V.6 becomes approximately

$$2 A_3 > ? \left(\frac{\Delta}{h} + 1 \right) f A_3 H_{2-3}$$

for stability $\left(\frac{\Delta}{h} + 1 \right) f H_{2-3}$ must be less than 2. Choosing an inherently compensated orifice sets $H_{2-3} = 2$ otherwise a more dangerous $H_{2-3} = 3$ will result. The stability condition reduces to $\left(\frac{\Delta}{h} + 1 \right) \cdot f < 1$. If $\frac{\Delta}{h} = 10$ f must be less than $\frac{1}{11}$.

Using the example of Fig. IV.2 it would require $\frac{a}{b} < \sqrt{\frac{1}{11}}$ and if $h = 20 \mu\text{m}$, $\Delta = .2 \text{ mm}$, a very shallow pocket. A more practical design removes the pocket completely from Fig. IV.2 and replaces it with a channel along the contour line 4 as in Fig. V.4. The channel is fed by N equally spaced orifices along the channel. Since there is no pressure gradient inside contour line 4 the pressure distribution experienced by the pocketed design would be duplicated and so would its lifting capacity. The ratio of the volumes of the two recesses is a measure of their relative influence on the stability.

$$\text{Ratio } \frac{\text{vol. channel}}{\text{vol. pocket}} = \frac{b^2 \times 2\pi a}{\pi a^2 \Delta} = \frac{b^2 2}{a \Delta}$$

above, $a = 100 \text{ mm}$, $\Delta = 0.2 \text{ mm}$ and b assumed at 2 mm yields a Ratio = $\frac{1}{2.5}$ that

is the channeled design has 2.5 x the stability margin attained by the .2 mm deep full pocket.

The analytics described above are basically similar to the simplified lumped parameter analysis of Licht and Elrod⁽¹⁾ of circular bearings such as Fig. IV.2. Another analysis by Licht and Elrod⁽²⁾ was refined to include the capacitance of the h film in domain 4-5. Tests were conducted on actual bearings. Confirmation by experiment was somewhat poor but it did provide useful design guidelines. That is that the simple lumped parameter⁽¹⁾ analysis results are pessimistic compared to the refined analysis⁽²⁾ but even the latter results are pessimistic compared to the test data⁽²⁾ when supply pressure is less than 85 psia. In the test domain of supply pressures between 85 psia and 95 psia the simplified analysis⁽¹⁾ gave somewhat optimistic results on allowable pocket depths while the refined analysis remained a bit pessimistic.

A circular thrust bearing is only infrequently used for linear guideways. More commonly the guideways will be rectangular as suggested by Fig. IV.1. However for the aerostatic case the pocket is to be avoided. Instead a series of orifices arrayed in parallel lines is employed. Stout and Sweeney⁽³⁾ have prepared design charts for this type of field. While there are no explicit pockets the authors did reckon with the unavoidable capacitance associated with each orifice subassembly. The design charts offer dimensional specifications to skirt pneumatic hammer instability. Other charts include load, clearance, supply pressure and orifice sizes for optimum configurations.

Stabilizing the EX.P Gas Bearing Slideway With Additional R-C Members

H. Mori & A. Mori⁽⁴⁾ have been able to suppress pneumatic hammer and yet retain a generous pocket by adding an additional restrictor and another chamber for a second capacitance. A gas bearing control system which they recommend is Fig. V.1a. Fig. V.1b is the analogous electrical circuit.

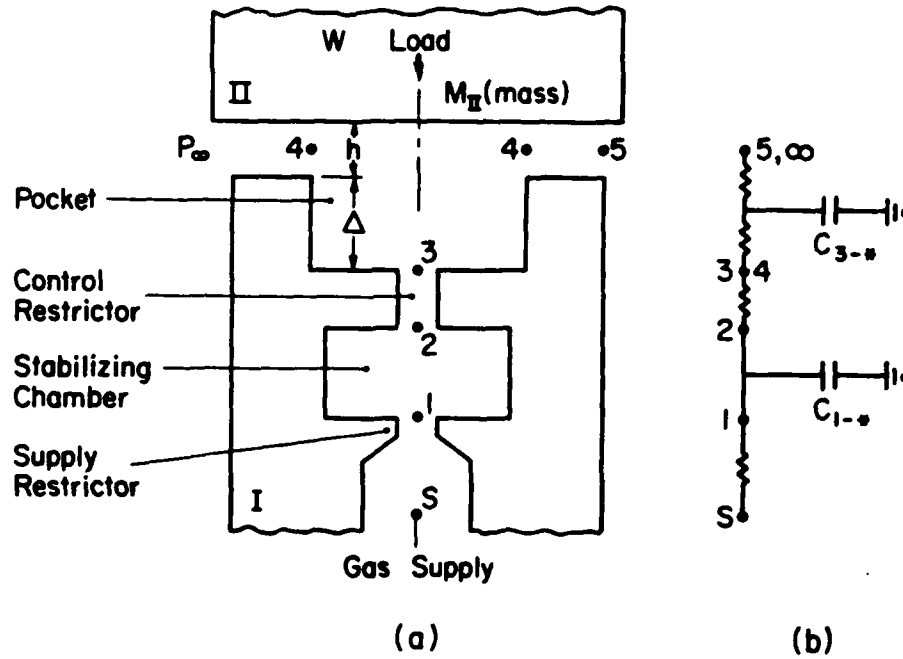


Fig. V.1 Schematic of Aerostatic Bearing with An Added R-C Element Ref. 4.

Let: Subscript 12 represent the envelop of the chamber containing nodes 1 and 2.

Subscript 34 represent the envelop of the chamber containing node 3 and the contour 4.

Subscript 45 represent the chamber between contours 4 and 5 occupied by bearing film h.

The perturbed mass flow equations of the cascaded system of Fig. V.1 become

$$\dot{m}_{3,12} + \dot{m}_{\infty,12} = \dot{m}_{3,12} = 0$$

$$\dot{m}_{2,34} + \dot{m}_{\infty,34} + \dot{m}_{4,34} + \dot{m}_{11,34} = 0$$

$$\dot{m}_{3,45} + \dot{m}_{\infty,45} + \dot{m}_{\infty,45} + \dot{m}_{11,45} = 0$$

$$\text{Let: } q' = C_{3-*} = \text{Vol}(34) \frac{\rho_3}{p_{3/*}}$$

$$s' = \text{squeeze flow } \rho h A$$

$$\theta = \frac{\partial \mathcal{M}_{3.5}}{\partial h} = \frac{\partial \mathcal{M}_{4.5}}{\partial h} = \frac{3\mathcal{M}_{4.5}}{h}$$

$$\xi = \frac{\partial \mathcal{M}_{s.1}}{\partial p_{1/*}} = \frac{\mathcal{M}_{s.1}}{p_{2/*}} \cdot \mathcal{F}_{s-1}$$

$$\eta = \frac{\partial \mathcal{M}_{2.3}}{\partial p_{2/*}} = \frac{\mathcal{M}_{2.3}}{p_{2/*}} J_{2-3}$$

$$\zeta = \frac{\partial \mathcal{M}_{2.3}}{\partial p_{3/*}} = \frac{\mathcal{M}_{2.3}}{p_{3/*}} \cdot \mathcal{F}_{2-3}$$

$$z' = \frac{\partial \mathcal{M}_{1.*}}{\partial p_{1/*}} = C_{1-*} = \text{vol}_{.12} \cdot \frac{\rho_1}{p_{1/*}}$$

$$\beta = \frac{\partial \mathcal{M}_{3.5}}{\partial p_{3/*}} = \frac{\mathcal{M}_{3.5}}{p_{3/*}} = \frac{2}{1 - \left(\frac{p_{5/*}}{p_{3/*}} \right)^2}$$

As in the conventional case discussed earlier the three simultaneous in equations are converted with the above influence coefficients into simultaneous equations involving perturbed pressures δp and movements z at the various points of the system. The equation $M_{II} \ddot{h} = M_{II} \ddot{z} = \int_3^5 \delta p \, dA$ is used to express perturbed pressures in terms of perturbed motions. A fourth order differential equation is generated just as a third order D.E. was generated by the earlier illustration that is:

$$\overset{\dots}{a_0} \ddot{z} + \overset{\dots}{a_1} \dot{z} + \overset{\dots}{a_2} z + \overset{\dots}{a_3} z + a_4 = 0$$

Where: $z = \delta h$ perturbed clearance

$$a_0 = q'z' , \quad a_1 = (\zeta + \beta')z' + (\xi + \eta)q'$$

$$a_2 = \xi(\zeta + \beta') + \eta\beta' + \frac{A_e}{M_{II}}s'z'$$

$$a_3 = \frac{A_e}{M_{II}} (z'\theta' + (\xi + \eta)s')$$

$$a_4 = \frac{A_e}{M_{II}} \theta' (\xi + \eta)$$

To apply the Routh-Horowitz stability criterion first establish the following determinates \mathcal{D} .

$$\mathcal{D}_1 = a_1 \quad \mathcal{D}_2 = \begin{vmatrix} a_1 & a_0 \\ a_3 & a_2 \end{vmatrix} \quad \mathcal{D}_3 = \begin{vmatrix} a_1 & a_0 & 0 \\ a_3 & a_2 & a_1 \\ 0 & a_4 & a_3 \end{vmatrix}$$

The necessary and sufficient set of conditions for stability are that $a_0 > 0$ and \mathcal{D}_1 , \mathcal{D}_2 , \mathcal{D}_3 are each positive. Fig. V.2 is a map of the stable and unstable zones of operation Mori, Mori⁽⁴⁾ calculated by the method similar to that described here and actual test values. Their results are for a circular bearing geometry such as shown in Fig. IV.2 but with an additional R-C component placed between stations 2 and 1. The good agreement between calculated and test values establishes the creditability of their theory. The results also showed that capillary restrictors do as well as orifice restrictors in this stabilizing scheme as long as dimensions are chosen from the restricted stabilized zone shown.

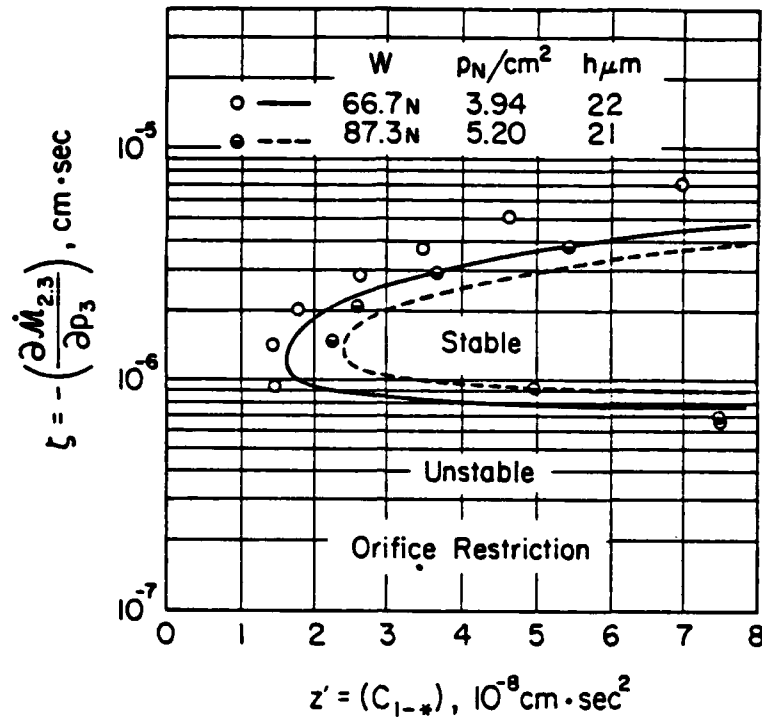


Fig. V.2 Zones of Stable and Unstable Operation From Ref. 4.

D. Wilcock⁽⁵⁾ developed the dynamics of EX.P thrust bearings somewhat along the lines above⁽⁴⁾ using servomechanism analytics. He includes more parameters such as oscillatory loading and inertance (inertance defined in Section I, Table A.I.c Element 1) into the 1-2 restrictor branch. No experimental confirmation is given however.

Precision Levels of Aerostatic Linear Guideways

A Kobayashi⁽⁶⁾ describes ultra-precision machine tool developments in Japan directed towards diamond cutting associated with the fabrication of computer memory disks, laser scanner mirrors etc.. Hydrostatic and aerostatic guidance play significant roles in these developments. Performance figures for linear guideways such as Fig. V.3 are given in the accompanying table. Exact construction details are not given but a plausible assumption is that the aerostatic lands contain no explicit pockets but rather

each land is fed by a straight line array of orifices essentially as described in reference (3). The table I indicates that the guidance fidelity of aerostatic slide ways can be made good to an order of 20 nanometers! This ultra precision is from a guideway which can nevertheless support loads of the order of 2000 N.

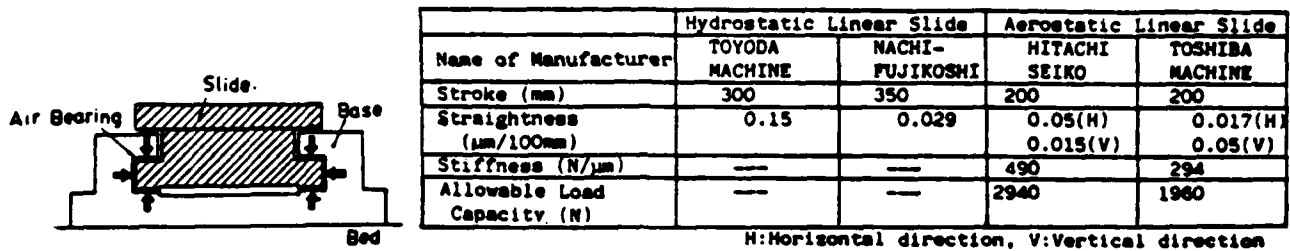


Fig. V.3 Aerostatic Linear Slide (Hitachi Seiko) Performance. Ref. 6

A High Precision Straight Line Positioning System.

In section IV, Fig. IV.6, a unique hydrostatic guideway system was described in which the conventional passive control restrictor 1-2 was replaced by a valve activated by the vertical position of the slide table relative to a horizontal straight edge. An important aspect of this concept is the removal of the bearings film thickness h as the parameter of position control. This therefore removes the influence of manufactured errors inherent in the guideway. Instead the more precise straightedge becomes the controlling datum. This concept is expanded by A. Shimokohbe et al⁽⁷⁾ to create a high precision positioning system to meet the needs of ultra precision tooling such as might be used in diamond turning machines. Figures V.4a,b show the system assembly. The object is to position the block so that five kinematic errors are held within fractions of microns or arc seconds. There is a primary table (mechanical slide of Fig. V.4a) running in a guide with conventional thin film lubrication. This guideway need possess only moderate precision since it provides merely nominal positioning. Fine positioning

is super imposed on top of the nominal position by controlling the film thickness of nine aerostatic circular thrust bearings Fig. V.4b which support the block. The table below demonstrates the position errors first observed without the feed back control and then with the feedback controls activated. The feedback system registers approximately a 30 fold improvement in position precision. The complexity of feedback position control is obviously acceptable when high precision is the object.

TABLE: Measured Position Errors

Error Type	Vertical	Horizontal	Roll	Pitch	Yaw
Free System	8 μ m	10 μ m	10 sec	10 sec	10 sec
Feed-Back System	0.1 μ m	0.4 μ m	0.2 sec	0.4 sec	0.2 sec

The system operates as follows. A pair of precision straight edges, Fig. V3.a, is probed by a pair of capacitance micrometers whose readings will be converted to signals registering the components of vertical and roll errors of the block relative to the straight edges. An autocollimator registers the pitching error of the block position. These data activate three servo valves. Each of these valves controls the gas flow rate to one of the three aerostatic pads bearing on the underside of the block. The principle involved is similar to that described for the adaptive control of the hydrostatic bearing of Fig. IV.5. In that case the probe data being mechanical, was converted directly to a valve opening. Thus time the probe signals being electrical they must be converted to mechanical valve opening by solenoids. While the electrical feedback involves a more complex system it has an advantage over the mechanical probe-valve controller of section IV. That is, computer modification of system characteristics can be readily imposed adding to versatility of performance.

The three aerostatic pads acting on the under side of the block tilt and lift the

block to negate the errors reported by the capacitance probes and the autocollimator. A second autocollimator beams across the top of the block to monitor the yaw errors. Its signal activates the servo valves associated with pads a_1 , b_1 , a_2 , b_2 . The laser system of Fig. V.4a beams onto a photodetector to register horizontal shift errors. This error also influences the servo valves associated with pads a_1 , b_1 , a_2 , b_2 . The combination of yaw and horizontal shift signals causes pads a_1 , b_1 , a_2 , b_2 to expand or contract to negate these errors.

The two pads oriented along the axis of table travel act as a pneumatic vise. Presumably if the outward travel of the block were measured by an interferometer these pads could be employed to add the sixth dimension of control.

The details of the air pads are also informative. Fig. V.5 shows that an annular channel is employed obviously to reduce the pneumatic capacitance of the pad in the interests of removing susceptibility to air hammer. The channel is unusually shallow suggesting great care was taken to develop the absolute minimum capacitance. This observation implies also that feedback control was not relied upon to suppress air hammer. The plot of Fig. V.5 also offers useful data regarding practical magnitudes of film thickness and pressures. The real character of the static load-clearance- supply pressure relationships might very well be compared with analytical results.

The example of the adaptive controlled hydrostatic slideway Fig. IV.5 shows a no-through-flow bearing. The side seals reduced the oil losses which with the high pressures involved in that example would translate both to extensive contamination of the machine area reduced effectiveness of the adaptive system by reintroducing the influence of pocket geometry errors. The no-through-flow concept was not used for the system of Fig. V.4a,b. The leakage of air out of aerostatic bearings does not equate to

contamination of the metrology environment (except for causing the laser beam to wander if it is not shielded from air currents).

Perimeter seals needed for no-through-flow pads would add complexity without profit.

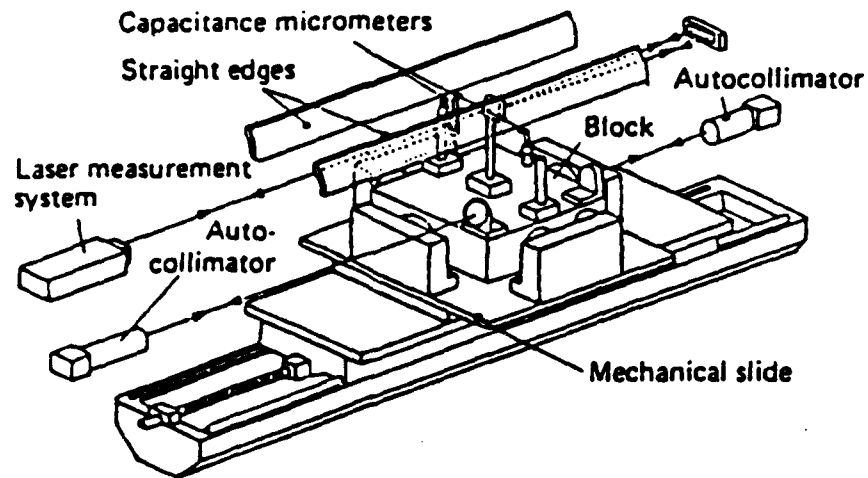


Fig. V.4a High Precision Straight Motion System. Ref.7.

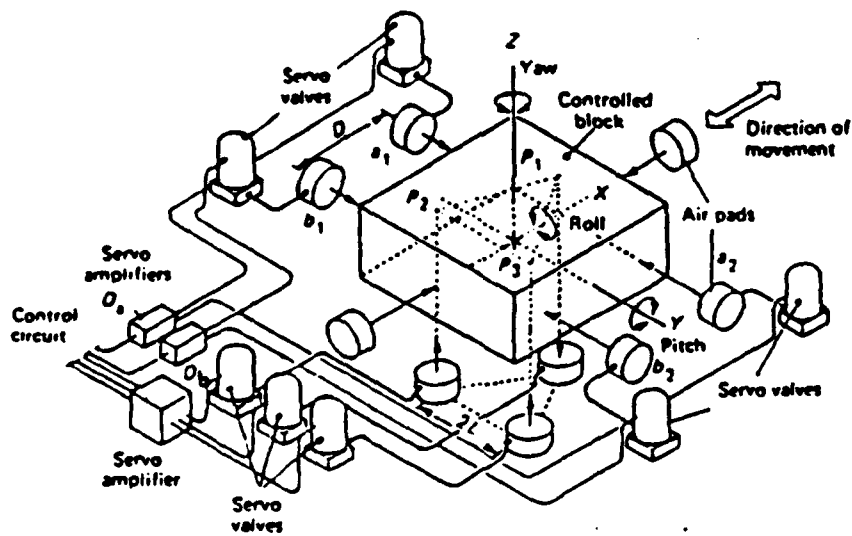


Fig. V.4b Pads, Servo Valves and Block Assembly. Ref. 7.

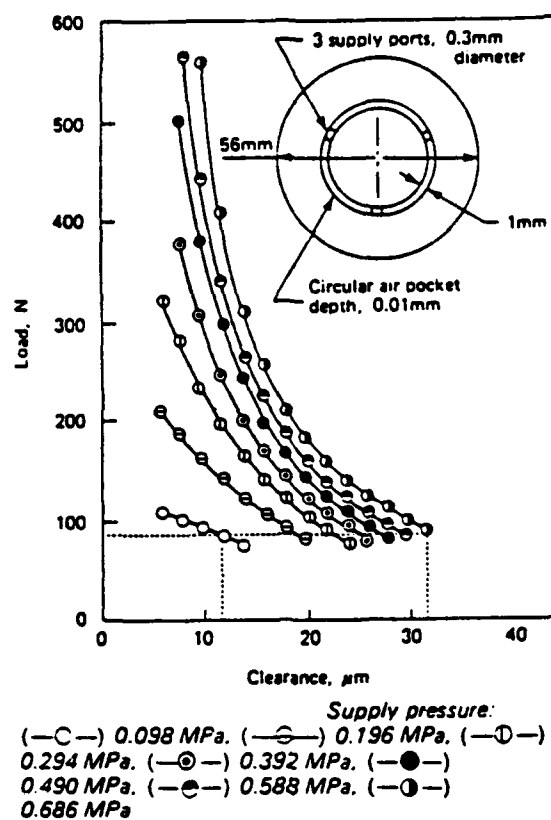


Fig. V.5 Load, Clearance and Supply Pressure of Pads. Ref. 7.

V. References

- (1) L. Licht and H. G. Elrod, Jr., "A Study of Stability of Externally Pressurized Gas Bearings", Journal of Applied Mechanics, Vol. 27, Trans ASME Vol. 82, 1960
- (2) L. Licht and H. G. Elrod, Jr., "An Experimental Study of the Stability of an Externally Pressurized, Gas Lubricated Thrust Bearing", Journal of Applied Mechanics.
- (3) K. J. Stout and F. Sweeney, "Design of Aerostatic Flat Pad Bearings Using Pocketed Orifice Restrictors", Tribology International V. 17, N4, Aug '84, 191-193.
- (4) H. Mori, A. Mori, "On the Stabilizing Methods of Externally Pressurized Thrust Bearings" Transactions of the ASME, Journal of Basic Engineering, 1967.
- (5) D. F. Wilcock, "Externally Pressurized Bearings as Seveomechanism. I - The Simple Thrust Bearing", Transactions of the ASME, Journal of Basic Engineering, 1967.
- (6) Akira Kobayashi, "Recent Development of Ultra-Precision Diamond Cutting Mechanics in Japan", Bull. Japan Soc. of Precision Engg., V17, N2, 1983, 73-80.
- (7) A. Shimokohbe, H. Aoyama and I. Watanabe, "A High Precision Straight-Motion System", Precision Engineering, Vol. 8, No. 3, July 1986.

APPENDIX: AV

Derivation of $\frac{\partial \dot{M}_{2.3}}{\partial p_{3/4}}$ and $\frac{\partial \dot{M}_{2.3}}{\partial p_{2/*}}$ where $\dot{M}_{2.3}$ is mass flow through a thin plate orifice. Upstream pressure is $p_{2/*}$, downstream pressure is $p_{3/*}$. The flow through an orifice is customarily described as

$$\dot{M}_{2.3} = C_d A_0 p_{2/*} \sqrt{\frac{2}{R T_2} \left(\frac{\gamma}{\gamma-1} \right) \left[\left(\frac{p_{3/*}}{p_{2/*}} \right)^{\frac{2}{\gamma}} - \left(\frac{p_{3/*}}{p_{2/*}} \right)^{\frac{\gamma+1}{\gamma}} \right]} \quad \text{E.AV.1}$$

where: R is the gas constant for the fluid involved

T_2 is the temperature at state 2. $R T_2 = \frac{p_{2/*}}{\rho_{2/*}}$,

γ is the polytropic constant $\gamma = 1.4$ (air)

Let: $\frac{p_{3/*}}{p_{2/*}} = \beta$ C_d = coefficient of discharge (assumed invariant in this analysis).

A_0 = orifice area = $\frac{\pi d_o^2}{4}$ or periphery x h for proximity orifice.

a) Evaluating $\frac{\partial \dot{M}_{2.3}}{\partial p_{3/*}}$

Rewrite E.AV.1 as

$$\dot{M}_{2.3} = B \lambda^{1/\gamma} \quad B = C_d A_0 p_{2/*} \sqrt{\frac{\rho_{2/*}}{p_{2/*}} \left(\frac{\gamma}{\gamma-1} \right)} \quad \text{E.AV.2b}$$

$$\lambda = \beta^{2/\gamma} - \beta^{1+\frac{1}{\gamma}}$$

$$\text{Then } \frac{\partial \dot{M}_{2.3}}{\partial p_{3/*}} = \frac{B}{2\lambda^{1/2}} \frac{\partial \lambda}{\partial p_{3/*}}$$

$$\frac{\partial \lambda}{\partial p_{3/s}} = \frac{\partial}{\partial p_{3/s}} \left(\beta^{2/\gamma} - \beta^{1+\frac{1}{\gamma}} \right) = \left(\frac{2}{\gamma} \beta^{2/\gamma-1} - \left(1 + \frac{1}{\gamma}\right) \beta^{\frac{1}{\gamma}} \right) \frac{\partial \beta}{\partial p_{3/s}}$$

$$\text{Since } \frac{\partial \beta}{\partial p_{3/s}} = \frac{1}{p_{2/s}} = \frac{\beta}{p_{3/s}} ; \frac{\partial \lambda}{\partial p_{3/s}} = \left(\frac{2}{\gamma} \beta^{2/\gamma} - \left(1 + \frac{1}{\gamma}\right) \beta^{\frac{1}{\gamma}+1} \right) \frac{1}{p_{3/s}}$$

$$\text{Therefore } \frac{\partial \mathcal{M}_{2.3}}{\partial p_{3/s}} = \frac{B}{2} \frac{\lambda^{1/2}}{\lambda} \left(\frac{2}{\gamma} \beta^{2/\gamma} - \left(1 + \frac{1}{\gamma}\right) \beta^{\frac{1}{\gamma}+1} \right) \frac{1}{p_{3/s}}$$

$$\text{or } \frac{\partial \mathcal{M}_{2.3}}{\partial p_{3/s}} = \frac{\mathcal{M}_{2.3}}{2p_{3/s}} \left(\frac{\frac{2}{\gamma} \beta^{2/\gamma} - \left(1 + \frac{1}{\gamma}\right) \beta^{\frac{1}{\gamma}+1}}{\beta^{2/\gamma} - \beta^{1/\gamma+1}} \right)$$

$$\text{Finally } \frac{\partial \mathcal{M}_{2.3}}{\partial p_{3/s}} = \frac{\mathcal{M}_{2.3}}{p_{3/s}} \cdot \mathcal{F}_{2-3} \quad \text{E.AV.3}$$

$$\mathcal{F}_{2-3} = \frac{2/\gamma \beta^{2/\gamma} - \left(1 + \frac{1}{\gamma}\right) \beta^{1/\gamma+1}}{\beta^{2/\gamma} - \beta^{1/\gamma+1}}$$

β	0	.1	.2	.3	.4	.5	.53
Air \mathcal{F}_{2-3}	.715	.562	.471	.368	.239	.065	-.001

b) Evaluating $\frac{\partial \mathcal{M}_{2.3}}{\partial p_{2/s}}$ from E.AV.2b.

$$\frac{\partial \mathcal{M}_{2.3}}{\partial p_{2/s}} = \frac{B \partial \lambda^{1/2}}{\partial p_{2/s}} + \frac{\partial B}{\partial p_{2/s}} \cdot \lambda^{1/2}$$

$$\text{Where } \frac{\partial \lambda}{\partial p_{2/s}} = \left(\frac{2}{\gamma} \beta^{2/\gamma-1} - \left(1 + \frac{1}{\gamma}\right) \beta^{1/\gamma} \right) \frac{\partial \beta}{\partial p_{2/s}}$$

$$\frac{\partial \beta}{\partial p_{2/\star}} = p_{3/\star} \left(-p_{2/\star}^{-2} \right) = -\frac{\beta}{p_{2/\star}}$$

$$\text{Therefore } \frac{\partial \lambda^{1/2}}{\partial p_{2/\star}} = - \left(\frac{2}{\gamma} \beta^{2/\gamma} - \left(1 + \frac{1}{\gamma}\right) \beta^{1/\gamma+1} \right) \frac{1}{p_{2/\star}}$$

$$\frac{\partial B}{\partial p_{2/\star}} = \frac{\partial}{\partial p_{2/\star}} \left[C_d A_0 p_{2/\star} \sqrt{\frac{p_2}{p_{2/\star}} \frac{\gamma}{\gamma-1}} \right] = \frac{B}{2p_{2/\star}}$$

$$\text{Finally } \frac{\partial \mathcal{M}_{2.3}}{\partial p_{2/\star}} = \frac{-\mathcal{M}_{2.3}}{p_{2/\star}} \mathcal{F}_{2-3} + \frac{\mathcal{M}_{2.3}}{2p_{2/\star}}$$

$$\text{or } \frac{\partial \mathcal{M}_{2.3}}{\partial p_{2/\star}} = \frac{\mathcal{M}_{2.3}}{p_{2/\star}} J_{2-3} \text{ , } J_{2-3} = \left(\frac{1}{2} - \mathcal{F}_{2-3} \right) \quad \text{E.AV.4}$$

c) Derivation of $\frac{\partial \mathcal{M}_{5.3}}{\partial p_{3/\star}}$ and $\frac{\partial \mathcal{M}_{5.3}}{\partial h}$

$$\mathcal{M}_{5.3} = \frac{\rho_\infty}{p_{\infty/\star}} \frac{h^3}{12\mu} \cdot \frac{1}{S_r} \cdot \Psi_{5/3}$$

$$\frac{\partial \mathcal{M}_{5.3}}{\partial p_{3/\star}} = -\frac{\mathcal{M}_{3.5}}{\Psi_{3/5}} \frac{\partial \Psi_{3/5}}{\partial p_{3/\star}}$$

$$\frac{\partial \Psi_{3/5}}{\partial p_{3/\star}} = \frac{\partial}{\partial p_{3/\star}} (p_{3/\star}^2 - p_{5/\star}^2) = 2p_{3/\star}$$

$$\text{Hence } \frac{\partial \mathcal{M}_{5.3}}{\partial p_{3/\star}} = -\mathcal{M}_{3.5} \left(\frac{2p_{3/\star}}{\Psi_{3/5}} \right) = -\frac{\mathcal{M}_{3.5}}{p_{3/\star}} \left(\frac{2}{1 - \left(\frac{p_{5/\star}}{p_{3/\star}} \right)^2} \right)$$

$$\frac{\partial \mathcal{M}_{5.3}}{\partial p_{3/}} = - \frac{\mathcal{M}_{3.5}}{p_{3/}} \cdot \mathcal{F}_{3-5} \quad \mathcal{F}_{3-5} = \frac{2}{1 - \left(\frac{p_{5/}}{p_{3/}}\right)^2} \quad \text{E.AV.5}$$

$p_{5/}/p_{3/}$	0	.1	.2	.3	.4	.5
\mathcal{F}_{3-5}	2.00	2.02	2.08	2.20	2.38	2.67

$$\text{d) } \frac{\partial \mathcal{M}_{5.3}}{\partial h} = \frac{3 \mathcal{M}_{5.3}}{h} = -3 \frac{\mathcal{M}_{3.5}}{h} \quad \text{E.AV.6}$$

$$\text{e) } \underline{\text{Derivation of } \frac{\partial \mathcal{M}_{2.3}}{\partial h}}$$

$$\frac{\partial \mathcal{M}_{2.3}}{\partial h} = \frac{\partial \mathcal{M}_{2.3}}{\partial A_0} \cdot \frac{\partial A_0}{\partial h} = \frac{\mathcal{M}_{2.3}}{h}$$

$$\frac{\partial \mathcal{M}_{2.3}}{\partial h} = \left\{ \begin{array}{ll} = \frac{\mathcal{M}_{2.3}}{h} & \text{Inherently compensated orifice} \\ = 0 & \text{Orifice or capillary} \end{array} \right\} \quad \text{E.AV.7}$$

$$\text{f) } \underline{\text{Derivation of squeeze coefficient}}$$

$\delta \mathcal{M}_{II(3-4)}$ = mass flow into volume bordered by 3 and 4 (recess) due to transla-
tory velocity of plate II.

$\delta \mathcal{M}_{II(4-5)}$ = Mass flow into film domain 4-5.

$$\delta \mathcal{M}_{II(3-4)} = -A_{3-4} \cdot \dot{z}_{II/I} \cdot \rho_3$$

$$\delta \mathcal{M}_{II(4-5)} = -\dot{z}_{II/I} \int_4^5 \rho_4 dA = -\dot{z}_{II/I} A_0 \quad \text{E.AV.8}$$

g) Derivation of capacitance coefficient C_{3-}

From Table A.I.c element 3

$$C_{3-} = \frac{\text{mass of fluid in pocket 3-4}}{\gamma p_{3/}} = \frac{\rho_3 \text{ vol}_{3-4}}{p_{3/} (\gamma = 1.0)} \quad \text{E.AV.9}$$

APPENDIX VI
Project Staff 1983-1986

Faculty

M.M. Barash, Ransburg Professor of Manufacturing and Professor of Industrial Engineering	Principal Investigator & Project Director
C.R. Liu, Professor of Industrial Engineering	Principal Investigator
J. Modrey, Professor of Mechanical Engineering	Co-Principal Investigator
A.L. Sweet, Professor of Industrial Engineering	Co-Principal Investigator
K.S. Fu*, Goss Distinguished Professor of Engineering (Elec.Eng.)	Faculty Associate
W. Stevenson, Professor of Mechanical Engineering	Faculty Associate
J.J. Talavage, Professor of Industrial Engineering	Faculty Associate
R. Hannam**, Visiting Associate Professor of Industrial Engineering	Faculty Associate
W. Johnson***, Visiting Professor of Industrial Engineering	Faculty Associate
A. Shumsherrudin,† Visiting Associate Professor of Industrial Engineering	Faculty Associate
J.L. Batra,†† Visiting Professor of Industrial Engineering	Faculty Associate

*Deceased April 1985

**University of Manchester, England

***University of Cambridge, England (retired)

†Cranfield Institute of Technology, England

††Indian Institute of Technology, Kanpur, India

Graduate Research Assistants

*P. Chen
Y.C. Chou
*G. Eshel
P. Ferreira
*R. Khanna
G. Lang
*S.K. Lee
G.R. Llang
*Y.T. Lin
J. Lopez
A.I. Najashi

*D. Noller
Y.S. Ouyang
U. Roy
S. Shodhan
*R. Srinivasan
S. Venkatramen
*R. Venugopal
M.C. Wu
*J. York
Y.C. Yu

*Graduated

END

7-87

Dtic